Nanoscale excitations in emergent materials

NEEM 2015

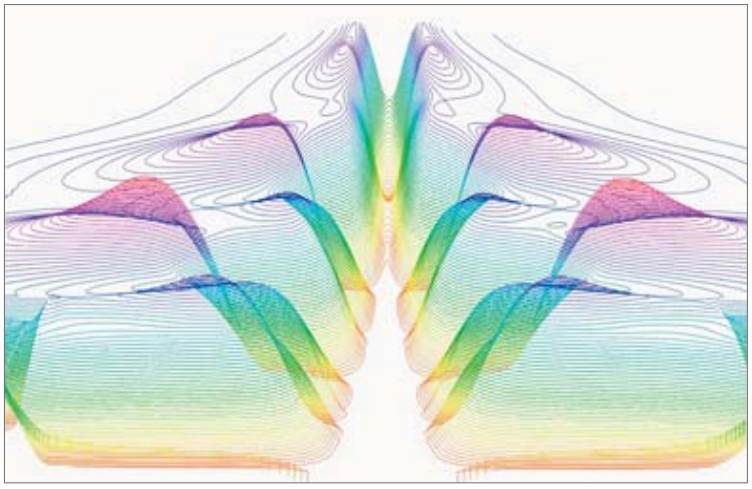

edited by
Augusto Marcelli
Chidambara Balasubramanian

superstripes press
science series

Nanoscale excitations in emergent materials

NEEM 2015

edited by
Augusto Marcelli
Chidambara Balasubramanian

superstripes press
science series

Science Series No.7

Title: Nanoscale excitations in emergent materials NEEM 2015

Published in Rome on November 2015
by Superstripes Press, Rome, Italy

http://www.superstripes.net/science/science.htm

ISBN 9788866830450
ISBN-A 10.978.886683/0450

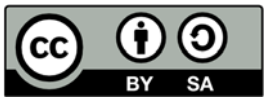

Cover page: *"Contour plot of the differential resistance dV/dI showing the critical behavior of a dynamic vortex Mott insulator."* (courtesy by Nicola Poccia)

Authors:

V.G. Achanta, A. Acquarelli, R. Ahuja, S. Allard, S. Anders, A. Annadi, F. Antolini, Ariando, G. Artioli, M. Autore, A. Ayrapetov, P. Ayyub, R. Bagga, G. Bais, C. Balasubramanian, S.K. Balijepalli, P. Ballirano, A. Banas, K. Banas, A.K. Bansal, T.I. Baturina, L. Begrambekov, F. Bellatreccia, A. Bellucci, S. Bellucci, E. Belluso, P.J. Bhatt, P.J. Bhatt, A. Bianconi, G. Bianconi, K. Bogle, D. Bora, S. Botti, M.B.H. Breese, A. Bregnocchi, A. Brinkman, G. Buonomo, I. Cacciotti, P. Calvani, G. Campi, L. Caneve, S. Capella, D. Cappelletti, M. Cestelli-Guidi, B.S. Chakrabarty, T.K. Chan, C.R. Chandraiahgari, M. Chen, G. Cibin, W. Ciccognani, S. Colangeli, F. Coneri, C. Cong, A.G. D'Aloia, R. D'Amato, F. D'Apuzzo, M.C. Dalconi, I. Davoli, G. De Bellis, F. De Matteis, A. D'Elia, G. DellaR.K. Desai, A. Di Cicco, D. Di Gioacchino, F. Di Pietrantonio, C. Dube, M. Dykas, A. Evsin, A. Fabbretti, M. Falconieri, M. Favero, G. Ferrari, S. Gagliardi, S. Gay, F. Giorgianni, E. Giovine, M. Girolami, A.M. Giuliodori, A.A. Golubov, K. Gopinadhan, F. Gozzi, C. Grisolia, A. Gruverman, R. Gunnella, M.Y. Hacisalihoglu, K. Hatada, K. Hayakawa, H. Hilgenkamp, A. Hirzer, P. Innocenzi, Y. Ito, G. Jona-Lasinio, B. Joseph, S. Kaciulis, D. Kanjilal, A. Kaplevsky, T. Kasponas, S.S. Khirwadkar, S. Kurhuzenkau, S. Laurenzi, A. Lausi, E. Limiti, S. Linzen, H. Lu, M. Lucci, S. Lupi, S. Macis, A. Marcelli, M. Marinelli, F. Marra, S. Mathew, D. Mencarelli, H.G. Meyer, E. Missale, T. Mizokawa, Y. Mizuguchi, C.G. Molenaar, B. Moroni, M.R. Motapothula, S. Mukherjee, M.K. Mukhopadhyay, F. Nanni, C.E. Nebel, D. Nikolaidu, F. Nobili, A. Notargiacomo, S.B. Ogale, P.B. Orpe, L. Ottaviano, E. Pace, A. Painelli, B. Pal, L. Paliotta, F. Palumbo, E. Paris, M. Pea, A. Perali, F. Perrozzi, R.A. Piacenti, L. Pierantoni, Y. Ping, N. Poccia, M. Polentarutti, C. Presilla, A. Proietti, A. Puri, G. Raciukaitis, A. Rana, M. Ranjan, P.M. Raole, S. Rezvani, A. Ricci, A. Rinaldi, T. Rindzevicius, F. Rondino, H. Rotella, A. Rufoloni, V. Russo, Y. Sadovsky, S. Saha, N.L. Saini, I.D.W. Samuel, M.G. Santonicola, S. Sanyal, D.D. Sarma, F. Sarto, M.S. Sarto, T.J. Sato, U. Scherf, D. Schlom, M. Schmelz, M.S. Schmidt, T. Schönau, M. Secco, G. Sharma, S.M. Sharma, Z. Shen, K. Shivaram, A. Sindona, C. Sissa, R. Spurio, A. Srivastava, R. Stolz, L. Stroea, T. Sugimoto, U. Susta, Y. Takano, A. Tamburrano, F. Terenziani, G. Terranova, V. Thakare, Y. Ting, L.J. Tomar, D.M. Trucchi, S. Ullah, N. Valanoor, L. Valentini, N.K. Varshney, R. Vasudevan, T. Venkatesan, C. Verona, G. Verona-Rinati, V.M. Vinokur, C. Viti, X.R. Wang, Z. Wang, A. Witkowska, A. Zakharov, V. Zakosarenko, D. Zhan, Q. Zhang

*These authors presented the scientific reports collected in this book at the NEEM 2015 conference held in Rome (Italy) on October 12-14, 2015.

Papers presented at the 2nd Bilateral Indo-Italian Workshop

NEEM 2015

Rome, Italy October 12-14, 2015

Organized with the support of the
Directorate General for the Country Promotion Ministry of Foreign Affairs and International Cooperation

by
Consorzio Hypatia
Department of Science & Technology of India
IMEM-CNR
Institute for Plasma Research (Ghandinagar)
Istituto Nazionale di Fisica Nucleare (INFN) – Laboratori Nazionali di Frascati
Rome International Center for Materials Science Superstripes RICMASS
Università Sapienza
Università di Roma Tre

With the patronage of
Accademia dei Lincei and *Regione Lazio*

Scientific Committee Chairpersons
Augusto Marcelli (INFN-LNF, Frascati)
Chidambara Balasubramanian (IPR, Gandhinagar)

Advisory Committee
A. Bianconi (RICMASS, Rome)
D. Bora (IPR, Gandhinagar)
C. Doglioni (Accademia dei Lincei, Rome)
P.D. Gupta (RRCAT, Indore)
A. Mottana (Accademia dei Lincei, Rome)

Scientific Programm Committee
Gaetano Campi (CNR - Istituto di Cristallografia, Rome)
Giancarlo Della Ventura (Università Roma Tre, Rome)
Daniele Di Gioacchino (INFN, Frascati)
Salvatore Iannotta (CNR - IMEM, Parma)
Flavio Lucibello (Consorzio Hypatia, Rome)
Subroto Mukherje (IPR, Gandhinagar)
Andrea Notargiacomo (CNR-IFM, Rome)
Mukesh Ranjan (IPR, Gandhinagar)
Naurang L. Saini (Università Sapienza, Rome)
Lidia Szpyrkowicz (Università Ca' Foscari, Venice)
Mariano Zarcone (INFN-LNF, Frascati)

Preface

This volume contains the extended abstracts of the contributions presented at the workshop *Nanoscale Excitations in Emergent Materials* (NEEM 2015) held in Rome from 12 to 14 October 2015, an event organized and supported in the framework of the Bilateral Cooperation Agreement between Italy and India within the project of major relevance *Investigating local structure and magnetism of cobalt nano-structures*, funded by the Italian Ministry of Foreign Affairs and the Department of Science & Technology in India.

Materials research is a key component of the economic and industrial development of a country, a fundamental area to develop new technology and new products with a high added value. India is definitely one of the leading nations in Asia in this sector and, in particular, is investing heavily in the field of nano-technologies, an area at the border of Physics, Chemistry, Biology and Engineering with clear positive outcomes for the environment.

The meeting was the 2nd workshop among Italian and Indian researchers and followed the first event (NEEM2013) held in Ahmedabad (India) in November 2013 and organized by the Institute of Plasma Research in Gandhinagar.

Covering a modern interdisciplinary area the NEEM2015 meeting has been funded by the Directorate General for the Country Promotion - Ministry of Foreign Affairs and International Cooperation as well as by the Department of Science and Technology of the Government of India. It has been mainly focused on the recent advances in the area of nano-materials as well as on advanced techniques used to characterize nano-materials and nano-structures. The topics of the meeting spanned from nano materials for energy and fusion, nanoparticles, correlated nano-phase materials, functional nano-materials, composite nano-materials, to bio-materials and their applications.

The workshop provided an important opportunity and a unique forum to exchange ideas among qualified interdisciplinary teams with the main aim to promote scientific and technological exchanges and trigger partnership activities among institutions in an area of great potential interests for researchers and for industrial houses. With this purpose we invited experts in the different fields to give an overview of the field and present their latest results.

We really would like to thank all sponsors, the *Accademia dei Lincei* and the *Regione Lazio* that kindly gave their patronage to this international workshop and all scientists that enthusiastically participated in the meeting and immensely contributed to its success.

A. Marcelli

C. Balasubramanian

Index

Role of Catalysts & Nano Structuring in Hydrogen Storage Materials

Rajeev Ahuja
Department of Physics & Astronomy
Uppsala University, Uppsala, Sweden

Email: *rajeev.ahuja@physics.uu.se*
Keywords: hydrogen storage, catalysis, molecular dynamics, MOF, metal-hydrides

The purpose of this talk is to provide an overview of the most recent theoretical studies undertaken by us in the field of hydrogen storage materials research. On selected examples, the application of our computational tool of choice, density functional theory, will be illustrated to show how *ab initio* calculations can be of use in the effort to reach a better understanding of hydrogen storage materials and to occasionally also guide the search for new promising approaches. A deeper theoretical understanding of the catalytic mechanism involved in kinetic enhancement should be a very valuable guide in the design of new catalysts. Systems to be discussed include: Metal-organic frameworks, where we have studied hydrogen physisorption in three different types of iso-reticular MOFs, namely Zn-/Mg-/Ca-MOF16, decorated with either Li, Na, or K [1]. Lithium ion diffusion in lithium imide (Li_2NH) and lithium amide ($LiNH_2$) was studied by us using both *ab initio* molecular dynamics simulations and the nudged elastic band method [2,3]. Finally, catalysts play an important role in many hydrogen desorption processes. We found (through a combination of experiment and theory) that carbon nanostructures, in particular nanotubes and fullerenes, can be used as catalyzing agents for hydrogen uptake and release in complex metal hydrides (such as sodium alanate, $NaAlH_4$) and provide a model which could explain the mechanism of the catalytic effect [4].

References

1. Pornjuk Srepusharawoot, Andreas Blomqvist, C. Moysés Araújo, Ralph H. Scheicher and Rajeev Ahuja, *International Journal of Hydrogen Energy* 36, 555–562 (2011)
2. A. Blomqvist, C.M. Araújo, R.H. Scheicher, P. Srepusharawoot, W. Li, P. Chen, and R. Ahuja, *Physical Review B* 82, 024304 (2010).
3. C. Moysés Araújo, Andreas Blomqvist, Ralph H. Scheicher, Ping Chen and Rajeev Ahuja, *Physical Review* 79, 172101 (2009).
4. P.A. Berseth, A. Harter, R. Zidan, A. Blomqvist, C.M. Araújo, R.H. Scheicher, R. Ahuja and P. Jena, *Nano Letters* 9, 1501–1505 (2009)

Does particle size control crystal structure?

Pushan Ayyub
Department of Condensed Matter Physics & Materials Science Tata Institute of Fundamental Research, Homi Bhabha Road, Mumbai 400005, India

Email: *pushan@tifr.res.in*
Homepage: *http://www.tifr.res.in/ ~pushan*
Keywords: particle size effects, structural phase transitions

Most of the physical properties of a solid get modified – often drastically – when the particle or crystallite size is reduced below certain characteristic length scales, which usually fall in the 1-100 nanometer regime. The physical and chemical properties of nano-solids are known to be controlled by one or more of the following factors: (1) quantum size effects, (2) surface and interface effects, and (3) size-induced modifications in the lattice symmetry. While the first two topics are well researched and fairly well understood, in this talk I will introduce some of our observations on size-induced changes in crystal symmetry. A decrease in the particle size causes some degree of structural modification in a large number of solids, particularly those in which the bonding has a covalent character [1,2]. Such size-induced changes in crystal symmetry affect important physical properties such as ferroelectricity [3,4] and superconductivity in nanocrystalline systems.

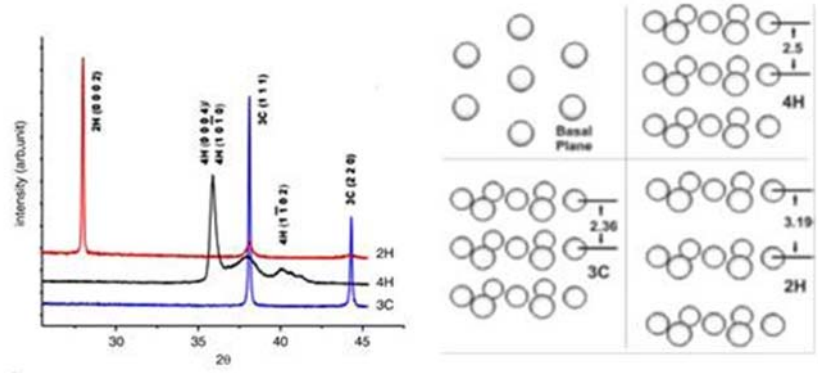

Figure 1: Left: XRD data from the three polytypic structures of silver: 3C, 4H, and 2H. Right: Pictorial representation of the 3C, 4H, and 2H polytypes of silver, depicting a progressive increase in the inter-planar spacing (in Å). The hexagonal-close-packed basal plane (top view) is shown on the top left [6].

We will also show that dimensional constraints can lead to the stabilization of various novel and unusual crystallographic phases. Though nanoparticles of typical metals usually exhibit only gradual changes, we observed traces of a hexagonal structure in nanocrystalline, predominantly cubic (*fcc*) silver [5]. More recently, we have succeeded in producing – in phase-pure form – two novel, crystallographic modifications of silver in dimensionally or kinetically constrained systems [6]. These are structurally anisotropic, low-density, poorly metallic forms of silver, whose optical, transport, vibrational, mechanical, and chemical properties are quite distinct from those of the canonical, cubic ground state [7]. At least one such phase is stable under ambient conditions, allowing therefore detailed physical measurements. First-principles calculations based on density functional theory confirm the relative stability of this hexagonal (4*H*) modification of "silver".
Similar size-induced structural transitions have also been observed in many other systems.

References

1. P Ayyub, V R Palkar, S Chattopadhyay, M S Multani; Effect of crystal size reduction on lattice symmetry and cooperative properties; Phys. Rev. B 51, 6135 (1995)
2. V R Palkar, P Ayyub, S Chattopadhyay and M S Multani; Size-induced structural transition in the Cu-O and Ce-O systems; Phys. Rev. B 53, 2167 (1996).
3. S Chattopadhyay, P Ayyub, V R Palkar and M S Multani; Size-induced diffuse phase transition in nanocrystalline ferroelectric $PbTiO_3$; Phys. Rev. B 52,13177 (1995).
4. S Chattopadhyay, P Ayyub, V R Palkar, A V Gurjar, R M Wankar, M S Multani; Finite size effects in antiferroelectric $PbZrO_3$ nanoparticles; J. Phys.: Cond. Mat. 9, 8135 (1997)
5. P Taneja, R Banerjee, P Ayyub, R Chandra. G K Dey: Observation of a hexagonal (4H) phase in nanocrystalline silver; Phys. Rev. B 64, 033405 (2001).
6. I Chakraborty, D Carvalho, S Shirodkar, S Lahiri, S Bhattacharyya, R Banerjee, U Waghmare, P Ayyub; Novel hexagonal polytypes of Silver: Growth, characterization and first principles calculations; J. Phys.: Cond. Mat. 23, 325401 (2011).
7. I Chakraborty, S N Shirodkar, S Gohil, U V Waghmare and P Ayyub: A stable, quasi-2D modification of silver: Optical, electronic, vibrational and mechanical properties, and first principles calculations; J. Phys.: Cond. Mat. 26, 025402 (2014).

Photoluminescence studies of Rare Earth doped nano glass-ceramics

Ruchika Bagga[1], Serena Gagliardi[*2], Mauro Falconieri[2], Venu Gopal Achanta[3], Gopi Sharma[1]
[1]*Department of Physics, Kanya Maha Vidyalaya, Jalandhar*
[2]*ENEA- Physical Technologies for Health and Security Division*
[3]*Department of Condensed Matter Physics, TIFR, Mumbai, India*

Email: **serena.gagliardi@enea.it*
Keywords: rare earth, glass ceramic, photoluminescence

In the last decade the use of Light Emitting Diodes (LED) deeply renewed illumination and displays technologies, replacing the conventional incandescent and fluorescent lamps and cathode ray tubes displays [1-3].
Since both these applications require the use of proper phosphors in order to achieve the white light and/or finely tuned colors, a large effort is devoted to the development of new white light emitting materials. Promising candidates are rare-earth (RE) doped glass ceramics, nanocomposite materials formed by a glass matrix hosting nanocrystals, thus combining the easy and economic manufacturing of glasses to the optical activity of doped crystals [4].
We investigated the emission properties of different rare earth (Dy^{3+}, Eu^{3+}) ions in oxyfluoride glass ceramics, since in these systems it is possible to produce white light by proper combination of the emission intensity of different intense bands in the visible spectral region. In fact, some of the emission bands of REs are associated to hypersensitive transitions (forced electric dipole transitions) so that their probability is affected by the crystal field surrounding the ion [5-7]; hence, fine tuning of the emission color can be obtained by proper sample preparation or by subsequent treatments. In particular, the effect of different thermal treatments on glass and glass ceramic properties and associated RE luminescence emission was investigated.
Different glass ceramic samples were on purpose prepared and characterized at Kanya Maha Vidyalaya, and also characterized at TIFR and ENEA C.R. Casaccia. Different characterizations, such as DTA, XRD, SEM and FTIR were employed to study the crystallization process and the structural properties of the precursor glass and corresponding glass–ceramics. The photoluminescence spectra at different excitation wavelengths were measured and the CIE chromaticity coordinates were calculated to investigate the feasibility of the studied materials for lighting applications.
The relative emission intensity of the visible bands of Dy^{3+} and Eu^{3+} ions were found to be tunable by the heat treatment which influenced the nanocrystal size

and concentration inside the glass matrix [8,9]. In particular white light emission was obtained from both RE ions in glass ceramics under UV excitation. Multi-color emission was also produced using different excitation wavelengths, by enforcing the formation of Eu^{2+} centers at the expense of the usual Eu^{3+} ones, by proper selection of the matrix composition.
In conclusion, thermal treatments have demonstrated to alter the RE environment on the nanoscale, influencing the emission properties, which, by suitable choice of the excitation wavelength, can be potentially exploitable for lighting devices.

References

1. Q. Luo *et al.*, J. App. Physics **105**, 4 (2009).
2. P. Babu *et al.*, Optics Express **19**, 3 (2011).
3. D.S. Jo *et al.*, Optical Materials **34**, 1362 (2012).
4. W. Hölland *et al.*, Glass Ceramic Technology, The American Ceramic Society (2002).
5. M. Dejneka *et al.,* J. Lumin. **65**, 227 (1995).
6. S. Zhang, *et al.,* J. Am. Ceram. Soc. **94**, 9 (2011).
7. S. Zhang, *et al.,* Chem. Mater. **23**, 5 (2011).
8. R. Bagga, *et al.,* Materials Science and Engineering B **178**, 218-224 (2013).
9. R. Bagga, *et al.*, Optical Materials **36**, 198-206 (2013).

In situ formation and photo patterning of emissive quantum dots

A.K. Bansal[1], F. Antolini*[2], L. Stroea[2], T. Kasponas[3], G. Raciukaitis[3], A. Hirzer[4], V. Schmidt [4], S. Allard[5], U. Scherf[5] and I.D.W. Samuel[1]
[1]*Organic Semiconductor Centre, School of Physics and Astronomy, University of St Andrews, North Haugh, St Andrews Fife, KY16 9SS, United Kingdom*
[2]*ENEA Photonics Micro and Nanostructures Laboratory, Via E. Fermi 45, 00044 Frascati (Rome), Italy*
[3]*EKSPLA UAB, Savanoriu Ave. 231, LT-02300 Vilnius, Lithuania*
[4]*Joanneum Research, Forschungsgesellschaft mbH, MATERIALS - Institute for Surface Technologies and Photonics, Franz-Pichler-Straße 30, 8160 Weiz, Austria*
[5]*Institut für Polymertechnologie Bergische Universität Wuppertal, Gauss-Strasse 20, 42097 Wuppertal, Germany*

Email: *francesco.antolini@enea.it*
Keywords: quantum dots, precursors, laser patterning

Nanostructured composites of inorganic and organic materials are attracting extensive interest for electronic and optoelectronic device applications. Here we report a novel method for the fabrication of metal selenide nanoparticles in organic semiconductor films that is compatible with solution processable large area device manufacturing. Our approach is based upon the controlled in situ thermal decomposition of cadmium selenide precursor complex in a film of the electron transporting material 1,3,5-tris(N-phenyl-benzimidazol-2-yl)-benzene (TPBI).

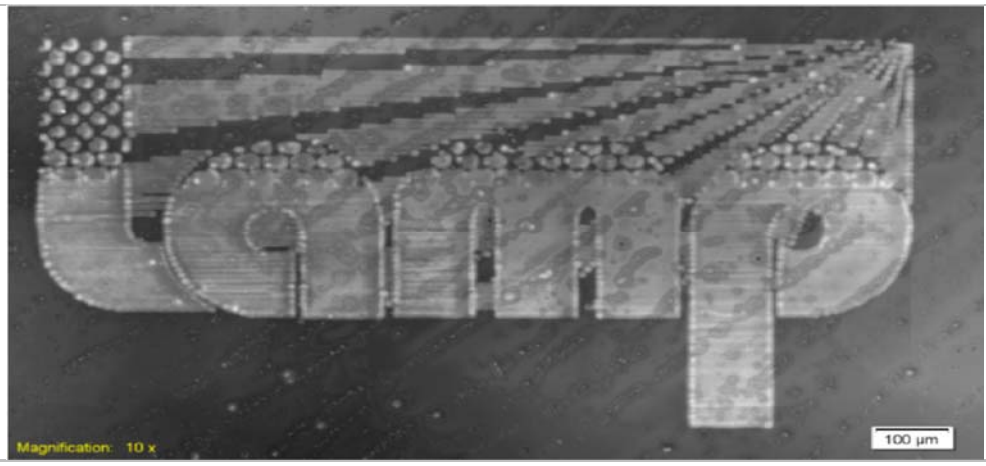

Figure 1: Laser writing of European project LAMP logo. Parameters: 1.05 mW, 100 kHz, 10.5 nJ, 0.75 mm/s, hatch 3 µm, nitrogen atmosphere.

Specifically we show that the photoluminescence quantum yield (PLQY) of the thermally converted CdSe quantum dots (QDs) in the TPBI film is up to 15%. The PLQY depends on the concentration of the solution, blend ratio of the precursor and the annealing temperature. Time-resolved photoluminescence studies show the fast energy transfer from the organic host to the emissive QDs. The results emphasize the importance of the alignment of energy levels between the host and guest dopants [1].

We also show that laser irradiation can form the QDs from the precursor [2]. This is an important result as it enables direct laser patterning (DLP) of the QDs. The DLP is performed on these blends with a picosecond laser at 266 nm wavelength at various irradiation doses. The confocal microscopy reveals the formation of the emissive QDs after laser processing (Figure 1).

The optical and structural properties of the QDs are also analyzed by means of UV-Vis, PL spectroscopy and transmission electron microscopy (TEM). The results show that the QDs are well distributed across the film and their emission can be tuned over a wide range by varying the temperature or laser power used on the blend films. Our findings provide a route to the low cost patterning of hybrid electroluminescent devices.

References

1. A.K. Bansal, F. Antolini, M.T. Sajjad, L. Stroea, R. Mazzaro, S.G. Ramkumar, K-J. Kass, S. Allard, U. Scherf and I.D.W. Samuel, Phys. Chem. Chem. Phys. 14, 9556-9564 (2014).
2. A.K. Bansal, M.T. Sajjad, F. Antolini, L. Stroea, P. Gecys, G. Raciukaitis, P. Andrè, A. Hirzer, V. Schmidt, L. Ortolani, S. Toffanin, S. Allard, U. Scherf and I.D.W. Samuel, In situ formation and photopatterning of emissive quantum dots in small organic molecules, Nanoscale 7, 11163-11172 (2015).

Hydrogen penetration through oxidized metal surface irradiated by oxygen added hydrogen flux

L. Begrambekov[1], A. Ayrapetov[1], A. Evsin[1], Ch. Grisolia[2], A. Kaplevsky[1], Ya. Sadovsky[1], A. Zakharov[1]
[1]*Plasma Physics Department, NRNU MEPhI, Moscow, Russian Federation*
[2]*CEA, IRFM, F-13108 Saint-Paul-lez-Durance, France.*

E-mail: *lbb@plasma.mephi.ru*
Keywords: hydrogen, oxygen, plasma, irradiation, oxidized surface, trapping, desorption.

1. Introduction

The oxide layers are known as effective diffusion barriers for hydrogen. At the same time, the barrier properties of the oxide layer are modified under plasma irradiation [1], causing, in particular, non-controlled hydrogen release from the plasma facing elements of plasma and fusion devices. The processes on the plasma irradiated oxidized surfaces are not known in details. The paper studies the hydrogen trapping and release from the metals with oxidized surface (stainless steel (SS), tungsten with aluminum oxide coating and zirconium alloy) irradiated by hydrogen (H) atoms and oxygen (O) and by O added H plasma.
Sample irradiation by deuterium (D) and H atoms and by D ions was performed in the plasma chamber of MICMA device [1]. Residual gas (95% H_2O and 5% H_2) pressure (P_{Res}) in the plasma chamber was $\leq 3\times10^{-3}$ Pa and that of TDS chamber $\leq 1{,}3\times10^{-5}$ Pa. Gas pressure during sample irradiation P_{Gas} was $\approx 6.6\times10^{-1}$ Pa. D and H atoms have been produced by molecular dissociation on heated tungsten cathode. The plasma was ignited between heated cathode and anode. Gas concentration during both irradiation and TDS analysis of the samples was measured by mass-spectrometer.

2. Stainless steel

Experiment. The SS wall of plasma chamber of MICMA (composition: 0.12% C, 18% Cr, 10% Ni, less than 1% Ti) was used as investigated "sample". The temperature of air cooled chamber wall did not exceed 315 K. In the first step, the chamber was filled by deuterium with oxygen additions, and the chamber wall was irradiated by mixture of D atoms and oxygen varied in the range (0.5, 2, 10, 20, 30 at %). Then a plasma was started, thus producing (D_2 + x%O_2) plasma irradiation of the wall being under floating potential regarding to plasma. Finally, deuterium was replaced by hydrogen and H atoms irradiated the wall. The average D- and H-atom fluxes on the wall were estimated as being equal $\approx 1.5\times10^{19}$ at/m^2, and these of D- and H-ion fluxes were equal to 0.5×10^{19} at/m^2.

Table 1. Total H release and D trapping within 40 minutes irradiation

Oxygen concentration in working gas, (at %)	Average hydrogen release rate, ($at/m^2 \times s$)	Hydrogen release (N_H) (at/m^2)	Deuterium trapping (N_D) (at/m^2)	N_H/N_D ratio
0,5	$2,5\times10^{17}$	$0,6\times10^{21}$	$0,3\times10^{21}$	2,0
2	$4,1\times10^{17}$	$1,0\times10^{21}$	$0,5\times10^{21}$	2,0
10	$7,2\times10^{17}$	$1,7\times10^{21}$	$0,9\times10^{21}$	1,9
20	$8,2\times10^{17}$	$2,0\times10^{21}$	$1,1\times10^{21}$	1,8
30	$12,3\times10^{17}$	$2,9\times10^{21}$	$1,5\times10^{21}$	1,9

Results and discussion. When cathode was heated, oxygen concentration decreased drastically. Instead, H_2O, HDO and D_2O, HD molecules were formed on the wall surface with D atoms from gas and H atoms mainly from the bulk of stainless steel. Consecutive irradiation of the wall by H atoms in (H_2 + x%O_2) mixture led to release of the early trapped deuterium. In all cases, hydrogen release did not change remarkably during wall irradiation with plasma. The increase of oxygen concentration activated H release and D trapping (Table 1). The action of low energy ions and deuterium/hydrogen atoms was reduced to activation surface processes leading to water molecule formation and release from the surface. It means that removal of hydrogen atoms from the surface appears to be the limiting act in the series of processes leading not only to hydrogen trapping but also to its de-trapping and release from the metal.

3. Tungsten covered by aluminum oxide layer

Experiments. The samples with dimensions $7\times7\times1$ mm^3 were mechanically and then electrochemically polished and washed in ethanol in the ultrasonic bath. The samples have not been annealed, and hydrogen with concentration $8.7\times10^{20}m^3$ was contained in the samples subjected to implantation with D ions. The parameters of implantation were as follows: ion energy E=300 eV/at, ion flux $j=7.3\times10^{19}m^{-2}s^{-1}$, ion fluence $\Phi=2.6\times10^{23}m^{-2}$. Sample temperature in these and the next experiments was 450-500. One of the irradiated samples was kept in Ar+4 at% O_2 gas mixture, and the second one in the plasma of the same composition during 2 hours. Other samples were coated with layer of aluminum oxide. Deposition was made in Ar plasma and in the mixtures (Ar+4 % O_2) and (Ar+8 % O_2). The coating was formed with Al atoms sputtered by plasma ions from aluminum target. The deposition condition was as follows: residual gas (95% H_2O and 5% H_2) pressure $P_{Res}=5\times10^{-4}$ Pa, Ar pressure $P_{Ar}=1.3\times10^{-1}$ Pa, 200-nm-thick layer was deposited on each side of the sample within 1 h.

Results and discussion. Gas concentration was not changed in the samples during two first experiments, but ≈85 and ≈55% of deuterium and hydrogen, respectively, left the samples during alumina oxide deposition in the plasma with oxygen addition. One can point out that the results of this experiment were

for the most part similar to those described in the previous sections despite the fact that tungsten was covered by oxide of other metal, and the argon atoms and ions impinging alumina did not play a principal role in the observed processes.

4. Zirconium alloy

Experiments. The samples of zirconium alloy (Zr + 1% Nb) with dimensions $7\times7\times1$ mm^3 before experiments were washed in ethanol in the ultrasonic bass, but was not annealed and contained hydrogen with concentration 2.8×10^{23} m^3. They were irradiated by the ions of Ar plasma under different pressures $(1.3 – 40) \times10^{-1}$ Pa of residual gas. Ar pressure was kept equal to 1.3×10^{-3} Pa in all experiments. Irradiation ion energy, ion current density, irradiation fluence, and sample temperature were equal to 250 eV, 7.5×10^{-19}m^{-2}c^{-1}, 9×10^{22}m^{-2}, and ≈530 K, respectively. Hydrogen content in the reference sample and in investigated samples after their irradiation was measured by TDS.

Results and discussion. Hydrogen retention in the zirconium alloy was practically doubt during its irradiation by ions of argon plasma, when P_{Res} was equal to 1.3×10^{-3} Pa,. The increase of P_{Res} led to intensification of oxide surface irradiation by hydrogen and oxygen ions/atoms appeared in plasma due to residual gas dissociation and ionization. The rate of hydrogen release from the surface and zirconium outgassing was increased. When P_{gas} grow up to ≈ 3×10^{-3} Pa, the rate of hydrogen penetration and trapping in zirconium alloy appeared to be equal to the rate of hydrogen release. Under further increase of P_{gas} hydrogen concentration in zirconium alloy dropped down during irradiation. The sense of the processes in this experiment seems to be similar to these considered above. At the same time, in the experiment oxygen was not added to the plasma. Thus, one can conclude, that presumable direction of hydrogen penetration through the surface depends on oxygen concentration in the irradiating flux, but not on oxygen/hydrogen ratio in it. In addition, it is seen that Ar ion irradiation did not play principle role in the phenomenon.

5. Concluding remarks

In all experiments, we met the same phenomenon initiated on oxidized metal surface by simultaneous irradiation with hydrogen atoms and oxygen, or with oxygen added hydrogen plasma. The phenomenon started with radiation-activated formation of molecules H_2O, D_2O, HDO, HD and H_2 and their release from the surface. The reactions of impinging particles with the surface oxides providing formation of hydrogen-contained molecules are presented in the report. The event activates hydrogen penetration through the surface in both directions. When oxygen irradiation is low, the hydrogen flux into the metal exceeds the flux in opposite direction. Metal outgassing takes place when intensity of oxygen concentration reaches the certain level.

References

1. L.B. Begrambekov, J. Surf. Inv. Xray, Syn. Neut. Tech. 9, 190–195 (2015).

Excitation of surface-waves at terahertz frequencies on a suspended graphene sheet

Stefano Bellucci[1*], D. Mencarelli[2,1], A. Sindona[3], L. Pierantoni[2,1]
[1]*INFN-LNF, Frascati (RM) Italy*
[2]*Dipartimento di Fisica, Università della Calabria, Via P. Bucci Cubo 30C, Rende (CS), Italy*
[3]*Dipartimento di Fisica, Università della Calabria, Via P. Bucci Cubo 30C, Rende (CS), Italy*

Email: **bellucci@lnf.infn.it*
Keywords: plasmons, grapheme, terahertz

Spatial dispersion effects upon local excitation of extrinsic plasmons in graphene micro-discs, is studied by a full-wave electromagnetic solver, in order to evaluate the effects of spatial dispersion when the infinite sheet is cut into various sizes and shapes at the microscopic scale. General considerations about the spatially dispersive anisotropic conductivity of graphene are used to select the conductivity response to be provided as input in a simulation of surface plasmons launched by the near field of a wire antenna, which is placed at sub-micrometric distances from a graphene micro-disk. The spatial dispersion of the graphene patch is shown to play a significant role not only in plasmon propagation free of external sources, but also in typical scanning probe microscopy configurations, recalling how a THz beam impinging on a metal atomic force microscope tip has been recently used to generate guided THz waves on graphene [1]. Our analysis shows how spatial dispersion affects the excitation strength, or coupling, between the field sources and the surface plasmons.

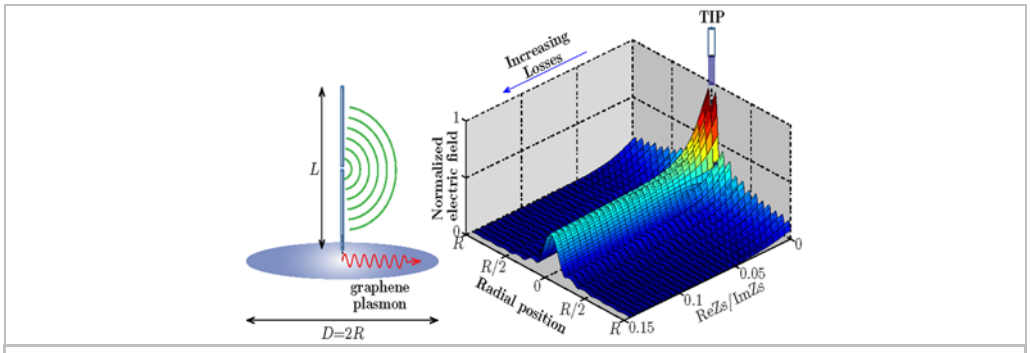

Figure 1: Left: wire antenna placed at sub-micrometric distance (L/200) from a graphene patch (left); Right: plasmon distribution (normalized electric field), with Im(Zs)=5000 Ohm, as a function of Re(Zs)/Im(Zs).

References

1. Low T, Avouris P, ACS Nano 8 (2), 1086-1101 (2014).

Assessment of the environmental pollution caused by natural and synthetic inorganic fibres: a TEM-SEM-EDS study

Elena Belluso[*], Silvana Capella[2]
[*]*Department of Earth Sciences; Interdip. Centre for Studies and other Toxic Particulates "G. Scansetti", University of Torino; CNR-Institute of Geosciences and Earth Resources, Torino Unit*
[2]*Department of Earth Sciences; Interdip. Centre for Studies and other Toxic Particulates "G. Scansetti", University of Torino*

Email: **elena.belluso@unito.it*
Keywords: inorganic fibers, environmental pollution, TEM-SEM-EDS study

Inorganic fibres is a term including both natural species (as asbestos in the case of minerals) and synthetic ones.
There is sufficient evidence for the noxiousness (and even carcinogenicity) to humans when high doses of several kinds of inorganic fibres penetrated in the respiratory organs (breathed fibres). Sometimes, other organs where fibres migrated from lungs become places of disease.
The correlation between exposures to high doses (of certain inorganic fibres) as in professional or para-professional environments and some pathologies is known since a long time [e.g. 1]. Currently the question is to understand if low dose exposure as in natural or certain anthropic outdoor environments also represent a potential risk for the same pathologies.
However, other variables make this issue very complicated. In fact the measurement of the airborne fibres in outdoor environment can vary day by day and through the same day in the same area according to meteorological conditions (e.g. wind, rain, humidity, dry weather) and to anthropic activities (e.g. vehicular passage, excavating). The outdoor areas are not a closed system and therefore the assessment of the background level and pollution situation about inorganic materials (and not only) is not very reliable.
A method to investigate the possible pollution situations caused by inorganic contaminants in the environment, even at low dosage, is to analyze the lung fiber burden (expressed as breathable fibrous mineral fraction) in animals. This approach has been used in a number of studies [e.g. 2, 3, and 4]. A non-experimental animal model (called "sentinel animal") [5] is used as an alternative to a human-based model. The sentinel animal model is preferred because some complicating factors such as occupational and para-occupational exposure as well as the habit of smoking do not occur in animals. Additionally, animal lung samples are more easily available in the large numbers necessary for sound statistical studies.

With this approach, by investigating the inorganic fibres present in the animal lungs, it is possible to evaluate which fibres are breathed (and not only present in air), the kind and extent of their background in air and the possible situations of pollution. By discerning, when feasible, natural and anthropogenic sources of inorganic fibre dispersion, it is possible to identify the pollution source for specific pollutants allowing stakeholders to carry out programs to reduce or eliminate dispersion.

To these targets, in collaboration with pathologist and veterinarians, we collected many lung samples of humans lived in various towns and animals lived in different areas of the Piedmont Region (NW Italy) with different anthropization level. The sample preparation for TEM-SEM-EDS investigation is based on chemical digestion and in detail described in two papers [6, 7].

In lungs of wild rats from Casale Monferrato (Alessandria district), an urban area where a big factory produced asbestos-cement materials until 25 years ago, many kinds of fibres have been detected. Some of them, such as asbestos crocidolite and amosite, vitreous silicates, metallic oxides, are correlated to air pollution from anthropogenic sources. Instead, tremolite asbestos are released from natural sources (e.g. rocks used for railway base). Chrysotile (Figure 1) can be airborne from both sources. In lungs of cows lived in grazing land and of wild animals lived in mountain the different kinds of detected inorganic fibres are related to the different environment of life. A large amount of titanium dioxide fibres are present in lungs of animals lived in a very strongly anthropized area (low Susa Valley).

The large amount of tremolite asbestos fibres detected in lungs of cows lived in a valley with a modest anthropization level are related to extended outcropping serpentinites bearing this kind of asbestos (Ala Valley).

In human lungs, the kind and amount of the detected fibres are related not only to the environment of life but they are also or mainly (in some cases) due to professional exposure. In addition, some life habits contribute to certain exposure. Synthetic inorganic fibres and asbestos fibres from anthropogenic sources (amosite, crocidolite) were detected in lungs from human lived in an anthropized area (low Susa Valley). In lungs from humans lived in an area where the anthropization level is low (Lanzo Valley), tremolite asbestos and chrysotile fibres were detected and correlated to dispersion in air from natural sources (i.e. the outcropping of serpentinites bearing this asbestos).

In the subjects professionally exposed to asbestos fibres, the very high lung burden of these fibres allowed to reveal pollution in the work environment. As an example, anthophyllite asbestos were detected in lungs of man working in a petrolchemical industry.

In conclusion, as it concerns the assessment of the pollution caused by natural and synthetic inorganic fibres, the investigation of the lung animals showed to be a very useful tool. Besides, this approach allows in many cases to distinguish between natural and anthropogenic sources of fibre air dispersion.

The investigation by SEM-EDS of inorganic pollutants extracted from biological samples is a very good technique useful to quantify the amount of inorganic pollutants as fibres, but to solve some ambiguous or uncertain identification (e.g., between chrysotile and asbestiform antigorite) TEM-EDS (by using electron diffraction) is essential: the two techniques have to be used as complementary.

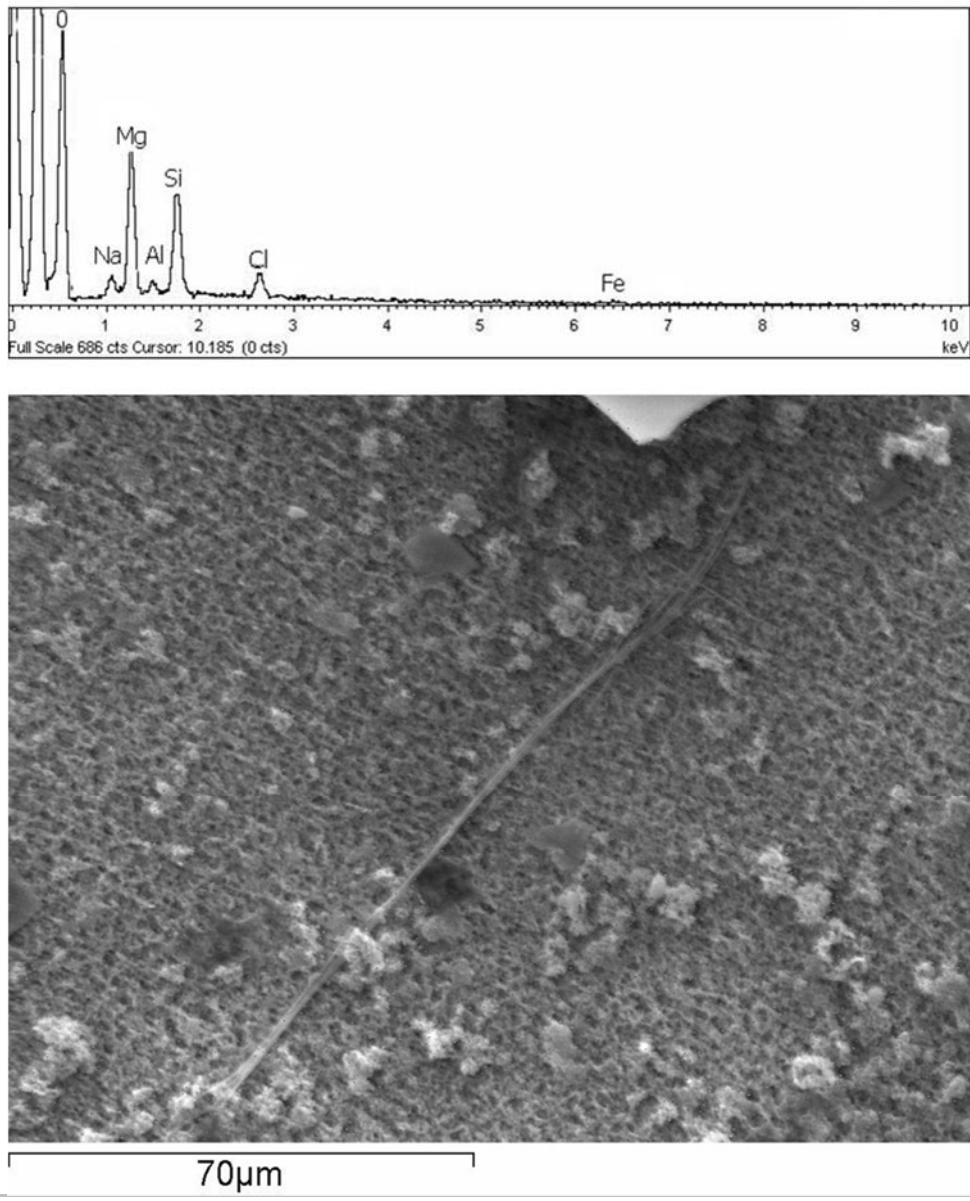

Figure 1: EDS-SEM spectrum and secondary SEM image of chrysotile fibers from wild rat lung asbestos. Na and Cl remained from the chemical digestion procedure.

References

1. R.F. Dodson, M.A. Atkinson, and J.L. Levin, Asbestos fiber length as related to potential pathogenicity: a critical review. Am. J. Ind. Med. 44, 291 (2003).
2. P. De Nardo, B. Bruni, L. Paoletti, R. Pasetto, and B. Siriani, Pulmunary fibre burden in sheep living in the Biancavilla area (Sicily): preliminary results. Sci. Total Environ. 325, 51 (2004).
3. P. Dumortier, L. Coplü, I. Broucke, S. Emri, T. Selcuk, V., P. De Vuyst, and I. Baris, Erionite bodies and fibres in bronchoalveolar lavage fluid (BALF) of residents from Tuzköy, Cappadocia, Turkey. Occup Environ Med. 58, 261 (2001).
4. E. Fornero, E. Belluso, S. Capella, and D. Bellis, Environmental exposure to asbestos and other inorganic fibres using animal lung model. Sci. Total Environ. 407, 1010 (2009).
5. National Research Council, Committee on Animals as Monitors of Environmental Health Hazards. Animals as Sentinels of environmental health hazards. Washington, DC: National Academy Press, 160, (1991)
6. E Belluso., D. Bellis, E. Fornero, S. Capella., G. Ferraris, S. Coverlizza, Assessment of inorganic fiber burden in biological samples by scanning electron microscopy-energy dispersive spectroscopy. Microchim. Acta, 155, 95 (2006).
7. R. Vigliaturo, *Microstructures of potentially harmful fibrous minerals*, PhD thesis, University of Torino, Italy (2015)

Material design of room temperature superconductors

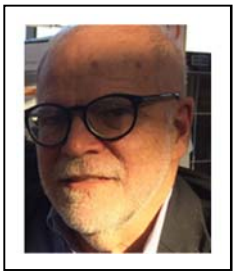

Antonio Bianconi
RICMASS, Rome International Center for Materials Science Superstripes, Via dei Sabelli 119A, 00185 Rome, Italy

Email: *antonio.bianconi@ricmass.eu*
Keywords: material design, Fano-Feshbach resonances, shape resonances

A road map for material design based for the synthesis of room temperature superconductors has been proposed in 1993 [1]. Recently it has been shown that superconductivity, with T_c= 203 K in pressurized sulfur hydride [2-4] is a practical realization of the proposed mechanism [1] based on the BPV (Bianconi-Perali-Valletta) theory [5,6]. In fact high temperature superconductivity in hydrides emerges where the pressure tunes the chemical potential of metallic H_3S around Lifshitz transitions where a shape resonance emerges between a first BCS condensate a second BCS-BEC condensate [2,3]. The complex electronic and structural landscape of the strongly correlated electronic structure of the quasi 2D copper oxide plane in cuprate superconductors, was first unveiled by XANES spectroscopy using synchrotron radiation [7-11]. It has provided first, the evidence of the orbital character of the itinerant holes (in the oxygen 2p orbital) [12] and second, the coexistence of two electronic states at the Fermi level: polarons [13] (where the ratio between the pairing interaction and the local Fermi energy is close to one) around the antinodal point and free quasi-particles around the nodal point of the Brillouin zone. Ordering of polarons forms the superstripes scenario [14] where inhomogeneous charge density wave (CDW) order coexists and competes with superconducting order [15]. A similar scenario occurs in iron-based superconductor where polarons in a shallow Fe($3dz^2$) orbital band, forming a very small Fermi surface, coexist with free quasi-particles in multiple large Fermi surfaces [16]. The two electronic components segregates forming a nanoscale phase separation, extending in the mesoscale, forming non Euclidean geometries favoring the superconducting phase [15]. Similar nanoscale phase separation scenarios have been observed recently in complex superconducting oxides [17,18] and functional systems [19,20]. The high temperature superconductivity mechanism in this particular two components scenario has been described by BPV theory [5,6] where the configuration interaction between first BCS pairs in the large Fermi surface and second pairs in the BCS-BEC condensate (made by polarons) gives a Fano Feshbach resonance, called shape resonance in superconducting gaps, which provides a contact pairing interaction, like well known Feshbach resonances in ultracold gases.

References

1. A. Bianconi, *"Process of increasing the critical temperature Tc of a Bulk Superconductor by Making Metal Heterostructures at the Atomic Limit"* US Patent **6,265,019** (2001)
2. A. Bianconi and T. Jarlborg *"Superconductivity above the lowest earth temperature in pressurized sulfur hydride."*EPL (Europhysics Letters) **112**, 37001 (2015) http://dx.doi.org/10.1209/0295-5075/112/37001.
3. A. Bianconi and T. Jarlborg, *"Lifshitz transitions and zero point lattice fluctuations in sulfur hydride showing near room temperature superconductivity"* Novel Superconducting Materials **1**, 37 (2015) http://dx.doi.org/10.1515/nsm-2015-0006.
4. T. Jarlborg and A. Bianconi, *"Breakdown of the Migdal approximation at Lifshitz transitions with giant zero-point motion in H_3S superconductor"* preprint arXiv:1509.07451 (2015).
5. A. Bianconi, A. Valletta, A. Perali, and N.L. Saini, *"High Tc superconductivity in a superlattice of quantum stripes"* Solid State Communications **102**, 369 (1997) http://dx.doi.org/10.1016/s0038-1098(97)00011-2.
6. A. Bianconi, *"Feshbach shape resonance in multiband superconductivity in heterostructures"* Journal of Superconductivity **18**, 625 (2005) http://dx.doi.org/10.1007/s10948-005-0047-5.
7. A. Bianconi, S. Doniach, and D. Lublin, *"X-ray Ca K edge of calcium adenosine triphosphate system and of simple Ca compunds"* Chemical Physics Letters **59**, 121 (1978) http://dx.doi.org/10.1016/0009-2614(78)85629-2.
8. J.Garcia, A. Bianconi, M. Benfatto, and C.R. Natoli, *"Coordination geometry of transition metal ions in dilute solutions by XANES"* Le Journal de Physique Colloques **47**, C8 49 (1986) http://dx.doi.org/10.1051/jphyscol:1986807.
9. D. Bazin, M. Benfatto, A. Bianconi, R.Clement, H. Dexpert, J. Galy, J. Garcia, P. Lagarde, P. Laggner, Y. Mathey, et al., *Synchrotron radiation in chemistry and biology 1*, vol. 145 (Springer, Berlin Heidelberg, 1988), ISBN 9783540183853 http://www.springer.com/us/book/9783540183853.
10. S. Della Longa, A. Soldatov, M. Pompa, and A. Bianconi *"Atomic and electronic structure probed by x-ray absorption spectroscopy: Full multiple scattering analysis with the G4XANES package"* Computational Materials Science **4**, 199 (1995) http://dx.doi.org/10.1016/0927-0256(95)00027-n.
11. A. Bianconi, S. Della Longa, C. Li, M. Pompa, A. Congiu-Castellano, D. Udron, A. Flank, and P. Lagarde, *"Linearly polarized Cu L3-edge x-ray-absorption near-edge structure of Bi2CaSr2Cu2O8"* Physical Review B **44**, 10126 (1991) http://dx.doi.org/10.1103/physrevb.44.10126.
12. A. Bianconi, A. Clozza, A. Congiu-Castellano, S. Della-Longa, M. De-Santis, A. Di-Cicco, K. Garg, P. Delogu, A. Gargano, R. Giorgi, et al., *"Experimental evidence of itinerant Cu(3d9)-Oxygen-hole many body configuration in the High-Tc superconductor YBa2Cu3O7"* International Journal of Modern Physics B (IJMPB) **1**, 853 (1987) http://www.worldscinet.com/ijmpb/01/0103n04/S0217979287001213.html.

13. A. Bianconi, M. Missori, H. Oyanagi, H. Yamaguchi, Y. Nishiara, and S. Della Longa, *"The measurement of the polaron size in the metallic phase of cuprate superconductors"* Europhysics Letters (EPL) **31**, 411 (1995) http://iopscience.iop.org/0295-5075/31/7/012.
14. A. Bianconi, "*Superstripes*" International Journal of Modern Physics B **14**, 3289 (2000), URL http://dx.doi.org/10.1142/S0217979200003769.
15. G. Campi, A. Bianconi, N. Poccia, G. Bianconi, L. Barba, G. Arrighetti, D. Innocenti, J. Karpinski, N.D. Zhigadlo, S.M. Kazakov, et al., *"Inhomogeneity of charge-density-wave order and quenched disorder in a high-Tc superconductor"* Nature **525**, 359 (2015) http://dx.doi.org/10.1038/nature14987.
16. R. Caivano, M. Fratini, N. Poccia, A. Ricci, A. Puri, Z.-A. Ren, X.-L. Dong, J. Yang, W. Lu, Z.-X. Zhao, et al., *"Feshbach resonance and mesoscopic phase separation near a quantum critical point in multiband FeAs-based superconductors"* Superconductor Science and Technology **22**, 014004 (2009) http://dx.doi.org/10.1088/0953-2048/22/1/014004.
17. P. Giraldo-Gallo, Y. Zhang, C. Parra, H.C. Manoharan, M.R. Beasley, T.H. Geballe, M.J. Kramer, and I.R. Fisher, "Stripe-like nanoscale structural phase separation in superconducting $BaPb_{1-x}Bi_xO_3$" Nature Communications **6**, 8231 (2015) http://dx.doi.org/10.1038/ncomms9231.
18. A.P. Menushenkov, A.V. Kuznetsov, K.V. Klementiev, and Kagan, "Fermi-Bose mixture in Ba(K) superconducting oxide BiO3" Journal of Superconductivity and Novel Magnetism pp. 1-5, (2015) http://dx.doi.org/10.1007/s10948-015-3295-z.
19. P. Falcaro, L. Malfatti and P. Innocenzi, *Water Droplets to Nanotechnology: A Journey Through Self-Assembly*, Royal Society of Chemistry (Cambridge, 2013).
20. P. Innocenzi, L. Malfatti, S. Costacurta, T. Kidchob, M. Piccinini and A. Marcelli, J. Phys. Chem. A **112,** 6512–6516 (2008).

Challenges in Material Development for Fusion Reactors and India's initiatives

Dhiraj Bora
Institute for Plasma Research, Bhat, Gandhinagar

Email: **dbora@ipr.res.in*
Keywords: ITER, fusion materials, plasma

Any attempt to develop new and cleaner sources of energy to meet the future global requirement is welcome. Therefore, it is attractive to think of having fusion as an alternate clean source of energy to contribute in the energy mix towards the second half of the century. Abundant availability of fuel, inherent safety, negligible radioactive waste and no greenhouse emissions are some of the advantages of this source. These advantages have driven the world fusion research programme since its inception.
The International Thermonuclear Experimental Reactor (ITER) has now moved into the construction phase at the Cadarache site in south of France. Large number of components have started arriving at site. ITER is an international collaboration of seven parties including India building the first FUSION SCIENCE EXPERIMENT capable of producing a self-sustaining fusion reaction, called "burning plasma". Unique features will be its ability to operate for long durations and at power levels ~500 MW sufficient to demonstrate the physics of the burning plasma in a power plant like environment. It will also serve as a test-bed for additional fusion power plant technologies.
Fusion can fulfill its promise of providing safe, economical and environmentally acceptable energy if material science and engineering can meet the challenging service requirements of a fusion power reactor. New Developments in Materials Science and Technology can help in achieving this goal. However, it presents many materials challenges including, high thermal heat flux, induced radioactivity, sputtering/blistering of plasma facing components, radiation damage, chemical compatibility etc..
Therefore, it is imperative to look for appropriate materials to satisfy the stringent requirements. All fusion developing countries have realized this need and started material development and benchmarking them against known materials. India has also started an ambitious fusion reactor relevant materials development programme.
This talk will discuss material development issues for fusion reactor and the Indian national scenario.

DNA wrapping around MWNTs and graphene: a SERS study

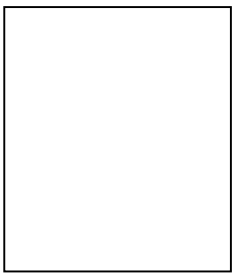

Sabina Botti[*,1], Stefano Gay[2], Susanna Laurenzi[3], Tomas Rindzevicius[4], Michael S. Schmidt[4], Alessandro Rufoloni[1], M. Gabriella Santonicola[5]
[1]*Department of Fusion and Technologies for Nuclear Safety and Security, ENEA Via E. Fermi, 27, 00044 Frascati, Italy*
[2]*Horiba Italia srl, Via L. Gaurico, 209, 00143 Rome, Italy*
[3]*Department of Astronautic, Electrical and Energy Engineering, Sapienza University of Rome, Via Salaria 851-881, 00138 Rome, Italy*
[4]*Department of Micro & Nanotechnology, Technical University of Denmark, Lyngby 2800, Denmark*
[5]*Department of Chemical Materials Environmental Engineering, Sapienza University of Rome, Via del Castro Laurenziano 7, 00161 Rome, Italy*

Email: **Sabina.Botti@enea.it*
Keywords: carbon nanotubes, graphene, Raman, SERS

In recent years, carbon nanostructure as nanotubes (CNTs) and graphene are at the centre of a significant research effort due to the strong scientific and technological interest because of their unique physical and chemical properties: large surface area, excellent thermal and electric conductivity, high electron transfer kinetics and strong mechanical strength. Recently, a great attention has been paid to the interaction of DNA with carbon-based nanostructures such as C_{60}, multiwalled-nanotubes (MWNTs), single-walled nanotubes (SWNTs) and graphene. The development of these studies is motivated by a wide spectrum of possible use of these materials e.g. as biosensors, drug delivery agents and diagnosis tools. In this work, we applied surface-enhanced Raman spectroscopy (SERS) to the study of DNA/MWNTs and DNA/graphene systems.
Since the discovery of the large Raman signal enhancement, occurring when a molecule is on or near a metallic nano-scale roughened substrate, SERS attracted a great interest in view of its possible applications [1-2]. It is widely recognized that the surface enhancement effect is based on the generation of an electromagnetic field at the surface of noble metals induced by the laser excitation. Although the electromagnetic mechanism is believed to be responsible of the main part of the enhancement, an additional enhancement is provided by the increase of polarisability of the adsorbed molecule, when a resonant charge transfer occurs between the metal and the adsorbate.
In our study, the carbon nanostructures were deposited as dilute dispersions on SERS active substrates with different morphologies.

Our investigation demonstrated that, since the SERS effect depends on the distance between the nanostructure and the adsorbed molecule, the Raman signal from the wrapped DNA or other molecules, deriving from functionalization/synthesis process and bound to the carbon surface, can be amplified.
We have previously investigated the wrapping of DNA double strands around the MWNTs, observing that the non-covalent interaction leads to the spectral shift of G line towards higher wavenumbers [3]. This finding indicates that the organic molecules are arranged among nanotubes leading to a debundling effect, which greatly enhances the MWNT solubility. Further, we studied the DNA-wrapping on graphene. Our findings indicate that the attachment of nucleotides to the graphene sheets occurs through hydrophobic interactions.

References

1. D.L. Jeanmaire, R.P. Van Duyne, Surface Raman Electrochemistry, J. Electroanal. Chem. 84, 1-20 (1977).
2. K. Kneipp, Y. Wang, R.R. Dasari, M.S. Feld, B.D. Gilbert, J. Janni, J.I. Steinfeld, Near-infrared surface-enhanced Raman scattering of trinitrotoluene on colloidal gold and silver, Spectrochimica Acta A 51, 2171 -2175 (1995).
3. S. Botti, S. Laurenzi, L. Mezi, A. Rufoloni, M. G. Santonicola, Surface-enhanced Raman spectroscopy characterisation of functionalised multi-walled carbon nanotubes, Phys. Chem. Chem. Phys. 17, 21373-21380 (2015).

Multifunctional composite systems based on biopolymers and natural fillers for food packaging

Ilaria Cacciotti[1,2*] and Francesca Nanni[2,3]
[1]*University of Rome "Niccolò Cusano", Via Don Carlo Gnocchi 3, 00166 Rome, Italy*
[2]*Italian Interuniversity Consortium on Materials Science and Technology (INSTM), Italy*
[3]*University of Rome "Tor Vergata", Department of Enterprise Engineering, Via del Politecnico 1, 00133 Rome, Italy*

Email: * *ilaria.cacciotti@unicusano.it*
Keywords: biopolymers, natural fillers, composites, thermal properties, mechanical properties, food packaging

In the food packaging sector biopolymers are considered as promising alternatives to the petrochemical-derived polymers, currently used in this sector, in order to reply to the urgent demand for a solution related to the environmental and ecological problems, associated to the non-biodegradable polymers.
However, the industrial application of these materials is avoided by their poor mechanical, thermal and barrier features. Thus, the formulation and design of multifunctional compostable systems with improved performances is strongly requested and motivated. To achieve this purpose, composite systems (both films and fibrous mats) based on compostable polymers (e.g. polylactide (PLA)) and natural fillers (e.g. diatomite, egg shell derived calcium carbonate, antioxidant and antimicrobial agents) were successfully prepared by solvent casting and electrospinning technique, respectively [1-3]. Suitable antioxidant/antimicrobial agents were stabilized by immobilization on particles surface via chemi/physi-sorption, in order to provide a double gas barrier effect, by mechanical action of the used particles that generate a tortuous path, preventing the gas flux, and oxygen scavenger activity of the used antioxidants. This novel approach allows not only to confer an enhanced barrier to gases but also to directly interact with the environment, extending shelf life and food quality.
The obtained systems were fully characterized in terms of microstructural, thermal, mechanical and antimicrobial properties by observation at scanning electron microscopy (SEM), X-ray diffraction, FT-IR spectroscopy measurements, differential scanning calorimetry (DSC), X-Ray diffraction (XRD) analysis, uniaxial tensile tests.

Defect-free composite films and electrospun mats consisted of randomly oriented fibers were obtained, showing the fillers good compatibility with the polymeric matrix. The addition of inorganic fillers allowed to improve the mechanical properties in terms of Young modulus and tensile strength, whereas the natural antioxidants usually act as plasticizers.

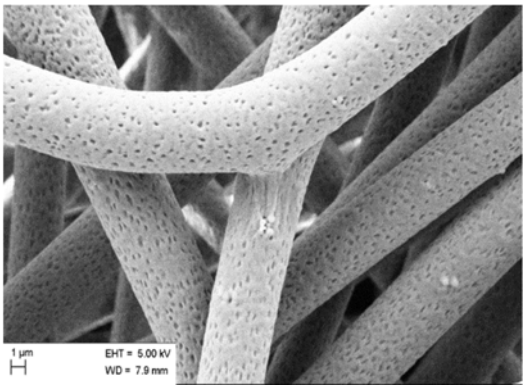

Figure 1: SEM micrograph of PLA fibers loaded with SiO_2 particles with physisorbed ascorbic acid.

References

1. I. Cacciotti, E. Fortunati, D. Puglia, J. M. Kenny, F. Nanni, Effect of silver nanoparticles and cellulose nanocrystals on electrospun poly(lactic) acid mats: morphology, thermal properties and mechanical behavior Carbohydrate Polymers 103, 22– 31 (2014).
2. I. Cacciotti, F. Nanni, Innovative composites based on compostable polymers and natural fillers for food packaging, Journal of Applied Biomaterials & Functional Materials (2015) *in press.*
3. I. Cacciotti, F. Nanni, Poly(lactic) acid fibers loaded with mesoporous silica for potential applications in the active food packaging, AIP (American Institute of Physics) Conference Proceedings (2016) *in press.*

Synthesis and systematic structural characterization of highly crystalline ZnO nanorods

C.R. Chandraiahgari,[*,1,3] G. De Bellis,[1,3] P. Ballirano,[2,3] S.K. Balijepalli,[4] S. Kaciulis,[4] L. Caneve,[5] F. Sarto,[5] and M.S. Sarto [*,1,3]

[1]*Department of Astronautics, Electrical and Energetics Engineering, Sapienza University of Rome, via Eudossiana 18, Rome 00184, Italy*

[2]*Department of Earth Sciences, Sapienza University of Rome, Piaz.le Aldo Moro 5, Rome 00185, Italy*

[3]*Research Center on Nanotechnology Applied to Engineering of Sapienza (CNIS), SNNLab, Sapienza University of Rome, Piaz.le Aldo Moro, 5, Rome 00185, Italy*

[4]*CNR - ISMN, P.O. Box 10, 00015 Monterotondo Stazione, Rome, Italy*

[5]*ENEA, Centro Ricerche Frascati, Via Enrico Fermi 45, Frascati 00044, Italy*

Email: **c.chandraiahgari@uniroma1.it, mariasabrina.sarto@uniroma1.it*

Keywords: Zinc Oxide nanorods-thermal decomposition method-XPS-PL

In the present work, we present a cost effective method for the mass production of high-purity ZnO nanorods (NRs) with uniform size distribution, based on the combination of thermal decomposition of zinc acetate dihydrate and probe sonication in acetone. The quality of the produced ZnO NRs, (which already showed antimicrobial properties in a previous study [1]) is assessed through various characterization techniques including field-emission scanning electron microscopy (FE-SEM), X-ray diffraction (XRD), transmission electron microscopy (TEM), X-ray photoelectron spectroscopy (XPS), and photo-luminescence spectroscopy (PL) and validated by comparison with ZnO microrods (MRs) and ZnO-nanoparticles (NPs). ZnO-NRs were synthesized through the thermal decomposition method, whereas ZnO MRs and ZNO NPs were synthesized through solvo-thermal methods [2]. Samples for morphological, structural, chemical composition and optical analyses were produced by dispersing the nanostructures in acetone by probe sonication and drop casting onto silicon substrates followed by drying at 120 °C for 30 min. The detailed analysis using FE-SEM and PL is shown in Fig.1 indicated that the produced ZnO nanostructures are chemically pure, high crystallographic quality and with excellent luminescence properties. It has also been demonstrated that the morphology of ZnO nanostructures can be tailored by controlling the process parameters [2]. Further, effect of probe sonication is one such process parameter was also being investigated using two different sonication cycles; (i) A short sonication (SS), having the scope of uniformly dispersing ZnO-NRs, without altering their initial diameter and length (NR2S); (ii) A long sonication

(LS) having the scope of chopping the longest nanowires in order to produce ZnO-NRs powder with uniform size in lengths (NR2L).

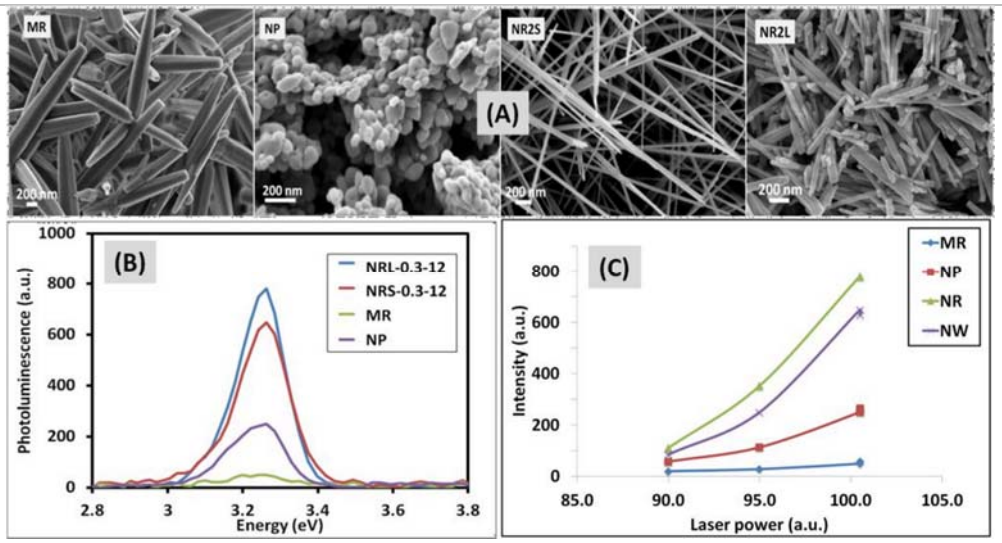

Figure 1: (A) FE-SEM images of MR, NP, NR2S and NR2L (B) PL band gap emission at 380 nm using laser power 1300 W/m^2 and (C) peak PL intensity of all the four types of ZnO nanostructures.

It resulted out that neither LS nor the SS does not affect diameter, purity and PL of the 1D nanostructures, but LS chops the longer rods and enables to obtain ZnO-NRs with a uniform distribution of diameters and lengths apart from the fact that it induces the surface oxygen defects. Hence, the possibility to control the ZnO-NRs morphology, combined with a cost-effective synthesis route, makes these nanostructures suitable for use as filler in a polymeric matrix for the development of new piezoresistive and piezoelectric materials [3].

References

1. I. Rago, C.R. Chandraiahgari, M.P. Bracciale, G. De Bellis, E. Zanni, M. Cestelli Guidi, D. Sali, A. Broggi, C. Palleschi, M.S. Sarto, D. Uccelletti, Zinc oxide microrods and nanorods: different antibacterial activity and their mode of action against Gram-positive bacteria. RSC Advances 99, 4 (2014).
2. C.R. Chandraiahgari, G. De Bellis, P. Ballirano, S.K. Balijepalli, S. Kaciulis, L. Caneve, F. Sarto, M.S. Sarto. Synthesis and characterization of ZnO nanorods with narrow size distribution. RSC Advances 62, 5 (2015).
3. C.R. Chandraiahgari, G. De Bellis, A. Martinelli, A. Bakry, A. Tamburrano, M.S. Sarto. Nanofiller Induced Electroactive Phase formation in Solution Derived Poly(Vinylidene Fluoride) Polymer Composites IEEE Nano 2015, Rome.

Nanoparticles for cement building materials

M.C. Dalconi[1*], G. Ferrari[2], V. Russo[2], G. Artioli[1], L. Valentini[1], M. Favero[1], M. Secco[1]
[1]*Department of Geosciences and CIRCe Centre, University of Padova, Padova I-35131, Italy*
[2]*Research & Development Laboratory, Mapei SpA, Milano I-20158, Italy*

Email: **mariachiara.dalconi@unipd.it*
Keywords: C-S-H nanoparticles, cement, hardening accelerator

A new accelerating additive for cement mixtures based on nanoparticles of polymeric metal silicate hydrates has been produced and characterized. The additive contributes in developing high early strength of hydrated cement paste and represents a new development in the field of concrete admixtures, based on the application of nanotechnology. The new additive consists of polysilicate nanoparticles, characterized by low Ca/Si ratio and high polymerization degree, acting as a catalyst for the crystallization of C-S-H (calcium-silicate-hydrate). C-S-H is the major volume phase in the matrix of portland cement concrete and plays the most critical role in strength development and durability of cement. The polymeric nature of the new silicate was demonstrated by Gel permeation Chromatography (GPC) and the nanoscale atomic ordering was investigated by XRPD, HR-TEM and ^{29}Si-NMR. Hydration kinetics of cement pastes containing different dosages of the new admixture were studied by in situ XRPD and compared to equivalent admixture-free cement pastes. The data confirmed that the new silicate hydrate accelerates the dissolution of alite (the main portland clinker phase) and the formation of C-S-H.
Synchrotron-based diffraction computed micro-tomography (XRD-CT) was also applied to visualize the 3D crystal phase evolution in the cement paste, thus enabling the direct analysis of the nucleation mechanisms and the microstructural developments. The data confirmed that the new silicate hydrates truly enhance the silicate network by inducing homogeneous nucleation and the rapid development of a diffuse interconnection between the hydration products.
Concrete mechanical tests confirmed a beneficial effect of the admixture on early strength development. The precipitation of C-S-H induced by the new polymeric silicate hydrates in the capillary porosity refines the microstructure of the cement paste, it reduces the water permeability and it improves the durability of concrete structures. In the precast industry, the strong acceleration of hydration rate achievable with this additive could reduce or even eliminate the steam curing, with considerable energy savings and consequent reduction of CO_2 emissions. In the ready-mixed concrete, the accelerated strength development permits an increase of productivity and a reduction of production cycles.

Synthesis and applications of nanoparticles by laser pyrolysis

Rosaria D'Amato[*1], Flaminia Rondino[1], Gaetano Terranova[1], Serena Gagliardi[2], Mauro Falconieri[2]
[1]ENEA, Department of Fusion and Technologies for Nuclear Safety and Security, TECFIS-MNF, CR Frascati, via Enrico Fermi 45, Frascati (Rome), Italy
[2]ENEA, Department of Fusion and Technologies for Nuclear Safety and Security, TECFIS, CR Casaccia, via Anguillarese 301, Rome, Italy

Email: **rosaria.damato@enea.it*
Keywords: laser pyrolysis, nanopowders, nanofluid, nanocomposites, porous electrode

Laser pyrolysis of gaseous molecules is a versatile method of synthesizing a wide variety of nanopowders. In this synthesis technique, the condensable products result from laser induced chemical reactions at the crossing point of the laser beam with the molecular flow of gas or vapour–phase precursors.
The physical and chemical properties of the nanoparticles (NPs) depend directly on the process parameters, such as flame temperature and residence time, that are determined by the nature and the flow rate of reagents and sensitizers, the reactor pressure and the laser power.
Using a CW CO_2 laser, we have synthesised Si, SiC, SiO_2, TiO_2 and C NPs of high purity, selected dimensions from 5 to 80 nm, different chemical characteristics and productivity up to 80g/h.
The produced nanopowders were characterized and tested for different applications: development of nanofluid coolants based on SiC and TiO_2 NPs; synthesis of nanocomposites for cultural heritage preservation by utilization of SiO_2 and TiO_2 NPs as fillers; production of TiO_2-based porous electrodes for photoelectrochemical devices.
The thermal conductivity enhancement in dispersions based on TiO_2 NPs was investigated using an optical technique known as forced Rayleigh light scattering. Measurements on these systems exhibited a linear relation between the thermal conductivity enhancement and the nanoparticle volume fractions with a maximum increase of 6% with respect to the base fluid ethanol at 0.6% TiO_2 content.
Nanocomposites constituted by SiO_2 and TiO_2 NPs dispersed in commercial polymeric matrices (acrylic polymer and silicon-based resin) were investigated as protective coatings for artistic stones. The results show that some properties of conservation materials can be improved by the presences of NPs because they induce substantial changes of surface morphology of the coating layer and reduce the physical damage observed during artificial weathering.

TiO_2 NPs were also used for energy applications in photoelectrochemical devices. In particular porous electrodes using pure and N-doped nanopowders were prepared by screen-printing and characterized. The electron transport in porous electrodes was evaluated by a photoelectrochemical method, determining the value of the electron diffusion length L_{diff}. The results show that L_{diff} in electrodes containing pyrolytic NPs compares well with that of the commercial standard. Taking the visible absorption of NPs as an estimate of the amount of the incorporated N, L_{diff} resulted to decrease with increasing N content.

Characterization of Aluminum Zinc Oxide Thin Films deposited by Solution Synthesis & Solution Combustion Synthesis

Ivan Davoli, Fabio De Matteis, Massimiliano Lucci, Sana Ullah
Dipartimento di Fisica, Corso di Scienza dei Materiali, Università di Roma "Tor Vergata", Via della Ricerca Scientifica, snc. 00133 Roma, Italy

Email: *ivan.davoli@uniroma2.it*
Keywords: transparent conducting oxide, optical transparency, electrical characterization

Transparent conducting oxides (TCO) are at the core of modern optoelectronic technologies particularly thin film photovoltaic and flat panel displays. Indium Tin Oxide (ITO) currently the best available TCO held 93% of the market until 2012 [1]. ITO thin films with transparency more than 90% and resistivity values in the range 10^{-4} Ω-cm are obtained mostly through vacuum-based techniques and chemical composition of these ITO films is usually 90% In and 8-10% Tin. Ever increasing demands of industry, scarcity of the indium material element and complex vacuum deposition systems all combine to increase the cost of end products. For a likely alternative among many material combinations as TCOs, zinc oxide (ZnO) a non-toxic, abundant and cheap material is getting exceeding popularity in the research and scientific community over the recent years.

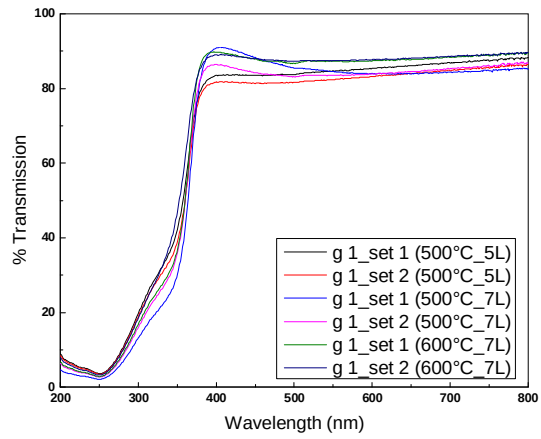

Fig. 1: Optical transmission obtained for Al:ZnO films with 5 & 7 layers with 1 mol% doping concentration with RTA at 500°C and 600°C. Details in the inset.

In addition to this, it is pertinent to mention that resistivity values for ITO remain almost same over the years while resistivity values for doped ZnO are decreasing continuously. This fact adds further to make ZnO stronger candidate for investigations in an effort to replace ITO. Pure ZnO however, is an unstable material due to adsorption of atmospheric oxygen, which decreases the conductivity and modifies its surface morphology. Higher valence elements of group-III (B, Al, Ga, ln) can be added to increase the conductivity by replacement of Zn^{2+} ions acting as effective donors and are used to enhance the electrical properties of doped-ZnO films [2-4].

Vacuum-based deposition methods offer the advantages of the highest conductivity and transparency, but the high cost of production involving complex systems and large-area device uniformity restrict its area of applications. Non-vacuum solution-based chemical deposition techniques offer the advantages of greatly reduced cost, compositional control, ease of fabrication and scalability. Solution combustion synthesis (SCS) has recently been exploited for production of transparent and conducting films for application in transistors. SCS offers additional advantage that heats are locally generated to convert reactants into desired oxides without the need of external heating source making possible the production of TCOs at low energy costs.

References

1. Ümit Özgür, Daniel Hofstetter, Hadis Morkoc, ZnO Devices and Applications: A Review of Current Status and Future Prospects, Proceedings of the IEEE 98, 7, 1255-1268 (2010)
2. Hyung Jun Cho, Sung Uk Lee, Byungyou Hong, Yong Deok Shin, Jin Young Ju, Hee Dong Kim, Mungi Park, Won Seok Choi, The effect of annealing on Al-doped ZnO films deposited by RF magnetron sputtering method for transparent electrodes, Thin Solid Films 518, 2941-2944 (2010)
3. Yung-Chen Cheng, Effects of post-deposition rapid thermal annealing on aluminum-doped ZnO thin films grown by atomic layer deposition, Applied Surface Science 258, 604-607 (2011)
4. Deok-Kyu Kim, Hong Bae Kim, The reason of degradation in electrical properties of ZnO:Al thin films annealed with various post-annealing temperatures, Current Applied Physics 13, 2001-2004 (2013)

Oxidation processes of Fe-amphiboles at high temperature

Alessandro D'Elia[1], Salvatore Macis[1], Giannantonio Cibin[2], Giancarlo Della Ventura[3], Augusto Marcelli[4], Umberto Susta[3]
[1]*Department of Mathematics and Physics Università di Roma Tre, Via della Vasca Navale 84, 00146, Rome, Italy*
[2]*Diamond Light Source, Harwell Science and Innovation Campus, OX11 0DE, Didcot, Oxfordshire, UK*
[3]*Department of Science Università di Roma Tre, Largo S. L. Murialdo 1, 00146 Roma*
[4]*Istituto Nazionale di Fisica Nucleare, Laboratori Nazionali di Frascati, 00044 Frascati, Italy*

Email: *ale9149@gmail.com*
Keywords: deprotonation, XRD, XAS pre-edge, amphiboles, crystal structure

Fe-bearing hydroxyl silicates are known to dehydrate at HT through a mechanism whereby the proton loss is related to the simultaneous oxidation of ferrous iron. The process has been studied in details during the 1960' because of the increasing technical interest for the capacity of fibrous amphibole silicates (e.g., "crocidolites") as heat-resistant materials. According to several authors [1] the whole process occurs substantially at the mineral surface. The reaction can be expressed as $4\ ^{[M1,3]}Fe^{2+} + 4\ ^{[O3]}OH + O_2 = 4\ ^{[M1,3]}Fe^{3+} + 4\ ^{[O3]}O^{2-} + 2\ H_2O$. In this reaction, ferrous iron at the M(1,3) OH-coordinated polyhedra oxidizes to ferric iron, the local charge balance being restored by a loss of hydrogen at the anionic O3 site while H_2 is removed as water molecules by means of atmospheric oxygen. The process is fed by a continuous diffusion of hydroxyl ions and electrons from the crystal core to the surface. There is evidence that the process produces a significant increase of the electrical conductivity of the amphibole, a feature that may have significant implications in geophysics [2]. In this work we monitored the evolution of the Fe^{3+}/Fe^{2+} ratio in a synthetic amphibole [3] during the heating experiments, by *in situ* X-ray absorption coupled with X-ray diffraction. Measurements have been performed up to 750° C at beamline B18 at the Diamond Light Source synchrotron radiation facility, at the energy of 8048 eV. XAS experiments [4,5] at the Fe K-edge have been also performed vs. temperature. The analysis of the pre-edge features of the Fe K-edge has been processed with the Athena software. The signal of the edge has been removed trough a background curve, and the pre-edge has been modeled by using three Voigt-shaped components. The energy centroid of all peaks has to be the same in all spectra [6]. Two of these peaks were assigned to the Fe^{+2} contribution and the third one to the Fe^{+3} contribution. The area ratio of

the fitted peaks was plotted vs. temperature to monitor the relative change in Fe^{+3} and Fe^{+2} generated by the deprotonation process. Refinement of the X-ray diffraction patterns, collected simultaneously to the Fe X-ray absorption spectra, was performed to characterize the structural modification as a function of the temperature. All cell parameter (a, b, c and the monoclinic β angle) were irreversibly modified during the heating experiment. In particular, a, b, c increase and β decreases in the initial stage of the thermal treatment, as a response to the thermal expansion. Around 300° C an abrupt drop of cell edges due to the deprotonation process was observed (see Fig. 1). Interestingly, as already observed by [2] using single-crystal XRD, in the same range there is an anomalous increase in the β parameter, suggesting that a structural adjustment, consisting of a chain sliding, is need to compensate for the relative dimensional modification of the structural (tetrahedral vs. octahedra) moduli. The mechanism of the transition remains open and additional work is required to clarify these complex processes [7].

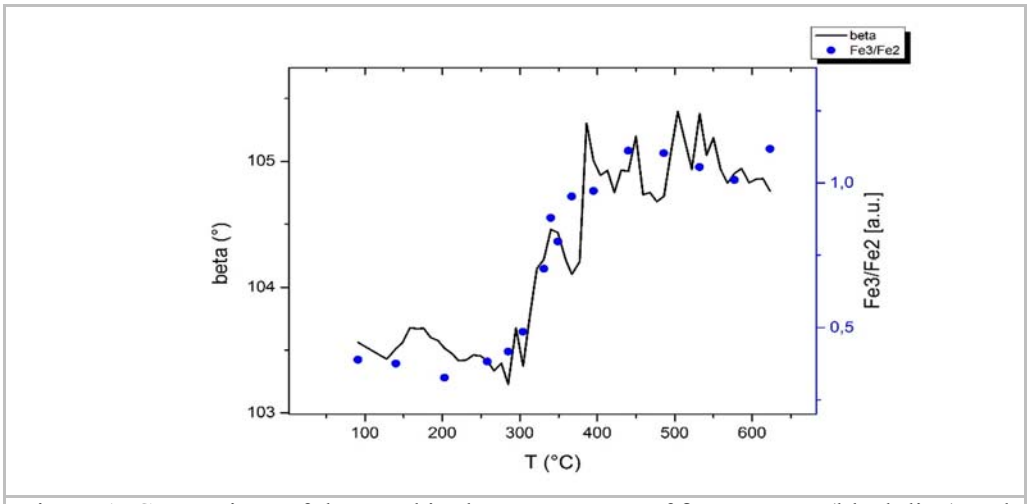

Figure 1: Comparison of the trend in the temperature of β parameter (black line) and the pre-edge peaks ratio (blue dots).

References

1. W.E. Addison J.H. Sharp, A mechanism for the oxidation of ferrous iron in hydroxylatedsilicates, Meeting of the Clay Minerals Group of the Mineralogical Society, Leeds 73-79 (1962)
2. R. Oberti, M. Boiocchi M. Zema G. Della Ventura, Synthetic potassic-ferro-richterite: 1. Composition, crystal-structure and HT behavior by in operando single-crystal X-ray diffraction. Canadian Mineralogist (2015) in press
3. Wang, D., Guo, Y., Yu, Y., Karato, S., Electrical condictivity of amphibole-bearing rocks: influence of dehydration, Contrib. Miner. Petr. 164, 17-25 (2012)

4. J. Garcia, M. Benfatto, C.R. Natoli, A. Bianconi, I. Davoli and A. Marcelli, Solid State Commun. 58, 595-599 (1986)
5. Z.Y. Wu, A. Marcelli, A. Mottana, G. Giuli, E. Paris and F. Seifert, Phys. Rev. B 54, 2976 (1996)
6. C. Bonadiman, S. Nazzareni, M. Coltorti, P. Comodi, G. Giuli, B. Faccini, Crystal chemistry of amphiboles: implications for oxygen fugacity and water activity in lithospheric mantle beneath Victoria Land Antarctica, Contrib. Miner. Petr. 167, 984 (2014)
7. G. Campi, et al., Inhomogeneity of charge-density-wave order and quenched disorder in a high-Tc superconductor, Nature 525, 359-362 (2015)

A new device for mobile monitoring of particulate matter. Preliminary result in an urban environment

Fernando Gozzi [1,2,*], Giancarlo Della Ventura [1,2], Augusto Marcelli [2,3]
[1]*Universita' degli Studi di Roma Tre, Dipartimento di Scienze Geologiche, Largo San L. Murialdo 1, 00146 Roma, Italy*
[2]*INFN - Laboratori Nazionali di Frascati, Via E. Fermi 40, 00044 Frascati, Italy*
[3]*RICMASS, Via dei Sabelli 119A, 00185 Rome, Italy*

Email **gozzifernando@gmail.com*
Keywords: particulate matter; air quality; mobile monitoring

Introduction

Particulate matter (PM) is a complex mixture of solid and liquid particles suspended in a gas phase that can be emitted by natural and anthropogenic sources. PM pollution has a considerable socio-economic impact, affecting public health, environment and climate. The finest the particles, the greater is the health risk. In particular, it has been demonstrated that ultrafine particles (UFP), i.e. particles with nanoscale size (<100 nm in diameter), are more effective in inducing respiratory diseases than larger particles with similar composition (e.g., Renwick et al., 2004). In this scenario, PM monitoring and characterization are fundamental aspects of this problem and, in the future, a great advancement is expected with the development of modern mobile instruments that integrate several and different quantitative and qualitative measurements (Gozzi et al., 2015a; Gozzi et al., 2015b). Nowadays, air quality is typically monitored by national environmental agencies through measurement of pollutants concentration at fixed stations and large and accurate databanks are available for statistical analysis. The position of the fixed sampling stations is chosen on the basis of well-assessed criteria: type of area, representativeness, exposure to atmospheric agents, etc., although limitations regarding the reliability of fixed PM stations exist. We present here the first data obtained with a novel device for PM mobile monitoring that we designed recently in the frame of the MIAMI (*Monitoraggio dell'Inquinamento Atmosferico della Montagna Italiana*) project. Preliminary tests using this compact prototype, installed on a car, have been performed in the suburb of Rome (Italy), under various meteorological and vehicular traffic conditions. The sampled materials have been characterized by means of Scanning Electron Microscope at the Laboratori Nazionali di Frascati of the INFN.

Device description

The device is equipped with a microcontroller, environmental sensors and a communication module. The device can be adapted to different means of transport (e.g., car, van, bicycle, bike, tram) by varying the dimension and the shape of the inlet system. It can monitor in real-time the mass concentration of Total Suspended Particles (TSP) and Volatile Organic Compounds (VOC). A set of sensors probing the main meteorological parameters (i.e., temperature, relative humidity, pressure) is integrated. The device communicates in real-time with a smartphone through Bluetooth® and can be managed by a dedicated applet for Android® and iOS®. All data are also associated with positioning information provided by the smartphone GPS. At the end of each run, data are saved on a single file and can be downloaded on the smartphone memory or other supports. Moreover, the device samples the TSP on a polycarbonate filter for further morphological and chemical analysis. The device can be also used for permanent indoor air quality monitoring (e.g., public premises, schools, offices, etc.).

Preliminar test and future developments

Preliminar tests were conducted in the metropolitan area of Roma, Italy. The concentration of TSP and VOCs, and environmental data were sampled with a temporal resolution of 1 s. In fig. 2 is reported the TSP concentrations measured along the route of the test, and the variation of the environmental data vs. time.

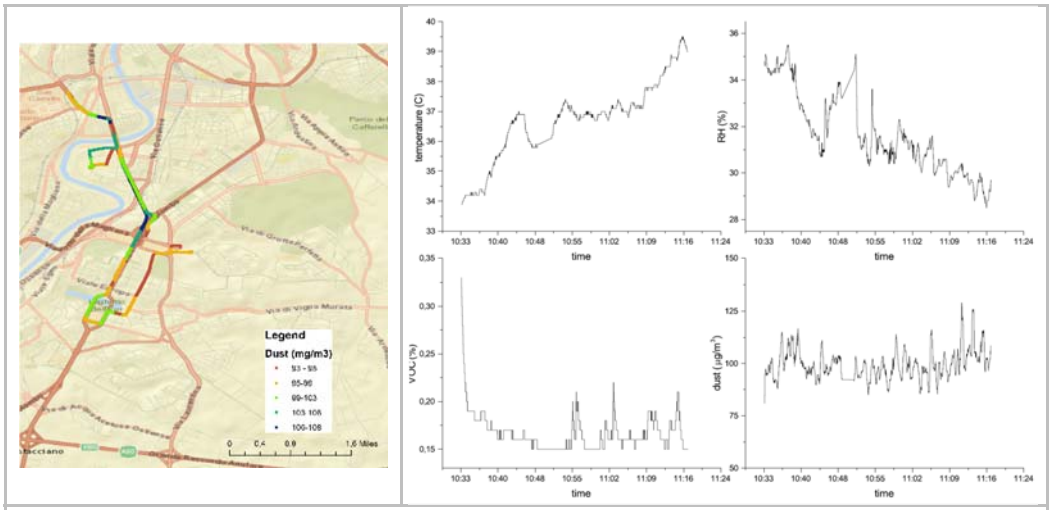

Fig. 1. Left: TSP variation along the route of the test, conducted in the urban area of Rome. Right: temporal variation of TSP, VOCs, temperature and RH measured during the test.

The sampled TSPs were analyzed manually by means of a electron-microscope coupled with energy dispersive X-ray analysis. An example of SEM analysis is

reported in Fig. 2. A further development of the device is the integration of a sensor to monitor the concentrations of UFP.

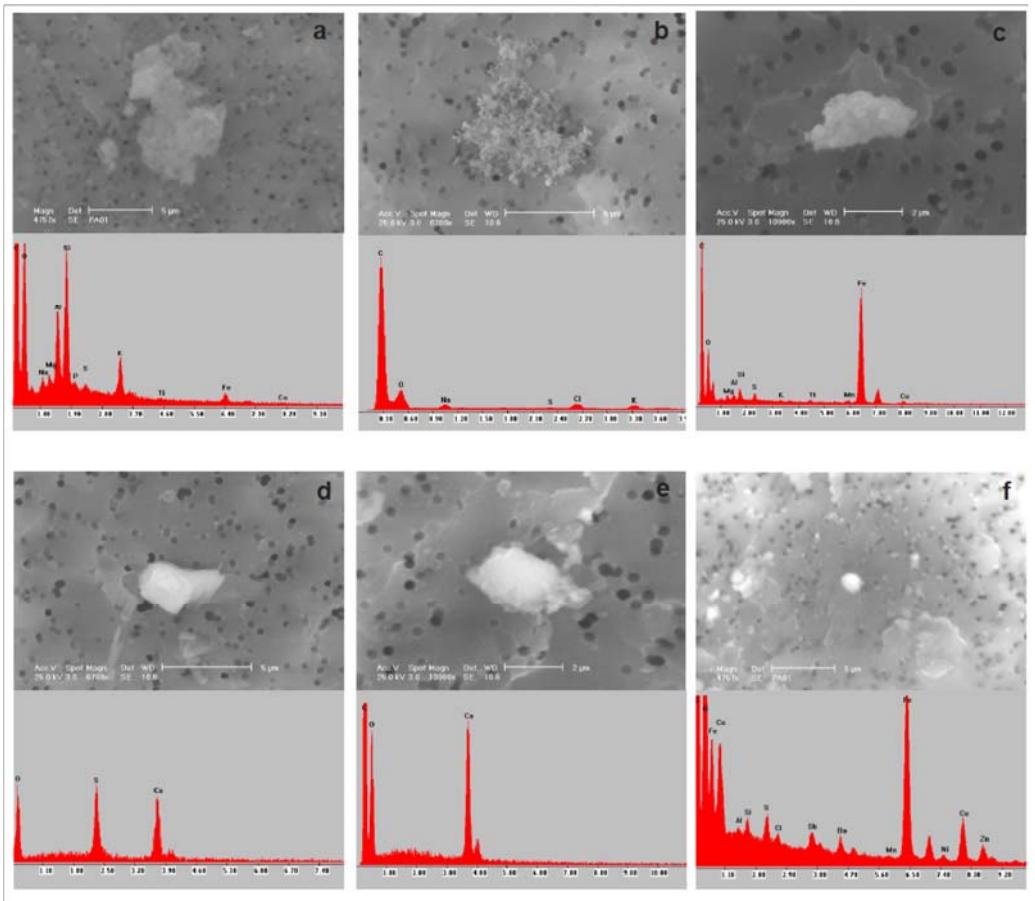

Fig. 2. Typical SEM photomicrographs and EDX spectra of different airborne particles sampled in the Rome urban area; a) terrigenous particle; b) soot aggregate; c) iron-oxide particle; d) gypsum crystal; e) carbonate particle; f) automotive brake wear particles.

References

1. F. Gozzi, G. Della Ventura, A. Marcelli. Mobile monitoring of particulate matter: existing methods and future perspectives. Atmospheric Pollution Research, 10.1016/j.apr.2015.09.007 (2015)
2. Renwick, L.C., Brown, D., Clouter, A., Donaldson, K., Increased inflammation and altered macrophage chemotactic response caused by two ultrafine particle type. Occup. Envir. Med. 61, 442-447 (2004).
3. F. Gozzi, G. Della Ventura, A. Marcelli, F. Lucci. Pollution hazards from particulate matter: state of the art and perspectives for PM monitoring, submit. (2015)

Characterization and properties of Portland cement incorporating iron nanoparticles

Fernando Gozzi [1,2,*], Giancarlo Della Ventura [1,2], Augusto Marcelli [2,3], Daniele Di Gioacchino [2], Fabio Bellatreccia[1], Giuliano Buonomo[1]
[1]*Universita' degli Studi di Roma Tre, Dipartimento di Scienze Geologiche, Largo San L. Murialdo 1, 00146 Roma, Italy*
[2]*INFN - Laboratori Nazionali di Frascati, Via E. Fermi 40, 00044 Frascati, Italy*
[3]*RICMASS, Via dei Sabelli 119A, 00185 Rome, Italy*

Email: **gozzifernando@gmail.com*
Keywords: nanoparticles; concrete; cement; thermal properties

The incorporation of nanoparticles (e.g., SiO_2, Al_2O_3, Fe_2O_3) into cement composites has emerged as a promising research field. It is known that concrete containing iron nanoparticles presents improved mechanical properties, e.g. increasing levels of compressive and flexural strength (Li et al., 2004), but few data are available on the variation of the electrical and thermal properties. Here we present preliminary data of our study on the electrical, and thermal properties of Portland cement doped with iron nanoparticles (Balasubramanian et al., 2014).
The electrical resistivity was calculated on the basis of measurements of electrical resistance (Tripodi, 2000, 2003, 2009). The measurements were realized using the 4Pt electrodes configuration (see McCarter et al., 2009). The electrical resistivity was calculated to be 1.8 kΩ·m and 1.6 kΩ·m for Portland cement and Portland cement doped with 10% nanoparticle, respectively.
The thermal conductivity was measured heating the cement samples by a resistor and measuring the ΔT between two ends placed at fixed distance (Fig. 1). The measure was stopped at achievement of steady state condition (i.e., no temperature variation).
The thermal conductivity is given by

$$\lambda = \frac{P\,L}{A\,\Delta T}$$

where $\Delta Q/\Delta t$ is the amount of heat transferred per unit time, ΔT is the temperature difference between the ends, Δx is the distance between the ends, A is the cross-sectional surface area, λ is the material's conductivity.

The thermal conductivity was calculated to be 0.58 W/m·K and 0.49 W/m·K for Portland cement and Portland cement doped with 10% nanoparticle, respectively.

Fig. 1. Experimental set up for the measurements of the thermal conductivity.

This research may offer in addition to practical applications really a new insight into the complexity of nanoscale phenomena in mesoscale systems that require modern and sophisticated approaches to be fully understood (Campi, 2015).

References

1. H. Li, H.G. Xiao, J. Yuan, and J. Ou, Microstructure of cement mortar with nano-particles, Composites Part B: Engineering 35(2), 185-189 (2004).
2. W.J. McCarter, G. Starrs, S. Kandasami, R. Jones, and M. Chrisp, Electrode configurations for resistivity measurements on concrete, ACI Materials J. 106(3) (2009)
3. C. Balasubramanian, B. Joseph, P. Gupta, N.L. Saini, S. Mukherjee, D. Di Gioacchino and A. Marcelli, X-ray absorption spectroscopy characterization of iron-oxide nanoparticles synthesized by high temperature plasma processing, J. Elect. Spectr. Rel. Phenom. 196, 125-129 (2014)
4. G. Campi, et al., Inhomogeneity of charge-density-wave order and quenched disorder in a high-Tc superconductor, Nature 525, 359-362 (2015)
5. P. Tripodi, M.C.H. McKubre, F.L. Tanzella, P.A. Honnor, D. Di Gioacchino, et al., Temperature coefficient of resistivity at compositions approaching PdH, Physics Letters A 276 (1), 122-126 (2000)
6. P. Tripodi, D. Di Gioacchino, R. Borelli, J.D. Vinko, Possibility of high temperature superconducting phases in PdH, Physica C: Superconductivity 388, 571-572 (2003)
7. P. Tripodi, D. Di Gioacchino, J.D. Vinko, AC electrical resistance measurements of PdH_x samples versus composition x, J. All. Comp. 486, 55-59 (2009)

SEI growth and characterization by soft XAS in nanostructured Li batteries anodes

R. Gunnella[1], F. Nobili[2], A. Witkowska[3], S. Rezvani[1] and A. Di Cicco[1]
[1]Physics Division, School of Science and Technology, University of Camerino, 62032 Camerino (MC) Italy
[2]Chemistry Division, School of Science and Technology, University of Camerino, 62032 Camerino (MC) Italy

Email: *roberto.gunnella@unicam.it*
Keywords: Electrochemistry, XAS, nanoparticles

Solid electrolyte interface (SEI)[1] formation during batteries charge and discharge cycles was monitored at the atomic level as a function of time by using XAS [2], a chemical sensitive and short range probe, and by selectively tuning the detection depth by collecting electrons, total and partial yield, and photon fluorescence yield. X-ray absorption experiments have been conceived and realized to study the modification of the signals related to the various atomic species in ZFO-C electrodes selected at different states of charge during the first Li insertion process and thickness and composition of the SEI layer with anisotropic growth depending on the nanostructuration of the anodes and on their characteristic coating.

Introduction

$ZnFe_2O_4$ Li-ion batteries (LIBs) represent a reliable, affordable, and safe energy storage technology for use in portable application. However, performances and durability of the cells are strongly influenced by the characteristics of the solid electrolyte interphase (SEI), [1–3] Materials and methods: Composite electrodes were prepared by using Na-carboxym-ethylcellulose (CMC, Sigma-Aldrich) binder dissolved in deionized water (5:95 wt/wt). ZFO and SuperP carbon (MMM-Carbon), previously mixed and ground in an agate mortar were added to the binder solution resulting in a slurry with a ZFO:SuperP:CMC composition equal to 75:20:5 (mass ratio) and electrodes preparation as reported in ref. [4].

Figure 1 reports the equilibrium capacity (Q) versus OCV (E) profile as acquired by GITT. The profile is consistent with previous findings [5] and describes the Li uptake by ZFO active material, leading to LiZn, Fe, Li_2O as final products of the mixed conversion/alloying processes, superimpose to the irreversible Li storage by the carbonaceous matrix, which leads to the formation of the SEI upon electrode surface. The discharge capacity is about 1200 mAh g^{-1}

which allows to estimate about 20% first-cycle capacity loss for irreversible processes with respect to the nominal reversible capacity (1000 mAh g^{-1}).
Specific points in Figure 1, marked as (A) (B), (C), (D), correspond to capacity and potential values of the electrodes that later underwent ex situ XAS characterization. The (A) point corresponds to the fresh electrode.

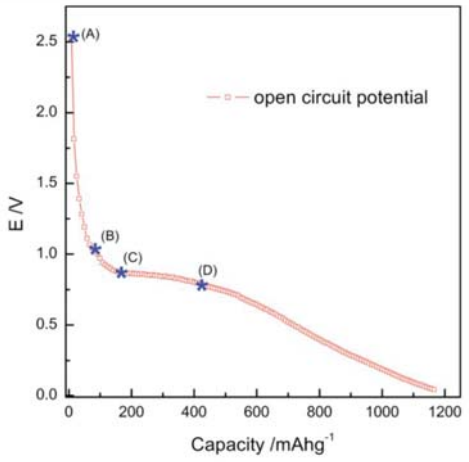

Figure 1: Open-circuit potential (E) vs. specific capacity (Q) of the ZFO-C vs. Li half-cell investigated during first Li uptake.

Samples characterization by XAS

Soft XAS experiments were performed in a wide photon energy range (50-1100 eV) at the BL8.1 BEAR end-station of the ELETTRA synchrotron facility in Trieste (Italy). All XAS spectra were collected in total electron yield (TEY) mode (i.e., drain current mode) up to the carbon K-edge (286 eV) while at higher photon energy the photon emission signal (fluorescence yield) was also collected. The thickness evolution of the SEI can be monitored by the fading of the Zn and Fe signal of the ZFO nanoparticles being covered by the SEI layer as reported in Fig. 2. A possible model of growth is reported in Fig. 3 together with SEM image of the SEI; the latter is found to grow preferentially over the active ZFO-C particles, and as reported already in ref. [4].
Changes are associated with the SEI layer growing on the two electrode-active materials. In particular, the SEM image in Figure 3 does not show a thick SEI layer growing all over the electrode when ZFO-C is concerned. The SEI is found to grow preferentially over the active ZFO-C particles, in agreement with present findings by XAS. The absence of a thick SEI layer covering the electrode allows the easy movement of Li^+ ions into the electrode pores facilitating the (de)lithiation process.

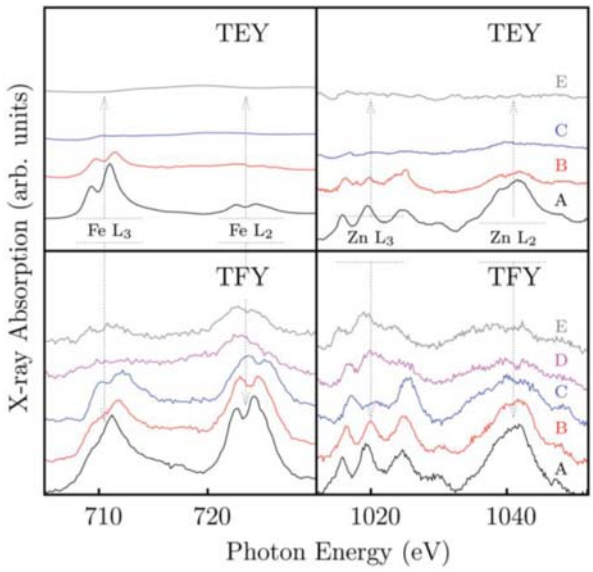

Figure 2. Left panel: total electron (TEY, top) and fluorescence (TFY, bottom) yield XAS spectra at Fe (left) and Zn (right-hand) L-edges for the ZFO-C electrodes under consideration (A–E, see text and previous figures). The intensity trends reflect the evolution of the SEI upon the electrodes.

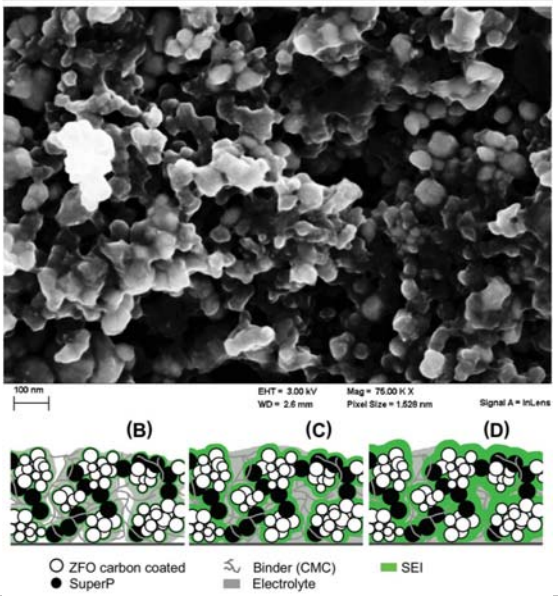

Figure 3: The SEM image shows the surface of a cycled electrode (10 full charge/discharge cycles) evidencing the absence of the SEI on the electrode surface.

Conclusions

The main conclusions that can be drawn by this work can be thus summarized as follows: 1) the evolution of the SEI takes place already during the first steps of the charging process and its thickness reach about 40 nm at about 1/3 of the full capacity, with a stable total thickness up to 20 working cycles; 2) the XAS technique is found to be very effective providing an estimate of the local thickness of the SEI, and indicates that the SEI grows preferentially around the ZFO nanoparticles.

References

1. E. Peled, J. Electrochem. Soc. 145, 3482 (1998)
2. A. Di Cicco et al., Adv. Enegy Mat. 1500642 (2015) DOI: 10.1002/aenm. 201500642

Temperature dependent local atomic displacements and disorder in $Ba(Fe_{1-x}Co_x)_2As_2$ superconductor

M.Y. Hacisalihoglu[*,1,2,3], E. Paris[1,4], B. Joseph[2], T.J. Sato[6], T. Mizokawa[7] and N.L. Saini[1]
[1]*Dipartimento di Fisica, Universita di Roma "La Sapienza" - P. le Aldo Moro 2, 00185 Roma, Italy*
[2]*Department of Physics, Recep Tayyip Erdogan University, 53100 Rize, Turkey*
[3]*Department of Physics, Karadeniz Technical University, 61080 Trabzon, Turkey*
[4]*Center for Life NanoScience@Sapienza, Istituto Italiano di Tecnologia, V.le Regina Elena 291, 00185 Rome, Italy*
[5]*Elettra, Sincrotrone Trieste, Strada Statale 14, Km 163.5, Basovizza, Trieste, Italy*
[6]*Institute for Solid State Physics, University of Tokyo, 106-1 Shirakata, Tokai, Ibaraki 319-1106, Japan*
[7]*Department of Applied Physics, Waseda University, Tokyo 169-8555, Japan*

Email: **m.y.hacisalihoglu@gmail.com*
Keywords: pnictides and chalcogenides, effects of crystal defects, doping and substitution, effects of disorder- X-ray diffraction and scattering

Since the discovery of superconductivity in $LaO_{1-x}F_xFeAs$ [1], several iron-based layered pnictides/chalcogenides are found to be superconducting [2-4]. Among these, the $Ba(Fe_{1-x}Co_x)_2As_2$ pnictide is one of the highly studied systems, due to the fact that large single crystals of this system can be produced with high purity in entire doping range of the phase diagram [2-6]. This also makes the system suitable for a variety of experimental probes, permitting to study physical properties with a great precision.

In this study we have studied the local structure of $Ba(Fe_{1-x}Co_x)_2As_2$ superconductor by temperature dependent extended x-ray absorption fine structure (EXAFS) measurements. Polarized EXAFS measurements at the Fe K-edge on optimally doped (x=0.06) single crystal have permitted to determine atomic displacements across the superconducting transition temperature (T_c). The Fe-As bond lengths hardly show any change with temperature, however, the Fe-Fe sublattice reveals a sharp anomaly across T_c, similar to the one known for cuprates and A15-type superconductors, consistent with the important role of Fe-Fe fluctuations in the superconductivity of $Ba(Fe_{1-x}Co_x)_2As_2$ materials.

We have found large atomic disorder around the substituted Co, revealed by polarized Co K-edge EXAFS measurements. The Co-Fe/Co bonds are shorter and more flexible than the Fe-Fe bonds with the As-height in Co-containing

tetrahedra being larger than the one in $FeAs_4$. The results suggest that local Fe-Fe fluctuations and atomic disorder should have important role in the superconductivity of Fe-based superconductors. The results will be discussed in connection to the nematic phases observed in different Fe-based superconductors.

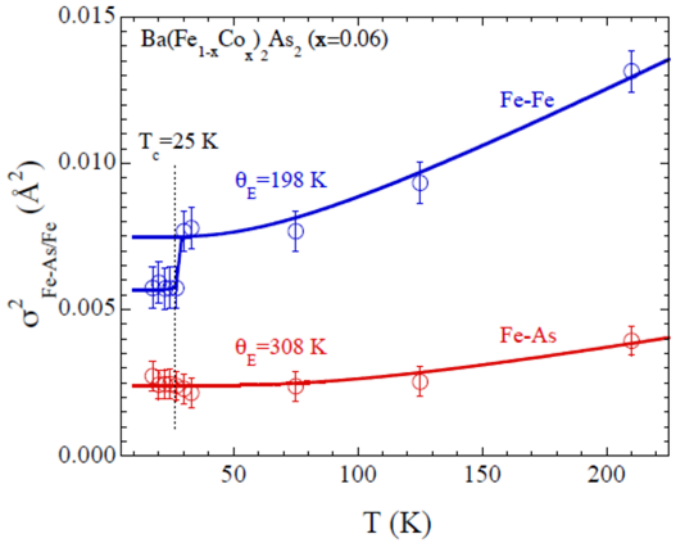

Figure 1: Mean square relative displacement (MSRD) of Fe-As and Fe-Fe are plotted as a function of temperature. The correlated Einstein model fits are shown by solid lines (for the Einstein model fits only the data above T_c are used in the case of Fe-Fe). Interestingly, the σ_i^2 for the Fe-Fe distance decreases sharply while the sample is cooled down to the superconducting state.

References

1. Y. Kamihara, T. Watanabe, M. Hirano and H. Hosono, J. Am. Chem. Soc. 130, 3296 (2008).
2. Celebrating 100 years of superconductivity - Special issue on Iron Based Superconductors, Report on Progress in Physics, 74 (2011)
3. D. C. Johnston, Adv. Phys. 59, 803 (2010).
4. D. Johrendt, H. Hosono, R.-D. Homann, R. Poettgen, Z. Kristallogr. 226, 435 (2011).
5. P.C. Canfield, S.L. Budko, Ni Ni, J.Q. Yan and A. Kracher, Phys. Rev. B 80, 060501 (2009).
6. Jiun-Haw Chu, James G. Analytis, Chris Kucharczyk and Ian R. Fisher, Phys. Rev. B 79, 014506 (2009).

A two rotor model with spin for magnetic nanoparticles

Keisuke Hatada[1,2], Kuniko Hayakawa[3], Augusto Marcelli[3,4] and Fabrizio Palumbo[3]
[1]*Département Matériaux-Nanosciences, Institut de Physique de Rennes, UMR UR1-CNRS 6251, Université de Rennes1, 35042 Rennes cedex – France*
[2]*Scienze e Tecnologie, Universita' di Camerino, Via Madonna delle Carceri 9, 62032 Camerino, Italy*
[3]*INFN-LNF, 00044 Frascati, Italy.*
[4]*University of Science and Technology of China, No. 96, Jinzhai Road, Hefei, Anhui 230026, P. R. China*

Email: *keisuke.hatada@univ-rennes1.fr*
Keywords: nanomagnetism, nanoparticle, scissors model

We consider single domain nanoparticles that can schematically be represented as a uniform magnetic lattice, the macrospin, rotating in a nonmagnetic lattice. While it seems to be natural to associate a rigid rotor with the nonmagnetic lattice [1], the macrospin is generally represented as a pure spin. We think, however, that in some cases, possibly in several cases, also the macrospin should carry a moment of inertia because the constituting spins will always, to some extent, drag the orbits.

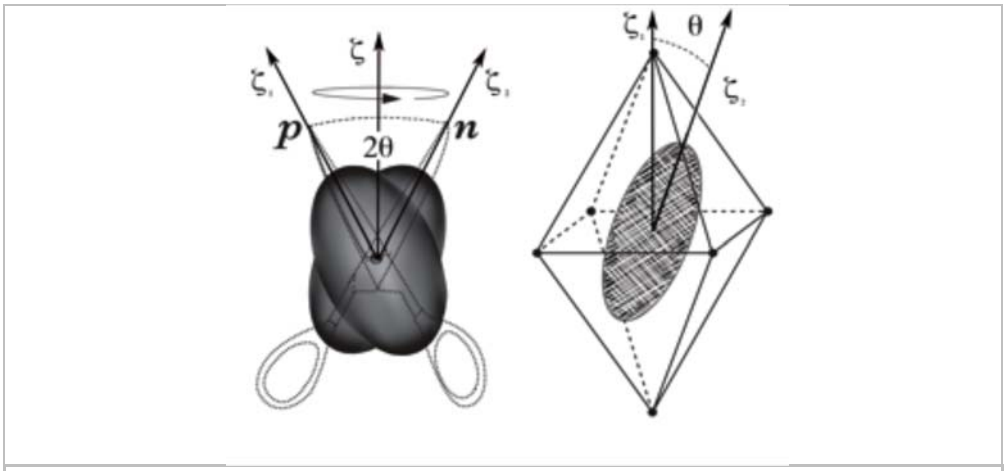

Figure 1: Two rotor model: on the left the proton (p) and neutron (n) rotors precess around the bisector ζ of their axes ζ_1, ζ_2. The lowest excited states are called scissors modes. The right figure represents also a nanoparticle if we identify the octahedron with the nonmagnetic lattice of easy axis ζ_1 and the ion with the macrospin pointing in the direction ζ_2.

One extreme example is given by structures in which the constituting spins belong to electrons that have such a strong spin–orbit coupling that they are rigidly locked to their orbits. Another example occurs when the macrospin has an electrically charged profile, so that its magnetic moment gets a contribution from the orbital motion. Concerning nanoparticles, an inertial parameter was often explicitly introduced in the treatment of tunneling.

We restrict our attention to nanoparticles that can be represented as two rigid rotors, one of which carries a large spin [3]. For such nanoparticles we adopt a model obtained by a modification of the two rotor model designed long ago [4] to describe deformed atomic nuclei, in which case the two rotors are the proton and neutron bodies as shown in Fig. 1. The two rotor model predicts collective excitations called scissors modes characterized by a strong magnetic dipole moment (generated by the rotation of the proton electric charge around the bisector of the proton and neutron axes), whose coupling with the electromagnetic field provides their signature.

By this model we can describe in a unified way the cases of nanoparticles free and stuck in anelastic or a rigid matrix. We evaluate the magnetic susceptibility for the latter case and under some realistic assumptions we get results in closed form. A crossover between thermal and purely quantum hopping occurs at a temperature much higher than that at which tunneling becomes important. Agreement with some experimental data is remarkable. [5]

References

1. E.M. Chudnovsky and D.A. Garanin, Phys. Rev. B: Condens. Matter Mater. Phys. 2010, 81, 214423.
2. M.F.O. Keeffe, E.M. Chudnovsky and D.A. Garanin, J. Magn. Magn. Mater. 324, 2871 (2012)
3. C. Balasubramanian, B. Joseph, P. Gupta, N.L. Saini, S. Mukherjee, D. Di Gioacchino and A. Marcelli, ‘X-ray absorption spectroscopy characterization of iron-oxide nanoparticles synthesized by high temperature plasma processing', J. Elect. Spectr. Rel. Phenom. 196, 125-129 (2014)
4. N. Lo Iudice and F. Palumbo, *Phys. Rev. Lett.* 41, 1532 (1978).
5. K. Hatada, K. Hayakawa, A. Marcelli and F. Palumbo, A two rotor model with spin for magnetic nanoparticles, *Phys. Chem. Chem. Phys.* **16**, 24055-24062 (2014).

Special effects at complex oxide interfaces

Hans Hilgenkamp
MESA+ Institute for Nanotechnology, University of Twente
P.O. Box 217, 7500 AE Enschede, The Netherlands

Email: *H.Hilgenkamp@utwente.nl*
Keywords: oxide interfaces, 2-DEGs, magnetism

In my contribution I will introduce special effects occurring at interfaces between complex oxides, with a particular emphasis on the $LaAlO_3/SrTiO_3$ and $LaMnO_3/SrTiO_3$ systems. In particular, I will discuss our research towards high-mobility 2-DEGs [1], field effect transistor-type devices [2] and magnetic effects [3].

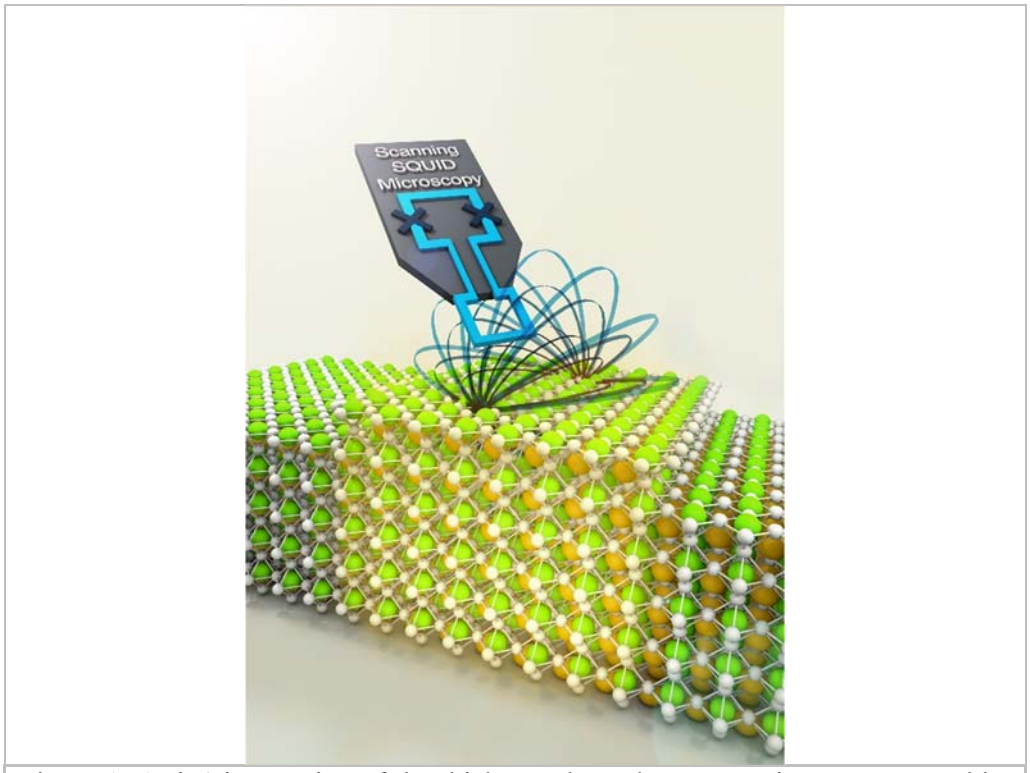

Figure 1: Artist' impression of the thickness dependent magnetism as measured by scanning SQUID magnetic microscopy experiments on thin layers of $LaMnO_3$ on $SrTiO_3$.

References

1. M. Huijben, G. Koster, M.K. Kruize, S. Wenderich, J. Verbeeck, S. Bals, E. Slooten, B. Shi, H.J.A. Molegraaf, J.E. Kleibeuker, S. van Aert, J.B. Goedkoop, A. Brinkman, D.H.A. Blank, M.S. Golden, G. van Tendeloo, H. Hilgenkamp, G. Rijnders, Defect engineering in oxide heterostructures by enhanced oxygen surface exchange, Advanced Functional Materials 23, 5240 (2013)
2. P.D. Eerkes, W.G. van der Wiel, H. Hilgenkamp, Modulation of conductance and superconductivity by top-gating in $LaAlO_3/SrTiO_3$ 2-dimensional electron systems, Applied Physics Letters 103, 201603 (2013).
3. X.R. Wang, C.J. Li, W.M. Lü, T.R. Paudel, D.P. Leusink, M. Hoek, N. Poccia, A. Vaillionis, T. Venkatesan, J.M.D. Coey, E.Y. Tsymbal, Ariando, H. Hilgenkamp, Imaging and control of ferromagnetism in $LaMnO_3/SrTiO_3$ heterostructures, Science 349, 716 (2015).

Mesoporous films: from self assembly to complex materials

Plinio Innocenzi
Laboratory of Materials Science and Nanotechnology (LMNT), D.A.D.U.,
University of Sassari, Porto Conte Ricerche,
S.P. 55 Porto Conte/Capo Caccia, Km 8.400 Località Tramariglio, 07041 Alghero (SS), Italy

Email: *plinio@uniss.it*

Self-assembly of ordered mesoporous films through templating micelles is a highly complex process, which involves a very fine tuning of different chemical-physical parameters. The final material, after removal of the organic template, contains mesopores with organized topology, which can be adjusted through the control of the film deposition conditions. Several ordered structures, such as lamellar, 2D hexagonal, or 3D cubic, just as an example, have been obtained so far in the films. On the other hand besides ordering the pores is also possible controlling the wall structure up to a very intimate level, which allows to adjust quite well the properties of the material.
The mesoporous films can be a platform, or a tool to make even more complex materials, such as hierarchical porous films, and the pores can host different types of functional molecules or particles, oxides, metallic and semiconductor nanoparticles. They can also be combined for the synthesis of an almost endless group of new functional materials whose possibilities of applications are only restrained by our limited imagination.

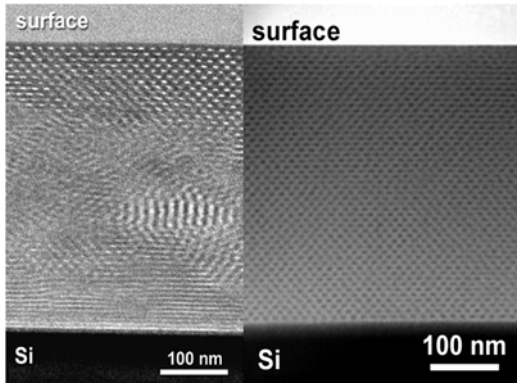

Some examples of self-assembled mesoporous materials will be presented, together with materials with higher ordered of complexity and functional properties.

References

1. L. Malfatti, T. Kidchob, P. Falcaro, S. Costacurta, M. Piccinini, M. Cestelli Guidi, A. Marcelli, A. Corrias, M.F. Casula, H. Amenitsch and P. Innocenzi, Highly ordered self-assembled mesostructured membranes: Porous structure and pore surface coverage, Microporous and Mesoporous Materials 103, 113–122 (2007)
2. P. Innocenzi, L. Malfatti, S. Costacurta, T. Kidchob, M. Piccinini and A. Marcelli, Evaporation of Ethanol and Ethanol-Water Mixtures Studied by Time-Resolved Infrared Spectroscopy, J. Phys. Chem. A 112, 6512–6516 (2008)
3. P. Falcaro, L. Malfatti and P. Innocenzi, *Water Droplets to Nanotechnology: A Journey Through Self-Assembly,* Royal Society of Chemistry (Cambridge, 2013)
4. G. Campi, et al., Inhomogeneity of charge-density-wave order and quenched disorder in a high-Tc superconductor, Nature 525, 359-362 (2015)

Chiral molecules and related asymmetries revisited

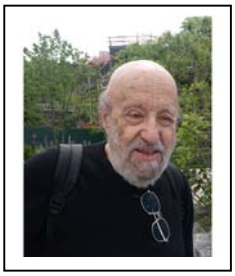

Giovanni Jona-Lasinio*, Carlo Presilla
Dipartimento di Fisica, Sapienza Università di Roma and INFN

Email: **gianni.jona@roma1.infn.it*
Keywords: chiral molecules, spontaneous symmetry breaking, localization, homochirality.

According to quantum mechanics, chiral molecules, that is, molecules, which are not superimposable on their mirror image, should not exist. The simplest molecules, which can be chiral have four or more atoms with two arrangements of minimal potential energy that are equivalent up to a parity operation. Chiral molecules correspond to states localized in one potential energy minimum and cannot be eigenstates of the Hamiltonian which is parity invariant. This has been a puzzle or a paradox since the early stages of quantum mechanics [1] and many different explanations have been attempted. A possible explanation is based on the mechanism of spontaneous symmetry breaking [2,3] which so far is the only one leading to quantitative estimates, reproduces satisfactorily existing spectroscopic data and suggests new experiments [4,5]. In particular experiments with gas mixtures as discussed in [5], may provide a critical test of the spontaneous symmetry breaking mechanism.
Another puzzling asymmetry is the homochirality in living matter, that is the dominance of left-handed molecules. Symmetry breaking in non-equilibrium may throw some light on this problem [6].

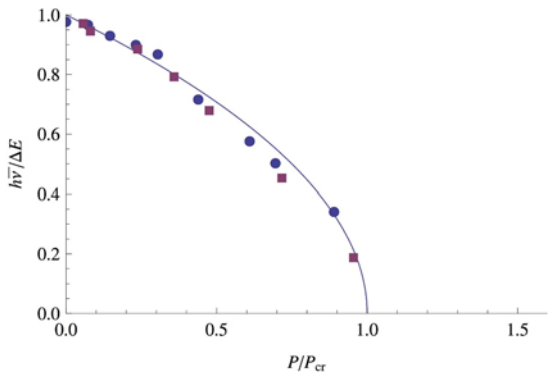

Figure 1: Inversion line frequency measured as a function of the pressure in a gas of NH_3 (circles) or ND_3 (squares). The solid line is the prediction, without free parameters, of Ref. [4]. A spontaneous symmetry breaking takes place at pressure $P=P_{cr}$, with the critical pressure given in terms of the microscopic parameters of the molecular species and the temperature of the gas.

References

1. F. Hund, On the interpretation of molecular spectra. III, Z. Phys. **43**, 805 (1927).
2. P. Claverie and G. Jona-Lasinio, Phys. Rev. A **33**, 2245 (1986).
3. G. Jona-Lasinio and P. Claverie, Prog. Theor. Phys. Suppl. **86**, 54 (1986).
4. G. Jona-Lasinio, C. Presilla and C. Toninelli, Interaction induced localization in a gas of pyramidal molecules, Phys. Rev. Lett. **88**, 123001 (2002).
5. C. Presilla and G. Jona-Lasinio, Spontaneous symmetry breaking and inversion-line spectroscopy in gas mixtures, Phys. Rev. A **91**, 022709 (2015).
6. G. Jona-Lasinio, Spontaneous symmetry breaking, Prog. Theor. Phys. **124**, 731 (2010).

Xpress – a joint Indo–Italian scientific partnership for a dedicated high pressure diffraction facility at Elettra Trieste

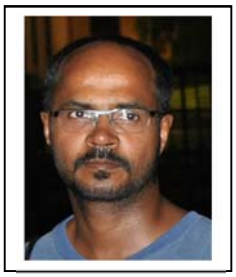

Boby Joseph[1*], Andrea Lausi[2†],
Nishant Kumar Varshney[1], Giorgio Bais[2],
Maurizio Polentarutti[2], S.M. Sharma[3]
[1]*ICTP-IISc Fellow, Elettra Sincrotrone Trieste, S.S. 14 Km 163.5 in Area Science Park, 34149 Basovizza, Trieste, Italy*
[2]*Elettra Sincrotrone Trieste, S.S. 14 Km 163.5 in Area Science Park, 34149 Basovizza, Trieste, Italy*
[3]*Physics Group, Bhabha Atomic Research Centre, Trombay, Mumbai, 400085 India*

Email: *bjoseph@ictp.it*
Keywords: synchrotron beamline facility, high-pressure x-ray diffraction, strongly correlated electron systems

High pressure x-ray diffraction is a basic step in understanding a plethora of extreme conditions phenomena relevant to several branches of science, to mention the most common one, the geophysics. It is recognized as a powerful tool to shed light on the physics issues of several strongly correlated electron systems. For example, important inputs were obtained from the high-pressure studies of the well-debated metal-insulator transition in vanadium dioxide [1,2]. Currently, a dedicated high pressure diffraction beamline, Xpress, is under the advanced stages of commissioning at Elettra Sincrotrone, Trieste.

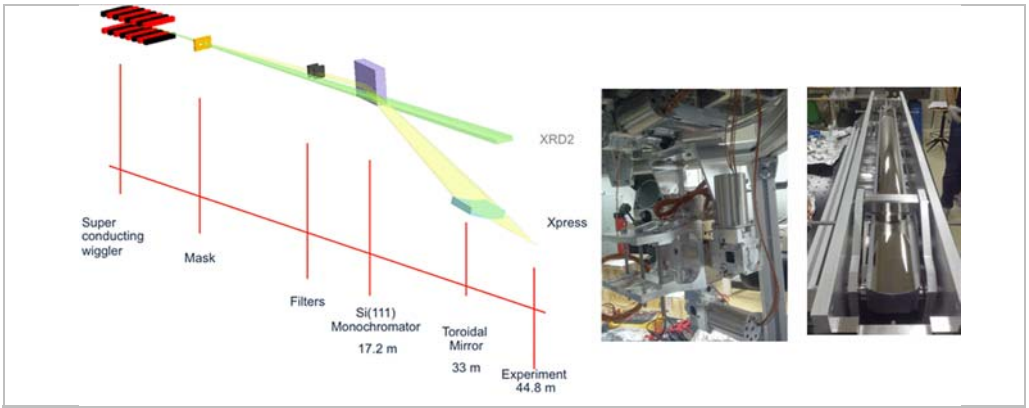

Figure: Left panel: Xpress beam line scheme. Middle panel: Inside view of the Splitter (a photograph taken during installation). Right panel: Inside view of the toroidal mirror (a photograph taken during installation).

This facility will start hosting scientific users from the last quarter of 2015. Xpress is part of a scientific partnership between the India and Italy under a project administered through the Indian Institute of Sciences (IISc) Bengaluru, for the development of a macromolecular and a high pressure x-ray diffraction facilities, respectively the XRD2 [3] and Xpress [4] beamlines.
A multipole superconducting wiggler (SCW) is the source of the Xpress and XRD2. The SCW will provide a factor of 14 higher flux compared to the permanent magnet wiggler of the already present diffraction beamline (XRD1) at 25 keV. The SCW also result in a smaller source size due to the shorter wiggler length. Detailed design and manufacture of the SCW has been done at the Budker Institute of Nuclear Physics, Novosibirsk. A liquid nitrogen cooled silicon single crystal (cut along the (111) direction) hosted in the splitter chamber in the *FrontEnd* section intercepts the beam from the source (SCW) and directs it to the focusing mirror of the Xpress at a fixed energy of 25 keV. The focusing mirror is a 1.4 m long torus, Pt coated to achieve 80% reflectivity at 25 keV and 2.9 mrad grazing angle. The focused beam from the mirror will be further optimized by custom made collimators (a minimum of 30 μm diameter) to have intense and well defined monochromatic beam required for the high pressure x-ray diffraction. A ruby fluorescence microscope connected side-by-side to the pin-hole stage will enable the on-line pressure monitoring. An image plate MAR 345 will be used to collect the diffraction pattern. Current experimental stage envisages room temperature – high-pressure measurements using various kinds of Diamond Anvil Cells in the pressure range 0-50 GPa. Detailed description of the Xpress beamline and some details about the academic user program of the Elettra will be described in the talk.

Acknowledgements. The authors thank Elettra staff, specially the alignment, vacuum, radio protection, safety, software and infrastructure groups for their enthusiastic participation and support to the new beamlines project. We thank Prof. D.D. Sarma, Scientific Director of the project for very effective and excellent leadership. We thank Dr. G. Paolucci for significant contribution in the initial stages of the project. We also thank Prof. J. Niemela and staffs of ICTP Trieste for important and continuous help in the co-ordination of the project. BJ and NKV acknowledge ICTP Trieste and IISc Bengaluru for the ICTP-IISc fellowship.

References

1. M. Mitrano, B. Maroni, C. Marini, et al., *Phys. Rev. B* **85**, 184108 (2012)
2. C. Marini, M. Bendele, B. Joseph, et al., *EPL* **108**, 36003 (2014)
3. https://www.elettra.trieste.it/Elettra-beamlines/xrd2.html
4. https://www.elettra.trieste.it/lightsources/elettra/elettra-beamlines/xpress/welcome-page.html

Controlled modification of surface and interface at nanoscale by energetic particles

D. Kanjilal
Inter-University Accelerator Centre (IUAC)
Aruna Asaf Ali Marg, New Delhi-110 067

Email: *dk@iuac.res.in*
Keywords: ion beams, surfaces and interfaces, controlled patterning

Ion beams in the energy range varying from a few tens of keVs to hundreds of MeVs available from the research facilities having various accelerators have been utilized to modify the properties at surface and interface of various materials and device structures in the spatial scale of nanometers and temporal scale of nano-seconds. Focused research activities in the related areas using the state of the art experimental facilities in various beam lines at IUAC Delhi have been carried out by various researchers. Ion beams at varied energies and doses are used for precise modification of materials at desired location in three dimensions. Some of the interesting results on controlled patterning on the surface, modification of phase near the surface and transport properties at the interface will be presented. Special emphasis will be given to the understanding of the fundamental interaction processes involved and various controlled experiments that can be performed to achieve the desired results. Low energy (keV) ion beams are generally used for ion implantation near or controlled sputtering of the surface at desired location. The modification of interface structures is carried out by dense electronic excitation during irradiation by ions at higher energies. Some of the interesting results on formation of different controlled structures and modification of device characteristics will be reviewed in this talk.

References

1. Tanuj Kumar, Ashish Kumar and D. Kanjilal, Appl. Phys.Lett. **103**, 131604 (2013)
2. Tanuj Kumar, Ashish Kumar, N.P. Lalla, Sonu Hooda, Sunil Ojha, Shammi Verma, D. Kanjilal, Applied Surface Science, **283**, 417 (2013).
3. Ashish Kumar, A. Hähnel, D. Kanjilal and R. Singh, Appl. Phys. Lett. **101**, 153508 (2012)

Overview of fusion materials and technologies developments at IPR for Divertor & Firstwall Applications

S.S. Khirwadkar*, P.M. Raole and Charulata Dube
Divertor and Firstwall Technology Development Division, Institute for Plasma Research, Bhat, Gandhinagar-382428, Gujarat, INDIA

Email: **sameer@ipr.res.in*
Keywords: divertor, first wall, tungsten, plasma facing component, tokamak, fusion

Developments of materials and technologies needed for Divertor & Firstwall Applications of a fusion grade tokamak constitutes an important area of research being actively pursued at the Institute for Plasma Research (IPR, India) in collaboration with national and international organizations of repute.
Tungsten being the only plasma facing material considered at present for fusion grade tokamaks, most of the materials research work is concentrated on development of bulk tungsten & tungsten alloy materials, tungsten based functionally graded materials and tungsten thick coatings on metallic substrates. Technological research includes activities related to fabrication plasma facing components and their support structures, joining and coating of plasma facing materials with actively cooled metallic substrates for heat transfer applications, welding of similar & dissimilar materials for structural support applications.
Characterization of materials/ coatings/ joints and evaluation of performance of materials & fabricated test mock-ups/ components under various loading conditions constitutes major part of the research activities.
This paper presents an overview of the research work being conducted at IPR on the above mentioned topics, including the following: (a) Material Damage Studies Under Energetic Heavy Ion Beams; (b) Characterization of tungsten materials; (c) Development of tungsten material through powder metallurgy route; (d) Performance of tungsten materials under thermal loads; (e) Studies on joining of tungsten-copper and copper-steel materials; (f) Welding of dissimilar steel materials; (g) Tungsten coating on steels;
It is believed from present day research that nano-structured materials will play an important role in divertor & first wall applications and hence it will be considered in future activities.

Terahertz and Infrared Plasmonic Absorption of 3-Dimensional Nano Porous Graphene

S. Lupi[*1], F. D'Apuzzo[2], R.A. Piacenti[2], M. Autore[2], F. Giorgianni[2], M. Cestelli-Guidi[3], A. Marcelli[3], Y. Ito[4], M. Chen[4]

[1]*INFN and Sapienza University, Rome, Italy*
[2]*IIT and Sapienza University, Rome, Italy*
[3]*LNF-INFN, Frascati, Italy*
[4]*WPI Advanced Institute for Materials Research, Tohoku University, Sendai, Japan*

Email: **Stefano.lupi@roma1.infn.it*
Keywords: graphene, nanostructured graphene, plasmons, Fano effects

Graphene Plasmons hold promise of wide applications due to low-losses, tunability and extreme confinement at the nanoscale, and have been investigate in all sorts of 2 Dimensional nanostructures and hybrid systems [1]. Three-dimensional Nanoporous Graphene (NPG) has recently been obtained with a new Chemical Vapor Deposition based fabrication process [2], obtaining to construct graphene in a 3D configuration (see Fig.1a) while retaining the unique characteristics of mass-less Dirac fermions with high electron mobility.

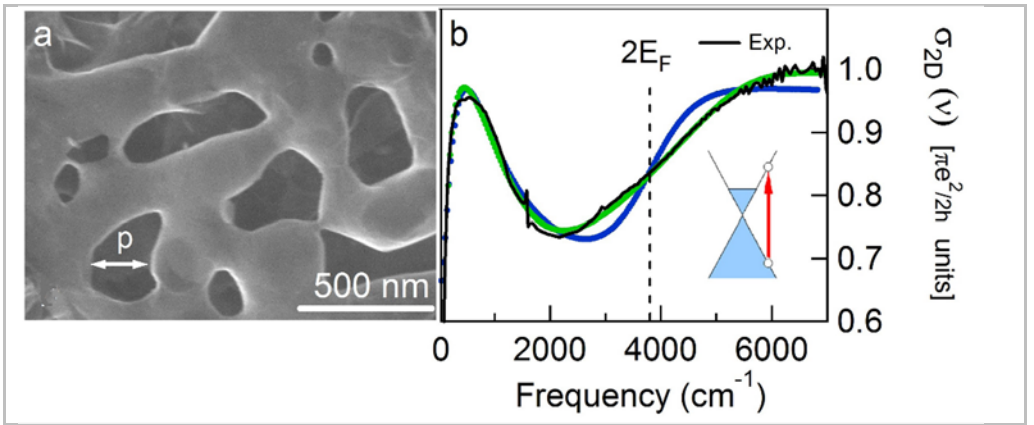

Fig. 1: a) SEM image of Nanoporous Graphene with average pore size p=200 nm. b) A typical Infrared absorption spectrum for a doped sample shows two absorption features: interband transitions and a plasmonic peak, at high and low frequency, respectively.

While NPG is the object of ongoing studies to demonstrate its application such as energy harvesting electrode [3], little is known about its optical properties. In

this work we performed terahertz and infrared optical conductivity measurements. The optical conductivity spectra, as in Fig.1b, exhibit, beside the typical interband absorption of graphene above the threshold of $2E_F$ (chemical potential of the system), i.e. in the near-infrared and visible part of the spectrum, a strong plasmonic absorption at terahertz (for low-doped samples) and Mid-Infrared (for E_F=250 meV) frequencies. We have shown that these plasmonic excitations strongly depend on the chemical doping and pore-size of the NPG 3D structure, following the behavior of 2D Dirac-Plasmons like in 2D graphene [4].

References

1. T. Low and P. Avouris, ACS Nano 8, 1086 (2014)
2. Y. Ito, M. Chen et al., Angewandte Chemie 126, 1 (2014)
3. Y. Ito, M. Chen et al., Angewandte Chemie 54, 2131 (2015)
4. F. D'Apuzzo et al., to be submitted (2015)

Microdrop deposition for ultra-diluted samples preparation

Salvatore Macis[1], Augusto Marcelli[2], Giannantonio Cibin[3]
[1]*Department of Mathematics and Physics, Università di Roma Tre, Via della Vasca Navale 84, 00146, Rome, Italy*
[2]*Istituto Nazionale di Fisica Nucleare, Laboratori Nazionali di Frascati, 00044 Frascati, Italy*
[3]*Diamond Light Source, Harwell Science and Innovation Campus, OX11 0DE, Didcot, Oxfordshire, UK*

Email: *salvatore.macis91@gmail.com*
Keywords: ultra-dilution, droplets, water, evaporation, XRF

The analysis of dust and solutes present in ultra diluted solutions is an important target for many researches, but difficult to achieve because of the extremely low concentration. The microdrop technique allows, through the evaporation of small droplets [1,2], the deposition of materials present in solution with a particular pattern of deposition and on a well-defined patterned area. The technique may produce drops with diameters in a range that goes from 30 to 200 μm. Evaporation deposits the non-volatile materials present in the solution in a relatively short time.

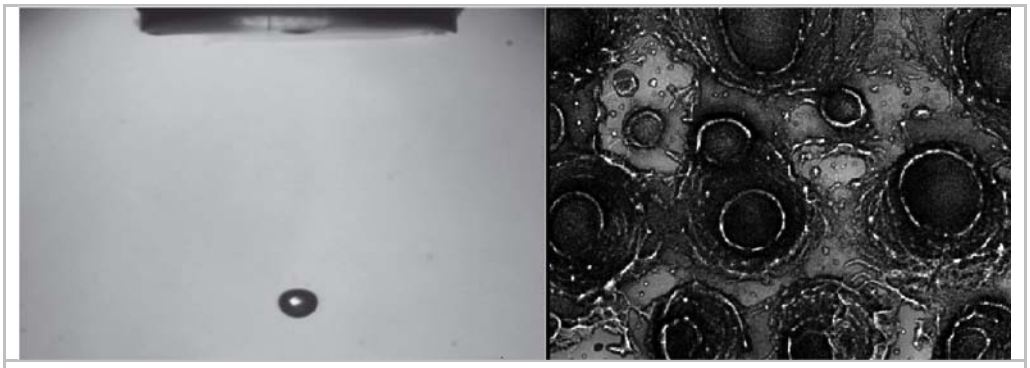

Figure 1: The droplets produced by the microdrop and the deposition pattern.

It is therefore possible to control the deposited density on very small areas with the aim to reach the highest density, with the smallest amount of materials, a result extremely difficult to achieve with other techniques - above all when high homogeneity is required. As a matter of fact, using microdrop deposition it is possible to obtain samples with density comparable to ones prepared with the filtering technique, but with a total amount of the solution ~25 times lower.

A second advantage of this technique is that it significantly minimizes and eventually rules out unwanted effects associated with the evaporation of large drops, such as coffee stains or cluster formations, allowing to achieve the highest sample uniformity [3,4].
In addition, unlike filtering techniques, the microdrop method can be applied and optimized for almost any liquid system, as microdrop heads are usually built using highly inert materials, and deposition can happen on any surface. It is then possible to select the most suitable substrate for the material to deposit and for the analysis to perform [5].
The technique here described may produce samples that could be used in many applications. Among the many, the deposition and the characterization of atmospheric particulate matter (PM) for pollution monitoring, studies of polluted water or the investigation of biological diluted materials contained in ultratrace, with concentration values that goes from hundreds to tens of ppm. An example application has been designed on the Antarctic ice for the X-ray absorption spectroscopy [6,7] of particulate trapped in ice cores to study the evolution of the climate during the Pleistocene and Holocene [8].

References

1. R.G. Picknett and R. Bexon, The evaporation of sessile or pendant drops in still air, Journal of Colloid and Interface Science 61, 336–350 (1977).
2. H. Hu, R.G. Larson, Evaporation of a sessile droplet on a substrate, The Journal of Physical Chemistry 106, 1334–1344 (2002)
3. F. Girard, M. Antoni, S. Faure, A. Steinchen, Evaporation and Marangoni Driven Convection in Small Heated Water Droplets, Langmuir 22, 11085-11091 (2006)
4. P. Innocenzi, L. Malfatti, M. Piccinini, D. Grosso, A, Marcelli, Stain Effects Studied by Time-Resolved Infrared Imaging, Anal. Chem. 2, 551-556 (2009)
5. G. Campi, et al., Inhomogeneity of charge-density-wave order and quenched disorder in a high-Tc superconductor, Nature 525, 359-362 (2015)
6. J. Garcia, M. Benfatto, C.R. Natoli, A. Bianconi, I. Davoli and A. Marcelli, Three particle correlation function of metal ions in tetrahedral coordination determined by XANES, Solid State Commun. 58, 595-599 (1986)
7. Z.Y. Wu, A. Marcelli, A. Mottana, G. Giuli, E. Paris and F. Seifert, Effects of higher coordination shells in garnet detected by XAS at the Al K-edge, Phys. Rev. B 54, 2976 (1996)
8. A. Marcelli, G. Cibin, D. Hampai, F. Giannone, M. Sala, S. Pignotti, V. Maggi and F. Marino, XANES characterization of deep ice core insoluble dust in the ppb range, J. Anal. At. Spectrom. 27, 33-37 (2012)

Tailoring of the conductivity of two-dimensional electron gas in $LAlO_3/SrTiO_3$ interfaces

Sinu Mathew[1,2,*], Anil Annadi[1], Taw Kui Chan[1,3], Da Zhan[4], Zexiang Shen[4], Ariando[1], Mark B.H. Breese[1,3] and T. Venkatesan[1,2,3]
[1]NUSNNI-NanoCore, National University of Singapore, Singapore 11741
[2]Department of Electrical and Computer Engineering, NUS, Singapore, 117576
[3]Center for Ion Beam Applications (CIBA), Department of Physics, NUS Singapore, Singapore 117542
[4]Division of Physics and Applied Physics, SPMS, Nanyang Technological University, Singapore 637371

Email **pmsmathew@gmail.com; elemathe@nus.edu.sg*
Keywords: hetrointerface; point defects; interface conductivity; localization; interface patterning

The two-dimensional electron gas (2DEG) formed at the interface between two insulators $LaAlO_3$ (LAO) and $SrTiO_3$ (STO) is one of the most fascinating systems in the field of oxide electronics [1,2]. This system attracts both fundamental as well as applied fields of research. Patterning of the interface 2DEG is a challenge in oxide electronics. Room temperature electronic devices, sensors and nano-photodetectors have been demonstrated in these interfaces [2]. Further, unconventional interfacial superconductivity along with magnetic order has been proposed in one-dimensional electron gas formed at this interface [3]. We demonstrate a novel way to tailor the conductivity and also to create an insulating state of the 2DEG at the interface using an ion beam exposure based single step strategy [4]. We found that this method can be utilized to manipulate the conductivity at the LAO/STO interface by carrier localization [Fig. 1(a) and (b)], arising from the defects created by the ion beam exposure, eventually producing an insulating ground state [Fig. 1(c)]. Magnetotransport measurements indicate that the irradiated (un-irradiated) samples showed a negative (positive) magneto-resistance along with simultaneous emergence of first-order (only second order) Raman modes.

This process of ion beam induced defect creation results in structural changes in $SrTiO_3$ as revealed by the appearance of first-order polar TO_2, and TO_4 vibrational modes which are associated with Ti-O bonds in the Raman spectra of the irradiated samples [Fig. 1(d)].

The creation of a spatially-selective insulating ground state by tuning the process parameters of an energetic ion beam based single step approach enable

to both pattern and also tune the electronic properties of interface 2DEG. We found that low Z ion irradiation can manipulate the conductivity of interface 2DEG by substrate engineering. A resist-free, single-step direct patterning of a conducting LAO/STO interface has been demonstrated by using a stencil mask with 0.5 MeV Helium ions [inset of Fig. 1(c)] while nanometer scale patterns may be possible with direct focused ion beam writing.

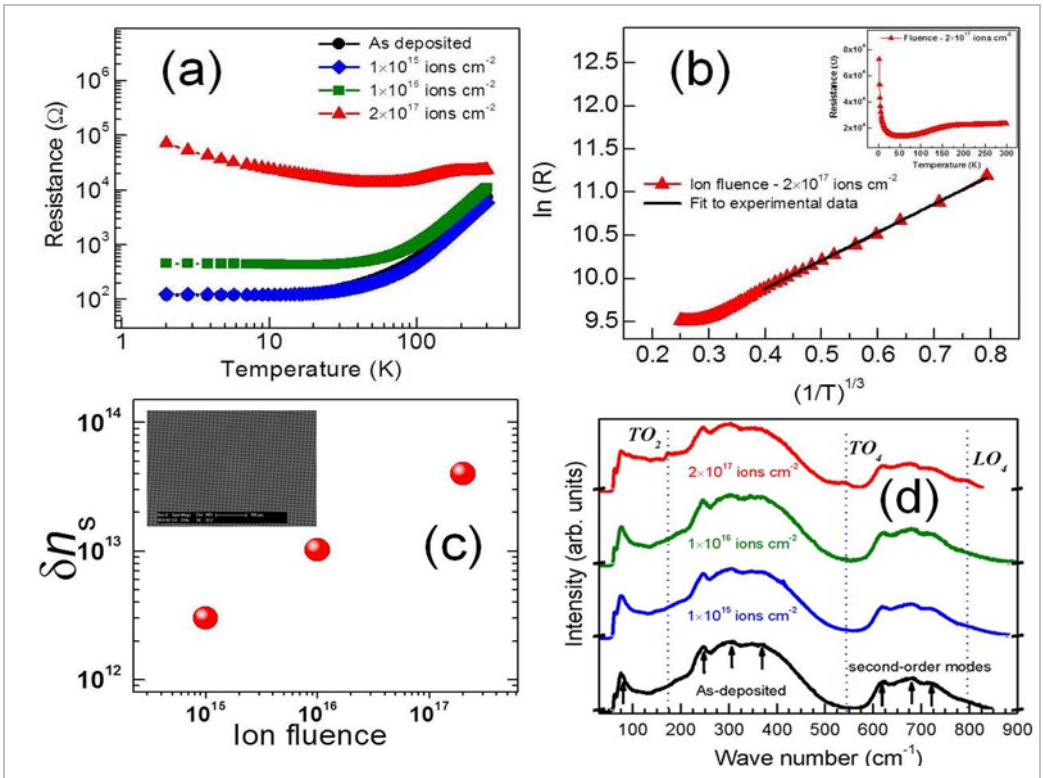

Figure 1: Electrical transport of an interface 2DEG in LAO/STO (a) Temperature dependent resistance of as-deposited and ion beam exposed samples at different proton fluences. (b) Variable range hopping fit to transport data of ion irradiated with 2×10^{17} ions.cm^{-2} fluence, the inset shows the non-saturating behavior of corresponding sample. (c) Reduction in carrier density δn_s with ion fluence at 300 K, here δn_s defined as the difference in n_s of as-deposited and irradiated sample sections ($\boldsymbol{\delta n_s = n_{s(as\text{-}deposited)} - n_{s(irradiated)}}$), an SEM image of the patterned interface 2DEG using 0.5 MeV Helium ions is shown at the inset. (d) Raman spectra of as-deposited and proton beam exposed samples.

References

1. A. Ohtomo, H. Y. Hwang, Nature **427**, 423-426 (2004)
2. J A. Sulpizio, S. Ilani, P. Irvin, J. Levy, Annu. Rev. Mater. Res. **44**,117–49 (2014)
3. L. Fidkowski, H.C. Jiang, R.M. Lutchyn, C. Nayak, Phy. Rev. B **87**, 014436 (2013)
4. S. Mathew, A. Annadi, T. K. Chan, et al. ACS Nano **7**, 10572 (2013) 10572

Verwey transition of magnetite nanostructures in a glass ceramic

Elena Missale[1], Augusto Marcelli[2,3],
Daniele Di Gioacchino[2], Ivan Davoli[1]
[1]*Department of Physics, University of Rome "Tor Vergata"*
Via della Ricerca Scientifica 1, 1-00133 Rome, Italy
[2]*INFN-LNF, Via Enrico Fermi 44, 00044 Frascati (RM), Italy*
[3]*RICMASS, via dei Sabelli 119 A, 000185 Rome, Italy*

Email: *elena.missale91@gmail.com*
Keywords: Verwey transition, magnetite, nanostructures, susceptibility.

We present the magnetic properties at low temperature of magnetite nanostructures embedded in a glassy matrix. The samples analyzed: borosilicate glassed with different amounts of iron oxides and two different nucleators: Cr_2O_3 and P_2O_5, obtained with a crystallization process at the temperature of ~ 1450° C, were synthesized at the National Institute of Material Physics in Maguerele (Romania). Additional details are available in Ref. [1].
To study the magnetic response of the samples we have measured the AC magnetic multi-harmonic susceptibility of four samples in order to detect the presence of magnetic phases. Actually, the measurement of the first harmonic component of magnetic susceptibility probes both linear and non-linear contributions of the magnetization, while the higher harmonic components refers only to the non-linear contributions such as magnetic phase transitions. In particular, the third harmonic exhibits the greatest amplitude signal respect to all higher harmonic components of the AC susceptibility [2-4].

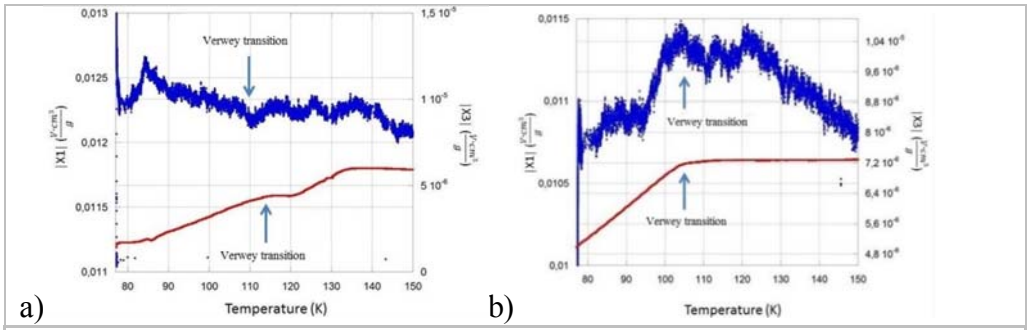

Figure 1: a) Curves of the first (red line) and the third (blue line) harmonic components of the magnetic susceptibility for the sample synthesized with P_2O_5 and b) with Cr_2O_3.

Because tuning the cooling procedure of the sample we may highlight weak magnetic phases present in these systems, we analyzed the magnetic response of the first and the third harmonic varying the temperature from 77 K to 150 K, at a frequency of 1070 Hz, in a Zero Field Cooling (ZFC) configuration, (i.e., cooling the sample without the application of the magnetic field) [5]. In Figure 1 different behaviors are shown and the agreement between the first and the third harmonic is excellent. Both curves in figure 1a) and 1b) show a magnetic transition from 100 K to 120 K. In fact, the magnetite phase (Fe_3O_4) of the iron oxide exhibits a magnetic transition known as Verwey transition at ~123 K. Moreover, at temperatures lower than that the Verwey temperature, the magnetite shows a metal to insulator transition with a decrease of the conductivity of two orders of magnitude [6]. This transition is due to a lattice distortion that changes the structure of magnetite from cubic to orthorhombic [7,8]. In addition, the third harmonic of these samples shows a more complex behavior vs. temperature that points out the presence of other weak magnetic transitions. These features are evident as small peaks in figure 1 a) and as a small step in figure 1b) around 85 K. These transitions are probably due to the presence of clusters of nanoparticles inside the glassy matrix present also in other nanoparticle systems [9]. These clusters facilitate the magnetic interaction among nanoparticles (figure 2). The observed behavior actually rules out the hypothesis that the magnetic transition observed at 85 K in the third harmonic corresponds to a superparamagnetic phase.
The same analysis can be successfully applied to many other correlated systems and superconductors [10,11].

We sincerely acknowledge V. Sandu for the synthesis of the samples used in this research.

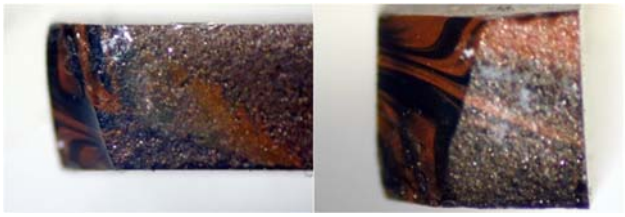

Figure 2: Optical microscope images of the sample synthesized with the P_2O_5 (data in figure 1.a.)

References

1. V. Sandu et al., Journal of Advanced Ceramic 1(2): 138-143 (2012)
2. P. Tripodi, D. Di Gioacchino, J.D. Vinko, Brazilian J. Phys. 34 (3B), 1177-1184 (2004)
3. D. Di Gioacchino, U. Gambardella, P. Tripodi, G. Grimaldi, Superconductor Science and Technology 16 (4), 534 (2003)

4. D. Di Gioacchino, A. Marcelli, P. Puri and A. Bianconi, J. Phys. Chem. Solids 71, 1046-1052 (2010)
5. S. Wang, A. Marcelli, D. Di Gioacchino, Z. Wu, Applied Mechanics and Materials, 568-570, 82-89 (2014)
6. Ze Zang and Sashi Satpathy, Phys. Rev, B 74, 174431 (2006)
7. E. Missale, Thesis, *Calibrazione di un gradiometro magnetico AC e caratterizzazione di nanostrutture di magnetite in vetri ceramici* (2015).
8. J. Garcia and G. Subias, J. Phys.: Condens. Matter 16, R145–R178 (2004)
9. C. Balasubramanian, B. Joseph, P. Gupta, N.L. Saini, S. Mukherjee, D. Di Gioacchino and A. Marcelli, J. Elect. Spectr. Rel. Phenom. 196, 125-129 (2014)
10. A. Bianconi, A. Clozza, A. Congiu Castellano, S. Della Longa, M. De Santis, A. Di Cicco, K.B. Garg, P. Delogu, A. Gargano, R. Giorgi, P. Lagarde, A.M. Flank and A. Marcelli, Intern. J. Modern Phys. B 1, 853-862 (1987)
11. G. Campi, *et al.*, Nature 525, 359-362 (2015)

Micro/nanostructures, bioaccessibility and toxic potential of welding and foundry industrial aerosols

Beatrice Moroni[1]*, Cecilia Viti[2], David Cappelletti[1]
[1]*SMAArt Research Center, University of Perugia, Italy*
[2]*Department of Earth Sciences, University of Siena, Italy*

Email: *b.moroni@tiscali.it*
Keywords: magnetite, electron microscopy, exposure doses, multiple exposure

Epidemiological studies have shown that, when compared to the general population, welders and iron foundry workers have a higher incidence of respiratory diseases and, possibly, cancer [1,2]. This occurrence has been usually related exclusively to the bulk chemical features (*i.e.*, total Cr, Ni, and Mn amounts) of the aerosols. This purely compositional approach does not take into account other important features, such as the particle size, the structural distribution of toxic elements within the particles, the surface characteristics of the hosting crystals, and the nature of chemical bonds. Detailed chemical and structural characterization of aerosol particles is, thus, necessary when reliable exposure and health risk factors are to be assessed.

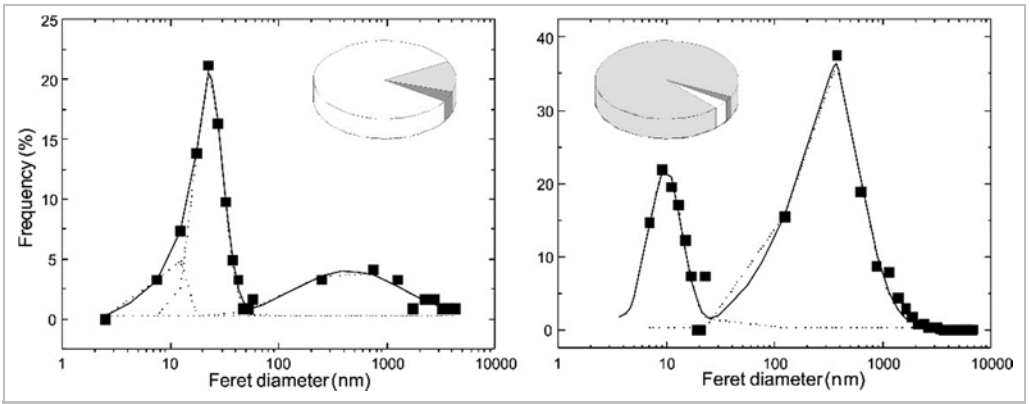

Figure 1: Size distribution of metal particles in welding fume (left) and cast iron foundry (right) aerosols. The pie plots report the relative abundance of ultrafine (white), fine (light grey) and coarse particles (dark grey).

To this purpose, particles from stainless steel welding fumes and cast iron foundry aerosols were characterized [3,4] by means of scanning and transmission electron microscopy coupled with image analysis, EDS microanalysis, electron diffraction and phase contrast imaging. In addition, the concentration and the solubility degree of Fe and other metals of potential

health effect (Cr, Ni, Mn, Zn and Pb) in the bulk samples were determined by inductively coupled plasma atomic emission spectrometry (ICP-AES).
Particle number size distributions revealed the dominant contribution of fine-ultrafine particles. The total surface area per unit mass of the aerosols was calculated giving high values in both aerosols. As the biological response to fine and ultrafine atmospheric particles is closely associated with surface area rather than mass concentration, these observations emphasize the necessity of employing surface area instead of gravimetric measurements when evaluating occupational exposure, particularly in the case of insoluble particles.
TEM structural determinations of nanoparticles revealed the major occurrence of randomly oriented, highly crystalline, ordered magnetite nanocrystals. Particles showed high Fe and variable contents of Mn, Si, Cr, Ni, Zn, and Pb. A trend of relative Ni, Mn, Si, Zn and Pb enrichment for decreasing particle size was also evidenced. These facts along with the measured low water-solubility of the dusts point to a remarkable toxic potential of both types of particles via cellular uptake. In addition, when considering the health risk in the foundry plant activities concomitant exposure to other cytotoxic and/or genotoxic agents (PAHs, graphite and crystalline silica) should be considered.

References

1. The Industrial Injuries Advisory Council, Position paper 29: Lung Cancer and Foundry Workers (2011).
2. The Industrial Injuries Advisory Council, Information note: Lung Cancer and welding Workers (2013).
3. B. Moroni, Grain size, chemistry, and structure of fine and ultrafine particles in stainless steel welding fumes, J. Aerosol Sci. 40, 939-949 (2009).
4. B. Moroni, Exposure vs toxicity levels of airborne quartz, metal and carbon particles in cast iron foundries, J. Expo. Sci. Environ. Epidemiol. 24, 42-50 (2014).

Self organization of nanoparticles and biomolecules on soft surfaces

Mrinmay K. Mukhopadhyay
Surface Physics & Material Science,
Saha Institute of Nuclear Physics, 1/AF Bidhannagar, Kolkata, 700064, India.

Email: *mrinmay.mukhopadhyay@saha.ac.in*
Keywords: biomembrane, nanoparticle, X-ray scattering

The understanding of self-organization of nanoparticles capped with organic molecules or the biomaterials is a matter of intense research in recent science due to its immense application in nanotechnology and biotechnology [1-3]. The physics behind this assembly arises from the competition of various forces like van der Waals, electrostatic, adhesion etc. between the molecules and the substrates. Solid substrates are being used routinely to understand the mechanism but strong interaction between the molecules and the substrates restricts the self-assembly and thus most of the time get the structures highly designed by the substrate morphology. Here we studied the structure of self-organization of nanoparticles and lipid bilayer membrane on water surface and polymer surfaces respectively using x-ray scattering techniques. We have measured the x-ray reflectivity (XRR) and grazing incidence small angle x-ray scattering (GISAXS) to understand the mechanism. A schematic of the sample environment for the nanoparticle and bio-membrane during x-ray scattering measurements is shown in Figure1.

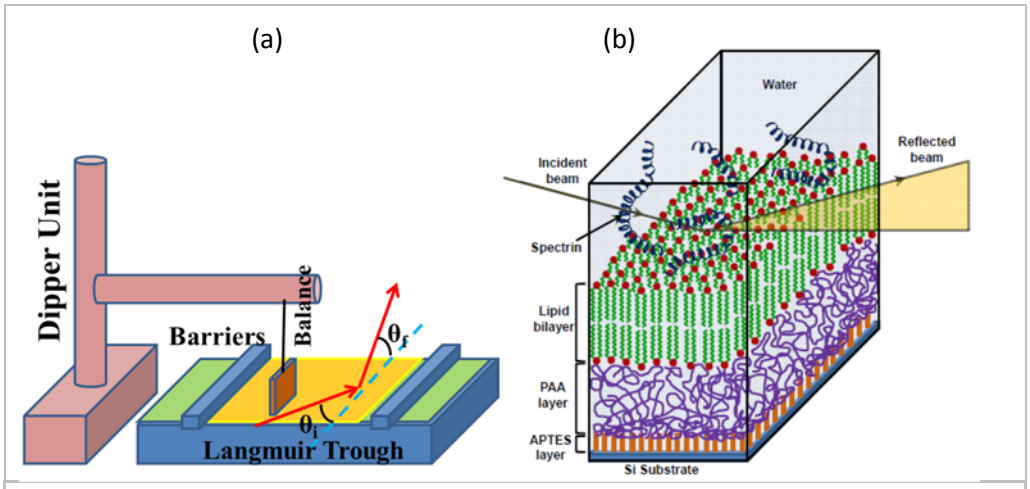

Figure 1: Schematic of the setup for x-ray scattering experiment from (a) monolayer on water surface and (b) lipid bilayer on polymer surface under water.

Two different shapes of nanoparticles were studied - (1) ODA coated spherical shape Au-nanoparticle and (2) ODA coated ZnS nanorods. These molecules were spread on water surface in a Langmuir trough and then XRR and GISAXS experiments were done at Indian Beamline, Photon factory, KEK, Japan. The results revealed a superlattice structure as a function of surface pressure for the Au nanoparticle. On the other side ZnS nanorods first grow along the length and then attach side by side to form a sheet on water surface.
Lipid bilayer membranes are stable only under water and we have prepared the membrane on a polymer brush to understand the transport mechanism of protein or other molecules through the lipid membranes [4]. The polymer brush maintains the fluidity of the lipid molecules and serves as the model system for the biological cells. XRR measurements were done at the X18A, NSLS, USA and Indian Beamline, Photon factory, KEK, Japan. The high energy of the incident x-ray beam allows us to measure the reflectivity from the samples under water. Results revealed the lipid head group specificity of the proteins attachment procedure and related organization of those molecules on the membrane surface.

Acknowledgement. I like to acknowledge the contribution from Mr. Rajendra Prasad Giri, Mr. Santanu Maiti, Prof. Somobrata Acharya and Prof. Milan K. Sanyal in this work.

References

1. Yugang Zhang et.al, A general strategy for the DNA-mediated self-assembly of functional nanoparticles into heterogeneous systems, Nature Nanotechnology **8**, 865 (2015).
2. Mrinal K. Bera et al, Reversible buckling in monolayer of gold nanoparticles on water surface, Europhys. Lett. **78**, 56003 (2007).
3. Somobrata Acharya et. al, A Bottom-up Approach Towards Fabrication of Ultrathin PbS Sheets, Nano Letters **13**, 409 (2013).
4. M. Tanaka, E. Sackmann, Polymer-supported membranes as models of the cell surface, Nature **437**, 656 (2005).

Diamond interfaces for protein and DNA sensing

Christoph E. Nebel
Fraunhofer-Institute for Applied Solid State Physics (IAF), Freiburg 79108, Germany

Email: *Christoph.nebel@iaf.fraunhofer.de*

In this presentation we introduce “diamond” with optimized surface properties to interact with DNA and the redox protein “cytochrome c”. For DNA sensing we bio-functionalize the diamond surface with nitrophenyl molecules and will describe the layer formation in detail. For protein-immobilization and -detection the diamond surface is terminated with a mixture of H-atoms and OH-molecules to generate a biomimetic surfaces.
We will introduce detailed properties with respect to a) surface modifications, b) sensing and c) chemical stability of these transduces applying a variety of electrochemical characterization methods, atomic force microscopy (AFM) with single molecule resolution, XPS, SEM and phenyl-grafting to identify H-bonding on the surface of diamond. The electrodes are single crystalline diamond layers with atomically smooth surfaces. The diamond films are grown by microwave-plasma assisted CVD. To achieve metallic conductivity at room temperature boron doping was applied with a boron density of about 10^{21} cm^{-3} as detected by SIMS.
These experiments reveal DNA sensitivities in the range of pico-mole with negligible degradation over 30 cycles of DNA hybridization and denaturation. For protein interaction we find that moderately OH-terminated diamond shows stable immobilization of Cytochrome *c* with high electron transfer activity, driven by a combination of electrostatic and hydrophobic interaction. This surface mimics natural binding partners, where coarse protein orientation is governed by electrostatic- and hydrophobic-interactions.

Laser and FIB assisted fabrication of conductive patterns on CVD diamonds

A. Notargiacomo[1*], D. Di Gioacchino[2], M. Pea[1], E. Giovine[1], A. Marcelli[2,3], G. Della Ventura[4], E. Pace[5], A. Puri[6]
[1]*Institute for Photonics and Nanotechnology, CNR-Rome, Italy*
[2]*INFN-Laboratori Nazionali di Frascati, Frascati (RM), Italy*
[3]*RICMASS, Rome International Center for Materials Science Superstripes, Rome, Italy*
[4]*Dipartimento di Scienze Geologiche, Università Roma Tre, Roma, Italy*
[5]*Università di Firenze, Dipartimento Fisica e Astronomia, Firenze, Italy*
[6]*CNR-IOM-OGG c/o ESRF, F-38043 Grenoble Cédex 9, France*

Email: *andrea.notargiacomo@ifn.cnr.it*
Keywords: diamond, conductive pattern, focused ion beam, laser

Diamond is an extraordinary material combining unique mechanical, optical and thermal properties [1] which make it suitable for applications in several research fields including high-power electronics, photo-detectors, devices for high-energy or astrophysics and high-pressure physics [2,3,4]. Many other applications demand diamond-based devices such as optimized micro-heaters and micro-thermometers [5] whose implementation is still at an early stage. In this framework we realized and characterized micro-conductive amorphous carbon paths by using either high-power laser or focused ion beam (FIB) techniques.

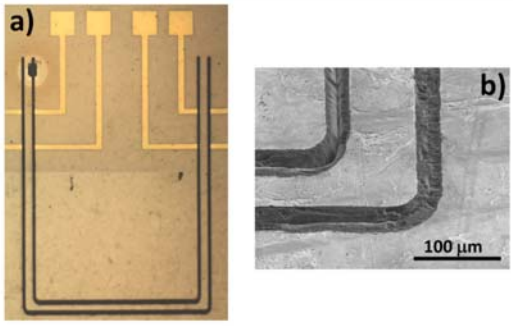

Figure 1: a) Optical image of diamond sample with a "u-shaped" laser pattern showing Au contact for current voltage characterization. b) SEM image detail of the laser pattern bend.

Graphitic resistive patterns were fabricated on a CVD diamond plate by a laser scriber [6]. Such a patterned device is rather low cost, can be easily manufactured and used both as temperature sensor and heating device. Different patterns (Fig. 1 shows double a "U-shaped" pattern) were fabricated by on the surface of the CVD diamond layers using a Nd:YAG laser under an inert protective gas. Black lines with different shapes and line resistance of ~15 Ω/mm were obtained at room temperature. The morphology of the graphitic lines was investigated by SEM showing a disordered structure of the darker regions treated with laser. Metallic contact pads were fabricated by electron beam lithography and lift-off in order to allow for electrical measurements in the four-probes configurations.
The graphitic patterns were fully characterized as thermometers or heaters. We measured the resistance vs. temperature data in a wide temperature range from 4.2 to 300 K (Fig 2a): the smooth behavior found allows to calibrate easily the thermometer response. Moreover, the simple interpolation allows to minimize the errors, thus improving the thermometer accuracy.

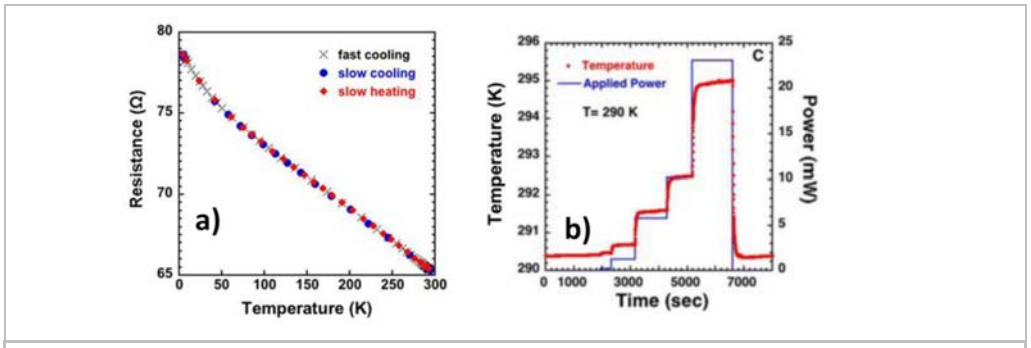

Figure 2: a) Resistance vs. temperature behavior of the thermometer device; b) temperature dependence vs. time as a function of applied power for the device used as heater.

In order to test the performance of the device as micro-heater we also characterized the heating response of the non-diamond carbon pattern using different electric current densities that provide different applied heat powers. We studied the response in different temperatures ranges between in the 4.2-and 300 K. Fig. 2b shows the dependence of temperature vs. time upon applying power at discrete parametric values as measured at room temperature. Moreover we have investigate the realization of the amorphous carbon layer using the focused ion beam Ga^+ ions implantation at 30 kV on a CVD diamond surface at ion currents in the (30 ÷ 300) pA range and ion dose between 0.1 pC/μm^2 and 300 pC/μm^2 [7]. Conductive layers were obtained with thickness up to ~20 nm (Fig 3a). High aspect ratio rectangular patterns were obtained and Ti electrical contacts were then deposited allowing for electrical characterization using a

four-probes configuration (Fig 3b). Electrical characterization showed an ohmic behavior (Fig 4a) and the conductivity of the FIB implanted stripes varied between 0.1 and 5.0 $(\Omega \cdot cm)^{-1}$ in the ion dose range investigated.

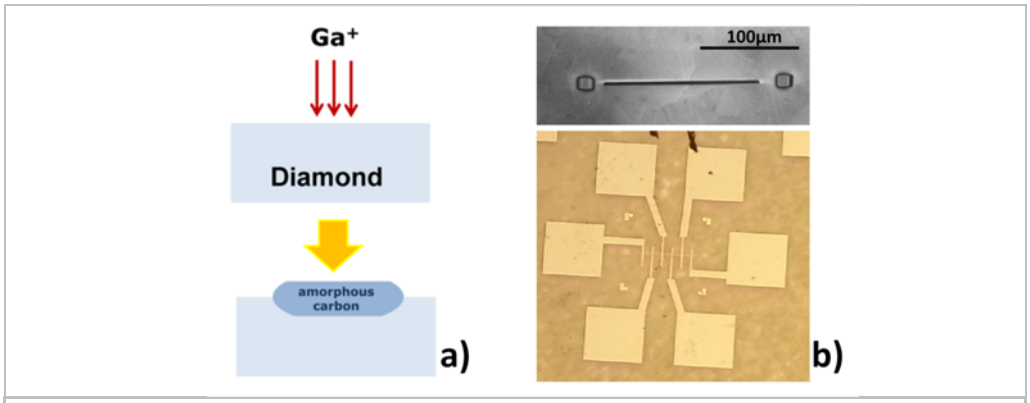

Figure 3: a) Schematic section of FIB implanted conductive area formation; b) SEM image of the implanted strip with markers; optical microscopy image of a device with contact pads.

The morphology of implanted areas were investigated by AFM showing surface swelling and rough surface with features that can be ascribed to chemical mechanical polishing of sample surface. In addition, conductive-AFM allowed to collect 2D current maps showing an inhomogeneous pattern of tip-sample current injection. I-V curves were collected in specific locations showed linear and non linear (not showed) behavior likely correlated to the level of conduction found in C-AFM maps.

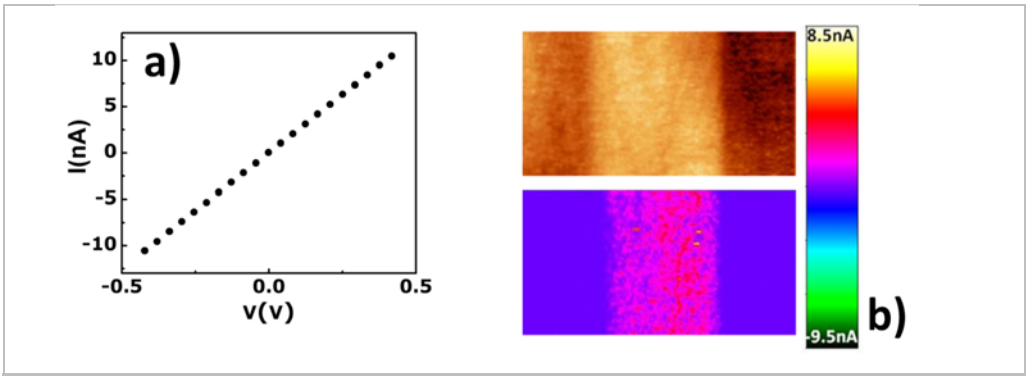

Figure 4: a) Current voltage measurement of a FIB implanted strip device. b) AFM (top) and corresponding current map (bottom) collected on a conductive diamond strip.

References

1. R. Kalish, Diamond as a unique high-tech electronic material: difficulties and prospects, J. Phys. D: Appl. Phys. 40, 6467-6478 (2007)
2. P. Tripodi, M.C.H. McKubre, F.L. Tanzella, P.A. Honnor, D. Di Gioacchino, et al., Temperature coefficient of resistivity at compositions approaching PdH, Physics Letters A 276 (1), 122-126 (2000)
3. P. Tripodi, D. Di Gioacchino, R. Borelli, J.D. Vinko, Possibility of high temperature superconducting phases in PdH, Physica C: Superconductivity 388, 571-572 (2003)
4. P. Tripodi, D. Di Gioacchino, J.D. Vinko, AC electrical resistance measurements of PdH_x samples versus composition x, J. All. Comp. 486, 55-59 (2009)
5. D.G. Cahill, K. Goodson, A. Majumdar, "Thermometry and Thermal Transport in Micro/Nanoscale Solid-State Devices and Structures, J. Heat Transfer 124, 223 (2002)
6. D. Di Gioacchino, A. Marcelli, A. Puri, A. De Sio, M. Cestelli Guidi, Y. Kamili, G. Della Ventura, A. Notargiacomo, P. Postorino, S. Mangialardo, E. Woerner, E. Pace, Graphitic patterns on CVD diamond plate as Microheating/Thermometer devices, ACS Appl. Mater. Interfaces 7, 10896 (2015)
7. M. Pea, E. Giovine, D. Di Gioacchino, A. Marcelli, G. Della Ventura, E. Pace, A. Notargiacomo, Morphological and electrical characterization of FIB implanted diamond surfaces, Microelectronic Engineering 141, 27-31 (2015)

Engineered Functional Nanomaterials for Energy Applications

Satishchandra B. Ogale
Department of Physics, Indian Institute of Science Education and Research, Dr. Homi Bhabha Road, Pune 411008, India

Email:*satishogale@gmail.com*
Keywords: engineered nanomaterials, solar energy, charge storage, solar water splitting, functional carbon.

Clean energy is possibly the most critical need of the present time in view of its implications for sustainable development. In all the three key sectors of renewable and clean energy research, namely conversion, storage and conservation, nanotechnology and new functional materials are contributing immensely to the domains of novelty, efficiency, versatility and potentially cost reduction. Nanomaterials, low dimensional materials, and their hybrid interfaces with molecular systems are of great interest in this regard in view of the diverse and interesting scenarios that are possible based on these platforms towards realization of effective device architectures for energy applications. A thrust towards clean energy is also bound to have a long term positive impact on our environment and by implication the health of living beings.

I will bring out some interesting elements of research being performed internationally in the area of clean energy through some examples derived from own work. The emphasis of the presentation in the case of energy conversion will be laid on solar energy harvesting; especially the sensitized and perovskite cells as well as solar water splitting for hydrogen generation. [1-7] Some examples of mechanical energy harvesting via nanogenerators will also be presented. The focus of the discussion on energy storage will be on functional carbon materials and other metal oxide/sulfide systems for ultracapacitor and battery applications. [8-14].

References

1. U Bansode, R Naphade, O Game, S Agarkar, SB Ogale, Hybrid Perovskite Films by a New Variant of Pulsed Excimer Laser Deposition: A Room-Temperature Dry Process *J. Phys. Chem. C 119*, 9177 (2015).
2. S Nagane, U Bansode, O Game, S Chhatre and SB Ogale, $CH_3NH_3PbI_{(3-x)}(BF_4)_x$: Molecular Ion substituted hybrid perovskite *Chem Comm.* 50, 9741 (2015).
3. R Naphade, M Tathavadekar, JP Jog, S Agarkar, SB Ogale, Plasmonic Light Harvesting of Dye Sensitized Solar Cells by Au-Nanoparticles Loaded TiO_2 Nanofibers, *J. Mater. Chem. A* 2, 975 (2014).

4. MC Tathavadekar, SA Agarkar, OS Game, UP Bansode, SA Kulkarni, SG Mhaisalkar and SB Ogale, Enhancing efficiency of perovskite solar cell via surface microstructuring: Superior grain growth and light harvesting effect, *Solar Energy* 112, 12 (2015).
5. A Deshpande, S Kelkar, S Rayalu, SB Ogale, Orthorhombic/Cubic Cd_2SnO_4 Nanojunctions: Enhancing Solar Water Splitting Efficiency by Suppression of Charge Recombination, *J. Mater. Chem. A* 2, 492 (2014).
6. A Sheikh, A Yengantiwar, M Deo, S Kelkar, SB Ogale, Near-Field Plasmonic Functionalization of Light Harvesting Oxide-Oxide Heterojunction for Efficient Solar Photochemical Water Splitting: The case of the Au NP / $ZnFe_2O_4$ / ZnO system, *Small* 9, 2091 (2013).
7. SA Kelkar, P Shaikh, SB Ogale, Nanostructured Cd_2SnO_4 as Energy Harvesting Photoanode for Solar Water Splitting, *Energy & Environ Sci.* 5, 5681 (2011).
8. D. Puthusseri, A Vanchiappan, M Srinivasan and SB Ogale, 3D micro-porous conducting carbon beehive by single step polymer carbonization for high performance supercapacitor: Role of in situ porogen formation, *Energy and Environ. Sci.* 7, 728 (2014).
9. D Puthusseri, B Anothumakkool, V Aravindan M, Srinivasan, K Sreekumar and SB Ogale, From waste paper basket to solid state and Li-HEC ultracapacitor electrodes: A value added journey for shredded office paper, *Small* 10, 4395 (2014).
10. A Banerjee, K Upadhyay, D Puthusseri, A Vanchiappan, M Srinivasan and SB Ogale, MOF-derived crumpled-sheet-assembled perforated carbon cuboids as highly effective cathode active materials for ultra-high energy density Li-ion hybrid electrochemical capacitors (Li-HECs), *Nanoscale* 6, 4387 (2014).
11. R Gokhale, V Aravindan, P Yadav, S Jain, D Phase, S Madhavi and SB Ogale, Oligomer-salt derived 3D, heavily nitrogen doped, porous carbon for Li-ion hybrid electrochemical capacitors application, *Carbon* 80, 460 (2014).
12. M Biswal, A Banerjee, M Deo, SB Ogale, From Dead Leaves to High Energy Density Supercapacitor, *Energy & Environ. Sci.* 6, 1249 (2013).
13. D Mhamane, A Suryawanshi, S Unni, CV Rode, S Kurungot, SB Ogale, Hierarchically nano-perforated graphene as a high performance electrode material for ultracapacitors, *Small* 9, 2801 (2013).
14. A Banerjee, S Bhatnagar, D Mhamane, V Aravindan, M Srinivasan and SB Ogale, Superior lithium storage properties of α-Fe_2O_3 nano-assembled spindles, Nano Energy 2, 5, 890 (2013).

Molecular materials for two-photon application in bioimaging and nanofabrication

Anna Painelli,* Cristina Sissa, Francesca Terenziani,
Siarhei Kurhuzenkau, Domna Nikolaidu,
Somananda Sanyal
Department of Chemistry, Parma University, Italy

Email: *anna.painelli@unipr.it*
Keywords: non-linear spectroscopy, 2-photon absorption, organic dyes and aggregates, theory and models.

2-photon absorption (2PA) is a third-order non-linear optical process where a material system is excited by the simultaneous absorption of two photons (we just refer for simplicity to one-beam processes, where two identical photons are absorbed). The probability of the 2PA process grows with the squared intensity of the light; so that using a focused laser beam it is possible to arrange things in such a way that 2PA only occurs in the tiny volume defined by the laser focus, the voxel (the elementary volume unit, in analogy with the pixel, the elementary surface unit). After excitation, the material may undergo different processes that can be exploited for different use. Here we focus on light-emission, exploited in 2-photon microscopy (2PM) and the generation of radicals, as needed for 2-photon induced polymerization (2PP). The two techniques have intrinsic 3D-resolution, opening new perspectives and possibilities in bio-imaging and fabrication.

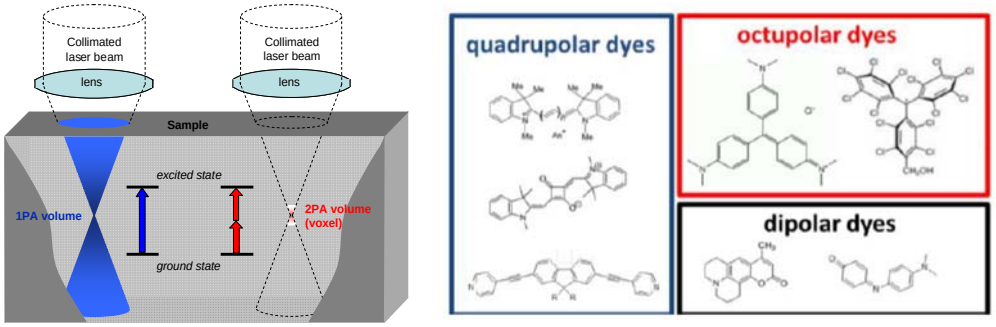

Figure 1. Left: a sketch of the excited sample volumes in a 1PA process (blue area) and in a 2PA process (red area). The volume excited in 2PA defines the unit voxel accessible in 2PM and 2PP applications. Right: the chemical structure of some dyes.

After a short introduction to the two processes, we address the requirements for the practical exploitation of the two techniques, putting special emphasis on the material requirements. Specifically, we are undertaking an extensive joint experimental and theoretical work to design optimized materials for the two applications. Our strategy of excited-state engineering combines results from quantum-chemical calculations and molecular dynamics to feed a family of parametric Hamiltonians (called essential-state models), with the aim to reliably describe low-energy spectral properties of a large family of chromophores, their aggregates and nanoparticles.
The models, validated through an extensive comparison with spectral data, are used to guide the synthesis of optimized materials for 2PA applications. The research leading to these results has received funding from the People Programme (Marie Curie Actions) of the European Union's Seventh Framework Programme FP7/2007-2013/ under REA grant agreement n°607721.

Local structural studies of BiS_2-based layered superconductors

E. Paris[*1,2], T. Sugimoto[3], Y. Mizuguchi[5], Y. Takano[6], T. Mizokawa[3,4], N.L. Saini[1]
[1]*Dipartimento di Fisica, Università di Roma Sapienza, Piaz.le Aldo Moro 2, 00185 Rome*
[2]*Center for Life NanoScience@Sapienza, Istituto Italiano di Tecnologia, Viale Regina Elena 291, 00185 Rome*
[3]*Department of Complexity Science and Engineering, University of Tokyo, 5-1-5 Kashiwanoha, Chiba 277-8561, Japan*
[4]*Department of Applied Physics, Waseda University, Tokyo 192-0397, Japan*
[5]*Department of Electrical and Electronic Engineering, Tokyo Metropolitan University, 1-1 Minami-osawa, Hachioji, Tokyo 192-0397, Japan*
[6]*National Institute for Materials Science, 1-2-1 Sengen, Tsukuba 305-0047, Japan*

Email: **eugenio.paris@uniroma1.it*
Keywords: superconductivity, lattice distortions, magnetism, electron doping

Discovery of superconductivity in $REOFBiS_2$ (RE = rare earth) has triggered theoretical and experimental efforts to understand the pairing mechanism. These materials show a layered structure with BiS_2 layers, which becomes superconducting after electron doping, alternated with rare-earth oxide layers, which act as a charge reservoir.

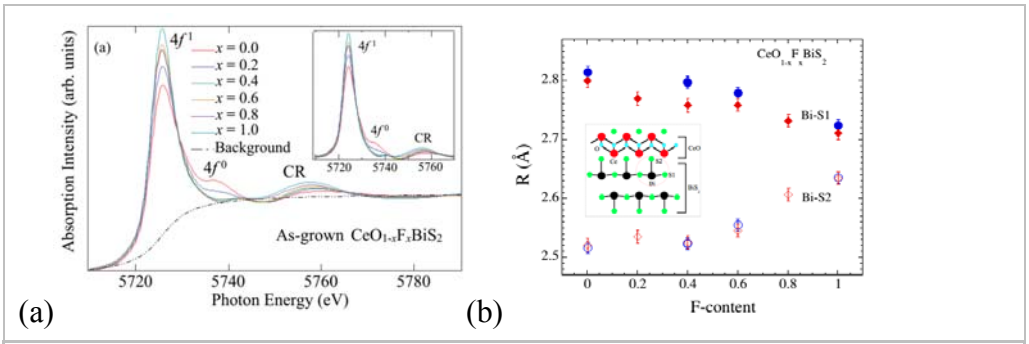

Figure 1: (a) Ce L_3-edge of $Ce(O/F)BiS_2$ as a function of fluorine doping, inset shows background subtracted data; (b) bismuth-sulphur distance as a function of fluorine doping, as extracted from Bi L_3-edge EXAFS.

These properties are shared by unconventional superconductors like the cuprates and the iron based family. The analogy with these materials is enriched

by the multiband nature of the Fermi surface, the indication of nesting and the coexistence of superconductivity and magnetism, which are peculiar characteristics of iron based superconductors.

A peculiar feature of the superconducting state is the high sensitivity to external pressure, chemical pressure and high-pressure sample synthesis. This is a clear indication of a strong interplay between structural distortions and transport and electronic properties in this class of materials. We have used X-ray absorption spectroscopy to study the effects of doping in the local structure and the valence electronic states in $CeO_{1-x}F_xBiS_2$. We find that Bi-S local correlations evolve systematically with fluorine substitution bringing the system to a decoupling between the BiS_2 and CeO layer, hence coexistence of superconductivity and ferromagnetism [1,2].

Results will be discussed in the frame of an interplay between local structural deformations and electronic properties in $CeO_{1-x}F_xBiS_2$. In addition, we have also investigated the effect of chemical pressure, which is known to dramatically affect superconductivity, by changing mean rare earth size. In particular the local effect of substitution of the rare-earth with Ce, Nd, Sm encompassing a wide range of ionic radius will be discussed [3].

References

1. T. Sugimoto, B. Joseph, E. Paris, A. Iadecola, T. Mizokawa, S. Demura, Y. Mizuguchi, Y. Takano and N. L. Saini, Phys. Rev. B 89, 201117 (R) (2014).
2. E. Paris, B. Joseph, A. Iadecola, T. Sugimoto, L. Olivi, S. Demura, Y. Mizuguchi, Y. Takano, T. Mizokawa & N. L. Saini, J. Phys. Condens. Matter 26, 435701 (2014).
3. Y. Mizuguchi, E. Paris, T. Sugimoto, A. Iadecola, J. Kajitani, O. Miura, T. Mizokawa, N. L. Saini, to be published (2015).

BCS-BEC crossover in quantum confined superconductors and superfluids at the nanoscale

Andrea Perali
School of Pharmacy, Physics Unit, University of Camerino, 62032 Camerino, Italy

Email: *andrea.perali@unicam.it*
Keywords: BCS-BEC crossover, multigap superconductivity, nanoscale superconductivity, shape resonances.

Superconductivity in iron-based, magnesium diborides, and other novel superconducting materials has a strong multi-band and multi-gap character [1,2] and recent experimental evidences support the possibility for a BCS-BEC crossover induced by strong-coupling and proximity of the chemical potential to the band edge of one of the bands [3,4]. BCS-BEC crossover at the band edge has been also predicted in superconducting stripes [2]. Here we study the simplest theoretical model which accounts for the BCS-BEC crossover in a two-band / two-gap superconductor, considering tunable interactions. Mean-field results - condensate fraction, correlation length, superconducting gaps - are reported in crossover diagrams to locate the boundaries of the different pairing regimes.

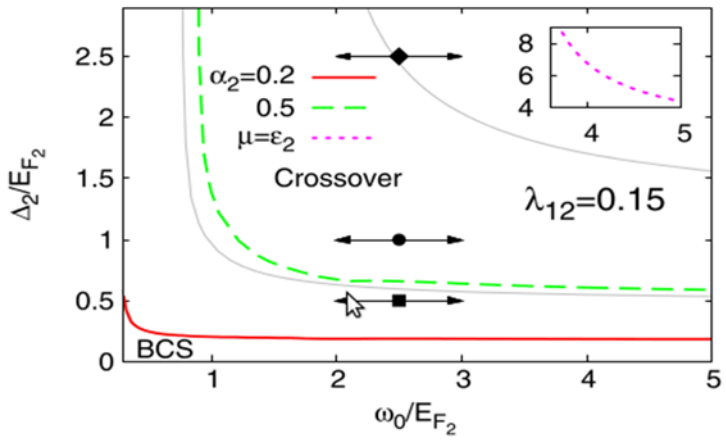

Figure 1: (from Ref. [6]). Crossover boundary diagram for the gap in the narrow band as a function of the cutoff frequency to which correspond condensate fractions $\alpha = 0.2, 0.5$ and chemical potential $\mu = \varepsilon 2$ in the two-band system with $\varepsilon 2 = 0.5$, $\lambda 11 = \lambda 12 = \lambda 21 = 0.15$. The lines for the one-band system (thin grey lines) for the gap to which correspond condensate fractions $\alpha = 0.2, 0.5$ and chemical potential $\mu = 0$ are also reported for reference. Inset: value of the $\Delta 2/EF2$ when $\mu = \varepsilon 2$. The points $\Delta 2/EF2 = 0.5, 1.0$ and 2.5 correspond to the experimental values for iron-based materials.

When the gap is of the order of the local chemical potential, superconductivity is in the crossover regime of the BCS-BEC crossover and the Fermi surface of the small band is completely smeared by the gap opening. In this situation, small and large Cooper pairs coexist in the total condensate, which is the optimal condition for high-Tc superconductivity [5]. The ratio between the gap and the Fermi energy in a given band results to be the best detection parameter for experiments to locate the system in the BCS-BEC crossover. Using available experimental data, our analysis shows that iron-based superconductors have the partial condensate of the small Fermi surface which is in the crossover regime of the BCS-BEC crossover [6], supporting in this way the recent ARPES findings [7,8] (see Figure 1).
We also discuss different physical systems in which the multigap and multiband BCS-BEC crossover can be realized. Two examples are considered here: (i) superconducting stripes in which shape resonances and multigap physics at the band edge play a cooperative role in enhancing superconductivity in the crossover regime of pairing [2], and (ii) superfluidity in ultracold fermionic gases confined in quasi-1D traps [9]. In the case of superconducting stripes, we review the experimental state of the art and recent progresses in this field.

References

1. S.V. Borisenko et al., Symmetry **4**, 251 (2012)
   see also: http://www.multisuper.org
2. A. Bianconi, A. Valletta, A. Perali, N.L. Saini, Physica C **296**, 269 (1998).
3. D. Innocenti, N. Poccia, A. Ricci, A. Valletta, S. Caprara, A. Perali, and A. Bianconi, Phys. Rev. B **82**, 184528 (2010).
4. A. Bianconi, Nature Phys. **9**, 536 (2013).
5. A. Perali, C. Castellani, C. Di Castro, M. Grilli, E. Piegari, and A. A. Varlamov, Phys. Rev. B **62**, R9295 (2000).
6. A. Guidini and A. Perali, Supercond. Sci. Technol. **27**, 124002 (2014).
7. Y. Lubashevsky, E. Lahoud, E. Chashka, E. Podolsky and A. Kanigel, Nat. Phys. **8**, 309 (2012).
8. K. Okazaki et al., Sci. Rep. 4, 4109 (2014).
9. A.A. Shanenko, M.D. Croitoru, A.V. Vagov, V.M. Axt, A. Perali and F.M. Peeters, Phys. Rev. A 86, 033612 (2012).

Enhancement of Structural and Optical Properties of TiO_2-ZrO_2 Nanocomposite by Zn, Ce, Co-doping

Piyush J. Bhatt*, Laxmi J. Tomar,
Bishwajit S. Chakrabarty
Applied Physics Department, Faculty of Technology & Engineering, The M. S. University of Baroda, Vadodara, Gujarat, India.

Email: **piyush.j.bhatt@gmail.com*
Keywords: nanocomposite, hydrothermal method, optical properties, structural properties

TiO_2 is a wide bandgap semiconducting material. Being chemically inert, cheap and easy to synthesis, it has been widely used in catalysis, photovoltaic, water splitting, paint etc. [1-2]. It has been reported that mixing of ZrO_2 with TiO_2 produces new crystallographic structure having large surface area and high porosity [5]. These mixed oxides show different optical and structural properties than the parent oxides [6]. In the present work we have tried to change optical and structural properties of TiO_2-ZrO_2 mixed oxides by doping Al and Ce which will be useful for dye sensitized solar cell application. A wide difference in ionic radius of Zn^{+2},Ce^{+3},Ti^{+3} and Zr^{+4} will produce defect and strain in material, hence significant change in optical and structural properties will be produced.
Zn, Ce co-doped TiO_2-ZrO_2 (TZ) nano composites have been prepared by hydrothermal method. The structural and optical properties of the obtained samples were investigated by X–ray diffraction (XRD) and UV-Visible spectroscopy, respectively. The composition of samples was confirmed by FTIR spectroscopy. It has been found that the crystallite size of all the samples was distributed in the range 6.02 to 17.41 nm. The content of Anatase phase varied in the range 48.71% to 93.50% depending on doping. The dopants produced lattice strain in material and it was found between 0.027 - 0.069. The absorption band for Ti-O-Ti bond has been observed in FTIR spectra. The absorptions related to impurity do not found in FTIR spectra, which show formation of material in pure form. A clear shift of absorption edge for different dopants has been observed from UV-Visible absorption spectra. The optical bandgap varies from 2.04 eV to 3.97 eV. The change in refractive index, absorption co efficient and optical conductivity was also evaluated from absorption spectra.

References

1. L. Yan, H. YanBing, J. Hui, S. QuanMin, W. Yan and F. ZhiHui, Photovoltaic properties of MEH-PPV/TiO_2 nanocomposites, Chinese Science Bulletin. 53, 2743 (2008).

2. J. Tang, J. R. Durrant and D. R. Klug, Mechanism of Photocatalytic Water Splitting in TiO_2. Reaction of Water with Photoholes, Importance of Charge Carrier Dynamics, and Evidence for Four-Hole Chemistry, J. Am. Chem. Soc. 130, 13885 (2008).
5. A. Kitiyanan, S. Pavasupree, T. Kato, Y. Suzuki and S. Yoshikawa, TiO_2-ZrO_2 mixed metal oxide electrode for a dye sensitized solar cell, As. J. Energy Env. 6, 165 (2005).
6. L. J. Tomar and B. S. Chakrabarty, Synthesis, structural and optical properties of TiO_2-ZrO_2 nanocomposite by hydrothermal method, Adv. Mat. Lett. 4, 64 (2013).

The dynamic vortex-Mott-insulator to metal transition

Nicola Poccia,[1,2,*] Tatyana I. Baturina,[3,4,5] Francesco Coneri,[1] Cor G. Molenaar,[1] X. Renshaw Wang,[1] Ginestra Bianconi,[6] Alexander Brinkman,[1] Hans Hilgenkamp, Alexander A. Golubov,[1,7] Valerii M. Vinokur[5]
[1]*NEST, Istituto Nanoscienze - CNR and Scuola Normale Superiore, P.za San Silvestro 12, I-56127 Pisa, Italy*
[2]*MESA+ Institute for Nanotechnology, University of Twente, 7500 AE Enschede, Netherlands*
[3]*A.V. Rzhanov Institute of Semiconductor Physics, Siberian Branch of the Russian Academy of Sciences, Novosibirsk 630090, Russia.*
[4]*Novosibirsk State University, Novosibirsk 630090, Russia.*
[5]*Materials Science Division, Argonne National Laboratory, Argonne, IL 60637, USA.*
[6]*School of Mathematical Sciences, Queen Mary University of London, London E1 4NS, UK.*
[7]*Moscow Institute of Physics and Technology, Dolgoprudnyi, Moscow District, Russia.*

Email: *nicola.poccia@nano.cnr.it*
Keywords: critical phenomena, non-equilibrium phenomena, Josephson junction, nanoscale superconductivity, vortex-Mott-transitions.

Equilibrium statistical mechanics described the physics of condensed matter for more than one hundred years. However, the preponderance of the natural phenomena, including life, involves energy flow (e.g. chemical, electric or thermal currents) [1]. From photosynthesis to earthquakes, we do not yet have the physics to describe it well. Phase transitions and criticality far from equilibrium are in fact less well understood since often arise in systems with multi-scale spatial inhomogeneities [2-6] and critical evolution [7,8]. However, the experimental evidence for universality of non-equilibrium phase transitions is still scarce, calling for intensified experimental efforts.
A network of superconducting islands realized on the top of a normal metal film offers a tunable realization of multi-scale superconductivity [9]. In this system the competition of vortex states can be investigated and the phase transitions between them induced. An eggcrate potential is created in a square network of superconducting islands and in which vortices can be induced by a magnetic field. At precise value of the magnetic field, vortices can be frozen into a vortex-Mott-insulator. An external applied electric current determines the dynamic vortex-Mott-insulator to vortex-metal transition. We can measure

therefore the critical exponents that coincided with those for thermodynamic liquid-gas transition.
The dip-to-peak reversal heralds a dynamic phase transition in the vortex system, jumping as a function of the applied current from a non-equilibrium vortex-Mott- insulating state to a non-equilibrium metallic state. Actually, this dip-to-peak reversal, that is not present in the resistance, rules out the explanation of this phenomenon as depinning.

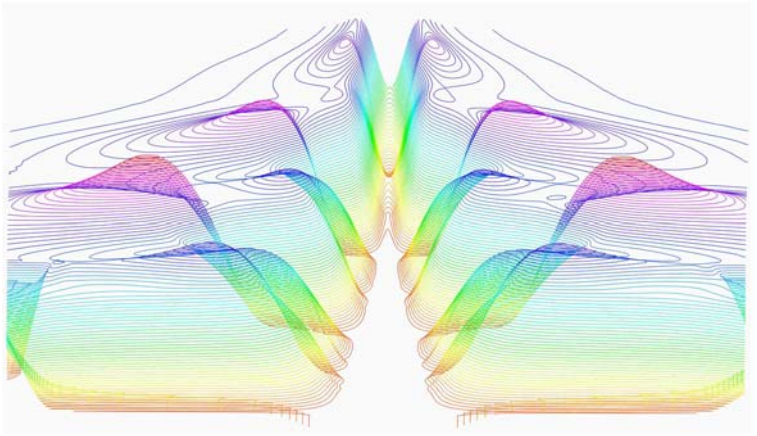

Figure 1: Contour plot of the differential resistance dV/dI. The current is displayed on the horizontal and the frustration factor along the vertical. At low current bias, the differential resistance minima at the frustration factors f = 1/3, 1/2, 2/3, 1, 3/2, 2, 7 are visible. When increasing the current a reverse of minima to maxima (violet) is observed [9].

The physics of Mott transitions driven by a current and their dynamic critical behaviour is unveiled by these results. The results also establish a connection between equilibrium and non-equilibrium phase transitions.
These results strongly encourage the search for artificial superconducting networks with novel phase transitions. Exploiting the dynamic Mott transition physics in artificial superconducting networks that make use of nanoscale phase engineering and of the sharp switch in the character of the differential resistance (differential conductance) is a promising possible prospect for applications in an emerging new generation electronics based on critical collective behaviours far-from equilibrium.

Reference

1. N. Poccia, A. Ansuini, and A. Bianconi, *International Journal of Molecular Sciences* **12**, 6810 (2011).

2. M. Fratini, N. Poccia, A. Ricci, G. Campi, M. Burghammer, G. Aeppli, and A. Bianconi, *Nature* **466**, 841 (2010)
3. N. Poccia, A. Ricci, and A. Bianconi, *Journal of Superconductivity and Novel Magnetism* **24**, 1195 (2011).
3. N. Poccia, A. Ricci, G. Campi, M. Fratini, A. Puri, D. Di Gioacchino, A. Marcelli, M. Reynolds, M. Burghammer, N. L. Saini, et al., *Proceedings of the National Academy of Sciences* **109**, 15685 (2012).
4. A. Ricci, N. Poccia, G. Campi, F. Coneri, A. S. Caporale, D. Innocenti, M. Burghammer, M. Zimmermann, and A. Bianconi, *Scientific Reports* **3** (2013).
5. A. Ricci, N. Poccia, G. Campi, B. Joseph, G. Arrighetti, L. Barba, M. Reynolds, M. Burghammer, H. Takeya, Y. Mizuguchi, et al., *Physical Review B* **84**, 060511+ (2011).
6. G. Campi, A. Bianconi, N. Poccia, G. Bianconi, L. Barba, G. Arrighetti, D. Innocenti, J. Karpinski, N. D. Zhigadlo, S. M. Kazakov, et al., *Nature* **525**, 359 (2015).
7. N. Poccia, M. Fratini, A. Ricci, G. Campi, L. Barba, A. Vittorini-Orgeas, G. Bianconi, G. Aeppli, and A. Bianconi, *Nature Materials* **10**, 733 (2011).
8. X. R. Wang, C. J. Li, W. M. Lü, T. R. Paudel, D. P. Leusink, M. Hoek, N. Poccia, A. Vailionis, T. Venkatesan, J. M. D. Coey, et al., *Science* **349**, 716 (2015).
9. N. Poccia, T. I. Baturina, F. Coneri, C. G. Molenaar, X. R. Wang, G. Bianconi, A. Brinkman, H. Hilgenkamp, A. A. Golubov, and V. M. Vinokur, *Science* **349**, 1202 (2015).

Influence of Arc Discharge Power on the Morphology and Magnetism of Cobalt based Nanostructures

Prachi B. Orpe[1,2,], Balasubramanian C.[1]
[1]*F.C.I.P.T Division, Institute for Plasma Research, A-10/B, G.I.D.C Electronics Estate, Sector-25, Gandhinagar -382044, India*
[2]*Nirma University, S-G Highway, Chandlodia, Ahmedabad, Gujarat- 382481, India*

Email: *prachi@ipr.res.in*

Keywords: arc discharge, cobalt based nanostructures, magnetism

The high temperature processing route such as arc discharge, always have been attractive method for synthesizing nanostructures, due to its low cost and bulk synthesis of nanopowders [1]. These high temperatures of the arc affect the morphology of the particles formed and so, the nanoparticles synthesize vastly differ in their properties from other low temperature synthesis processes [2-5]. It has been expected that this high temperature leads to high cooling rate which result into thermal stress onto the particles getting nucleated. Due to this, atomic ordering/disordering is also different from other nanoparticles.
In the present work, cobalt based magnetic nanostructures are synthesized using thermal arc plasma route under ambient He gas conditions. Herein we have studied the effect of arc power by varying three different currents 50 A, 100 A and 150 A, onto its morphology and thus on magnetism.

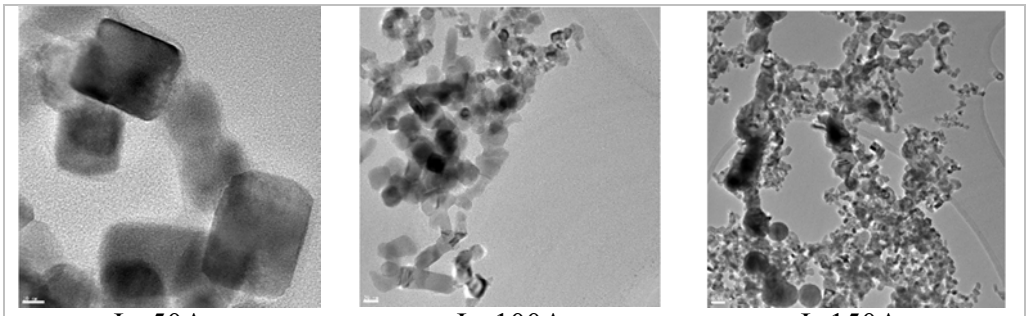

I =50A I =100A I=150A

Figure 1. TEM Images of cobalt based nanostructures for three different arc currents.

Morphological analysis is carried using Transmission Electron Microscopy technique wherein variation in the size distribution as well as shape diversity is observed with varying arc current. For low arc power, cubic nanoparticles with size in range of 25-30 nm were observed. While for higher arc power of 3.8

kVA, the growth of nanoparticles is higher resulting into large size particles. Therefore, the size distribution lies in the range of 50-55 nm. Diverse shapes such as hexagons and spheres are observed, apart from cubes. When the arc power is further increase to 6.750 kVA, drastic reduction in size distribution of 15-20 nm is observed. This is because of sharp temperature gradient, as more amount of power is given into the system, while arcing. The EDAX characterization also indicates the highest un reacted cobalt is found in 3.8 kVA samples which match with X-Ray Diffraction analysis were peaks of Co is observed apart from CoO.

Magnetic properties for as synthesized nanostructures were studied using Vibrating Sample Magnetometer (VSM). This characterization indicates that the highest coercivity is observed for the arc power of 3.8 kVA i.e. when arc current is 100 A. This matches with the EDAX data that with increasing number of unreacted cobalt, more amount of reverse field is required to bring it to original state.

The above result shows that arc power plays very crucial role on the morphology and is deciding factor for magnetic properties of cobalt based nanoparticles.

References

1. Wei Zhi-qiang, Xia Tian-dong, Ma Jun, Dai Jian-feng, Feng Wang-jun, Wang Qing, Yan Peng-xun, Growth mechanism of Cu nanopowders prepared by anodic arc plasma, Trans. Nonferrous Met. Soc. 16 (2006).
2. Caom s, Deng q g., Synthesis of nitride-iron nano meter powder by thermal chemical vapour-phase reaction method, J. Inorg. Chem. 12 (1996).
3. Karthikeyan J. Berndt C C, Tikkanen, Plasma spray synthesis of nanomaterials powders and deposits, J. Mater. Sci. Eng A238 (1997).
4. Gunther B, Kumpann A., Ultrafine oxide powders prepared by inter gas evaporation, J. Nanostruct. Mater. 1 (1992).
5. Chen D H, HE X R, Synthesis of nickel ferrite nanoparticles by sol-gel method, J. Mater. Res. Bulletin 36 (2001).

Effect of arc discharge currents on the structural and magnetic properties of iron based nanostructures

Prachi B. Orpe[1,2], Balasubramanian C.[1]
[1]*F.C.I.P.T Division, Institute for Plasma Research, A-10/B, G.I.D.C Electronics Estate, Sector-25, Gandhinagar - 382044, India*
[2]*Nirma University, S-G Highway, Chandlodia, Ahmedabad, Gujarat - 382481, India*

Email: *prachi@ipr.res.in*

Keywords: arc discharge current, magnetism, iron based nanostructures

Magnetic properties of the material are observed to change when a material dimensions are scaled down to nano scale [1]. This is mainly because of dependence magnetic properties such as coercivity, magnetic saturation, blocking temperature on the size, shape, surface chemistry which varies as dimensions are lower to nanoscale [2]. The enhanced magnetic properties of nanomaterials show wide range of applications from high density magnetic recording media to biomedical applications [3-4]. To synthesize such controlled size and shaped nanoparticles nanomaterials, there are top-down approaches and bottom-up approaches. Amongst all these route, thermal plasma is novel technique to synthesis the nanoparticles. The high temperature restricts the growth of particles during the nucleation stage itself and also the crystallinity of the material is also preserved. This high temperature is also responsible for inducing thermal stresses during the nucleation, due to which ordering of atoms is affected which further affect the size distribution and shapes of nanoparticles formed. The temperature in thermal plasma can be varied by changing discharge current.

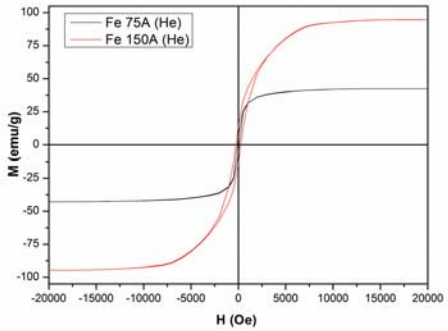

Figure 1: Hysteresis plot of iron based nanostructures for two different arc currents.

In the present work, iron based magnetic nanostructures are synthesized using thermal arc plasma route under ambient He gas conditions. Herein we have studied the effect of arc currents by varying three different currents 75 A and 150 A, onto its structure and thus on magnetism.

X-Ray Diffraction studies are done to observe the phase changes for these two arc current viz. 75 A and 150 A. The study shows that under He atmosphere, all peaks in case of 75 A arc current corresponds to Fe_2O_3 phase. The average crystallite size calculated from the Scherrer formula is 31 nm. While, a sharp peak of unreacted iron at higher arc current i.e. 150 A is seen. This indicates that higher arc currents due to sharp temperature gradient there is also possibility of formation of Fe nanoparticles, along with Fe_2O_3. The average crystallite size in case of 150 A is 18 nm. Decrease in size can be related to sharp gradient at higher arc current which restrict the growth of nanoparticles during nucleation stage itself.

The magnetic properties were studied using Vibrating Sample Magnetometer. This study indicated that higher coercivity is observed for higher arc current, i.e. for 75 A the coercivity is 118.8 Oe while for 150 A it is 266.7 Oe. Also the value of saturation magnetization has increased. This is due to formation of unreacted Fe nanoparticles along with Fe_2O_3. The remnant magnetization is observed to be higher for higher arc current. This also indicates that enhancement in magnetization is mainly achieved by increasing the arc discharge current.

References

1. Isabelle M.L. Billas, A. Chatelain, Walt A. De Heer, Magnetism from the Atom to the bulk in Iron, Cobalt and Nickel Clusters, Science 265 (1994).
2. I. Banerjee, Y.B. Khollam, Balasubramanian C., R. Pasricha, P.P. Bakre, K.R. Patil, A.K. Das, S.V. Bhoraskar, Preparation of γ-Fe_2O_3 nanoparticles using DC thermal arc-plasma route, their characterization and magnetic properties, Scripta Materialia 52 (2006).
3. Hwan-Gi kim, Heon Lee, Byung Hoon Kim, Sun-Jae Kim, Ji-Myon Lee, Sana-chul Jung, Synthesos Process of Cobalt Nanoparticles in Liquid-Phase Plasma, Jap. J. App. Phys. 52 (2013).
4. Nina Matoussevitch, Angelike Gorschinski, Wilhelm Habicht, Jens Bolle, Eckhard Dinjus, Helmut Bonnemann, Silke Behrens, Surface modification of metallic Co nanoparticles, J. Mag. & Mag. Mater. 311 (2007).

Electric Field Effects in Oxides Hetero-Interfaces with Bismuth Ferrite

Abhimanyu Rana[1,2*], Haidong Lu[3], Kashinath Bogle[1], Qi Zhang[1], Rama Vasudevan[1], Vishal Thakare[2], Alexei Gruverman[3], Satishchandra Ogale[2] and Nagarajan Valanoor
[1]*University of New South Wales, Sydney (Australia)*
[2]*National Chemical Laboratory (NCL), Pune (India)*
[3]*University of Nebraska – Lincoln (USA)*
**Currently at University of Twente (Netherlands)*

Email: **rana.abhimanyu@gmail.com*
Keywords: field effects, resistive switching, ferroelectrics

Electric field effects in oxides hetero-interfaces have been of immense interest in oxide electronics [1]. Ferroelectrics have particularly attracted significant attention as tunneling barrier [2,3] and gate dielectric materials [4]. In our recent work [5], we investigated the resistive switching in epitaxial multiferroic $BiFeO_3$ (BFO) heterostructure with $La_{0.67}Sr_{0.33}MnO_3$ for varying lengths scales in both the thickness and lateral directions. We combined the macroscale current–voltage measurements in conjunction with local scanning probe microscopy techniques to study resistive switching in current-perpendicular-to-plane configuration (as shown in the Figure). We discussed the polarization control of electron tunneling and an electronic reconstruction at the interface for distinct thickness regime. We further revealed the conduction through ferroelectric domains (as opposed to domain walls) in ultra-thin epitaxial heterostructures.

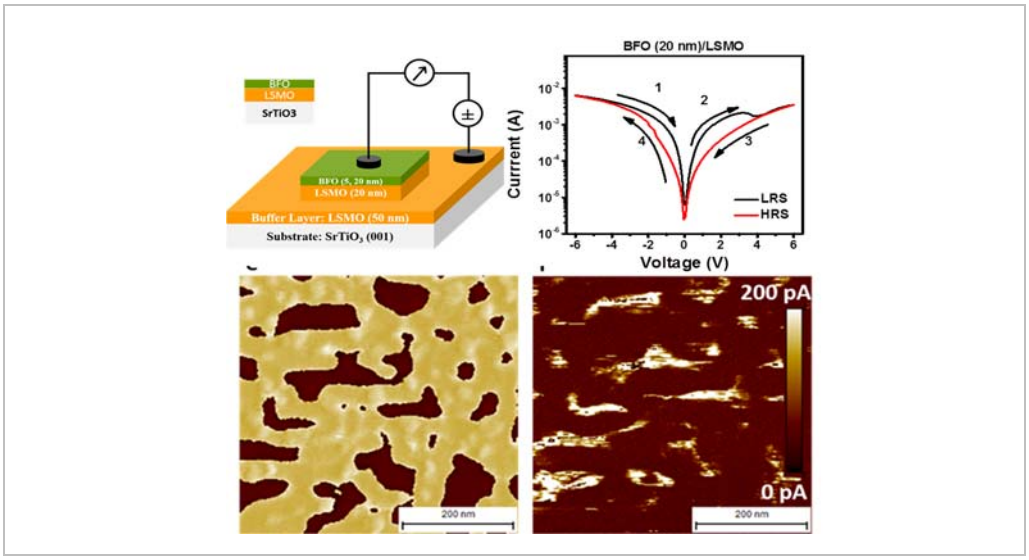

References

1. C.H. Ahn et al., Nature 424, 1015 (2003)
2. M. Hambe et al., Adv. Funct. Mater. 20, 2436 (2010)
3. Y. W. Yin et al., Nat. Mater. 12, 397 (2013)
4. S.M. Wu et al., Phys. Rev. Lett. 110, 0672202 (2013)
5. A. Rana et al., Adv. Funct. Mater. 24, 3962 (2014)

Investigation of sticking behaviour of silver atoms on patterned substrate with RBS

Mukesh Ranjan
FCIPT, Institute for Plasma Research, Gandhinagar, Gujarat

Email: *ranjanm@ipr.res.in*
Keywords: RBS, ripple pattern, silver nanoparticles, sticking

Rutherford Backscattering Spectrometry (RBS) is a widely used nuclear method for the near surface layer analysis of solids. A target is bombarded with ions at an energy in the MeV-range (typically 0.5–4 MeV), and the energy of the backscattered projectiles is recorded with an energy sensitive detector, typically a solid state detector. RBS allows the quantitative determination of the composition of a material and depth profiling of individual elements. In the current work in-situ RBS technique is used to study the sticking tendency of silver adatoms on flat as well as rippled patterned substrate.

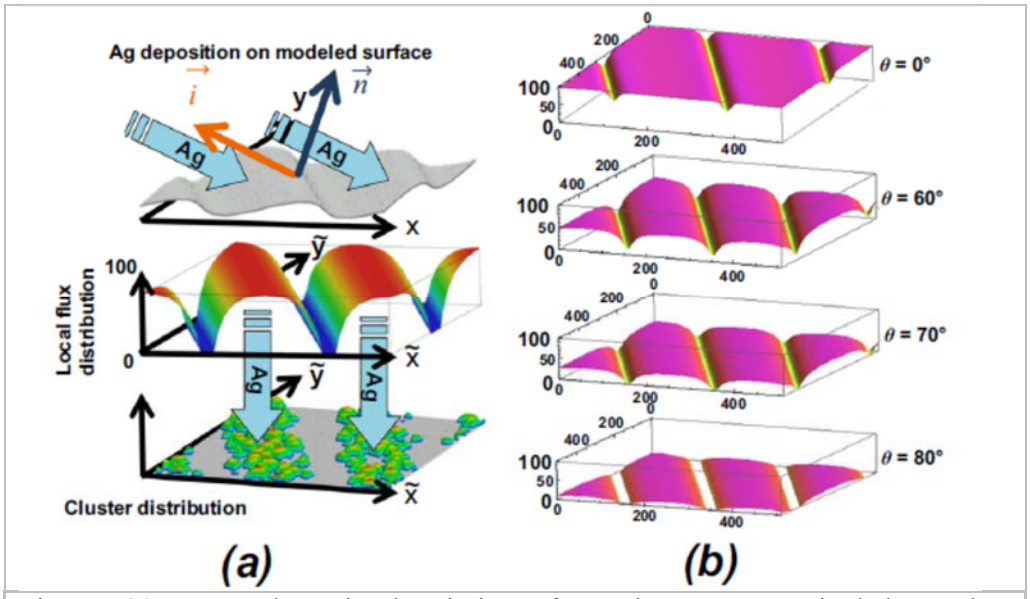

Figure: (a) Top: schematic description of angular PVD on rippled template represented by a surface fitting function z = h(x,y). Middle: normalized local flux distribution with respect to (x,y) plane. Bottom: a cluster growth simulation model under normal deposition with the corresponding inhomogeneous local flux on the flat surface. Used axis and vectors directions are shown in the top image. (b) Local flux distribution at different angle of incidence. The rate is normalized by the maximum flux observed at θ = 0°.

Study of the surface adatom diffusion kinetics and the local flux variation seems to be important for this self-assembly process on ripple pattern surface. It was observed that patterned substrate have higher sticking and it rises sharply below one monolayer of atom. We propose the local flux variation model based on the ripple asymmetric tilt and the local incident angle, which explains the self-assembly process nicely in terms of the nanoparticle size distribution. Based on RBS measurement and model best self-assembly at $\pm 70^{o}$ with respect to surface normal is explained even-though this angle is out of shadow deposition regime.

References

1. M. Ranjan, S. Numazawa and S. Mukherjee, *Mat. Res. Exp.* 1, 015038 (**2014**).
2. M. Bozoian, *Nucl. Instr. Meth.* B 82, 602 (**1993**).
3. Q. Zhou, Z. Li, J. Ni and Z. Zhang, *Mat. Trans.*, 52(3), 469 (**2011**).
4. Y. Suzuki, Y. Sumi,1 K. Kita, T. Miyanaga and K. Sagisaka, *Surf. Interface Anal.* 38, 1296 (**2006**).

Critical dynamics and inhomogeneity in complex materials

A. Ricci[1]*, G. Campi[2], N. Poccia[3], A. Bianconi[4]
[1]*Deutsches Elektronen-Synchrotron DESY, Notkestraße 85, D-22607 Hamburg, Germany*
[2]*Institute of Crystallography, CNR, via Salaria Km 29.300, Monterotondo Roma, I-00015, Italy*
[3]*MESA+ Institute for Nanotechnology, University of Twente, PO Box 217, 7500AE Enschede, Netherlands*
[4]*Rome International Center for Materials Science, Superstripes, RICMASS, via dei Sabelli 119A, I-00185 Roma, Italy*

Email: **alessandro.ricci@desy.de*
Keywords inhomogeneous superconductors, critical fluctuations, charge-stripes, spin-stripes, defects-stripes, nanoscale phase separation

Functional materials like high temperature superconductors (HTS) and complex oxides are characterized by an *intrinsic complexity*. Indeed, they show the coexistence of multiple striped-orders like Charge-Density-Wave (CDW), Spin-Density-Wave (SDW) and defects that get organized in different striped nano-domains and exhibit a strong dynamic competition. The study of the interplay among these multiple orders is challenging because their critical dynamics are strongly connected to the emerging of functional properties at the macroscopic scale. The first step to understand the competition between these multiple striped orders is the investigation of their spatial-organization. On this purpose we developed a set of innovative techniques like scanning micro X-ray diffraction (μXRD) and resonant scanning micro X-ray diffraction (RμXRD) to directly visualize the spatial-organization of the SDW, CDW and defects nano-domains. By the use of μXRD on several High temperature superconductors (HTS) we evidenced a common nanoscale phase separation scenario, characterized by the coexistence of competing scale-free networks of self-organized nano-domains promoting superconductivity [1-16]. Recently we discovered that the CDW stripes get self-organized in nano-domains defining a non-Euclidean space available for the superconducting order [17]. In this process the way how the nano-domains interact and evolve in time is still fundamental missing information. The formation of the striped nano-domains and their domain-wall fluctuations occur at two different time-scales ranging from picosecond up to several seconds. To study both processes we developed new experimental approaches that combine temporal and spatial resolution with bulk sensitivity like resonant IR-pump FEL-probe [18] and time-resolved X-ray Photon Correlation Spectroscopy (XPCS) [19,20]. Indeed, the developing of the new coherent x-ray sources like Free Electron Lasers or resolution limit

Synchrotron Facilities will allow the investigation of otherwise inaccessible phenomena opening the way to the development of new functional materials.

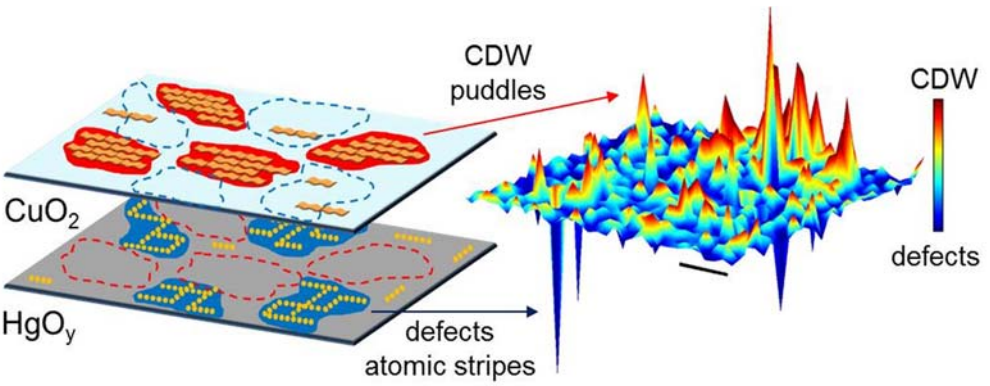

Figure 1. Anti-correlation between stripes and defects domains. (Left) The charge-stripes (CDW) rich areas (red) on the CuO_2 layers and defect-stripes rich areas (blue) on HgO_y layers. Spatial distribution of CDW and defects [9].

References

1. A. Bianconi, et al., *Intern. J. Modern Phys. B* 1, 853-862 (1987)
2. Y. Drees, Z. W. Li, A. Ricci, et al., *Nature Commun.* 5, 5731+ (2014).
3. A. Ricci, et al., *New Journal of Physics* 16, 053030+ (2014).
4. A. Ricci, et al., *Scientific Reports* 3, 2383+ (2013).
5. N. Poccia, et al., *Supercond. Science Tech.* 25, 124004 (2012).
6. N. Poccia, et al., *Nature Materials*, 10, 733-736 (2011).
7. A. Ricci, et al., *Physical Review B* 84, 060511+ (2011).
8. A. Ricci, et al., *Supercond. Science Tech.* 24, 082002+ (2011).
9. A. Ricci, et al. *Physical Review B* 91.2 020503 (2015).
10. M. Fratini, et al., *Nature* 466, 841 (2010).
11. N. Poccia, et al., *Proc. National Academy Sciences* 109, 15685 (2012).
12. D. Innocenti, et al., *J. Super. Novel Magn.* 22, 529 (2009).
13. A. Ricci, M. Fratini, A. Bianconi, *J. Super. Novel Magn.* 22, 305-308 (2009).
14. A. Ricci, et al., *J. Super. Novel Magn.* 22, 589-593 (2009).
15. N. Poccia, et al., *Advances in Condensed Matter Physics* 2010, 1-7 (2010).
16. A. Ricci, et al., *Superconductor Science Tech.* 23, 052003 (2010).
17. G. Campi, et al. *Nature* 525, 359-362 (2015).
18. A. Ricci, et al., *LCLS and FERMI proposals* (2015).
19. A. Ricci, *J. Super. Novel Magn.* 28, 1295-1298 (2015).
20. A. Ricci, et al. *Science* (submitted in 2015).

An Old Tale with a New Twist: Revisiting Metal-Insulator Transition of VO_2

Surajit Saha,[1,2,*] Amar Srivastava,[1,2] Helene Rotella,[1] Banabir Pal,[3] Zhe Wang,[4] M. R. Motapothula,[1,2] Kalon Gopinadhan,[1] Sinu Mathew,[1] Agnieszka Banas,[5] Krzysztof Banas,[5] Chunxiao Cong,[6] Yu Ting,[6] Michal Dykas,[1] Yang Ping,[5] Darrell Schlom,[4] D. D. Sarma,[3] T. Venkatesan[1,2]

[1]*NUSNNI-NanoCore, National University of Singapore, Singapore 117576*

[2]*Department of Physics, National University of Singapore, Singapore 117542*

[3]*Solid State and Structural Chemistry Unit, Indian Institute of Science, Bangalore 560012, India*

[4]*Department of Materials Science and Engineering, Cornell University, Ithaca, New York 14853-1501, USA*

[5]*Singapore Synchrotron Light Source, National University of Singapore, 5 Research Link, Singapore 117603*

[6]*Division of Physics and Applied Physics School of Physical and Mathematical Sciences, Nanyang Technological University, Singapore, 637371, Singapore*

Email: *physuraj@nus.edu.sg; saha.surajit@gmail.com*

Keywords: metal-insulator transition, VO_2 polymorphs, composites, dimerization.

Metal-insulator transition (MIT) in transition-metal oxides has been an important area of research for not only to understand the mechanism but also for various possible applications. In the d-electron systems, this transition is the result of instabilities arising from complex interplay of charge, spin, orbital and lattice degrees of freedom. Among them VO_2, a $3d^1$ system, has attracted a great deal of interest in last few decades for its MIT near room temperature (T_{MIT} ~ 340 K in bulk) concomitant with a structural phase transition at the same temperature. Recent findings suggest that it is both structurally and electronically driven, and perhaps, VO_2 is best described by a special case of a Pierels-Mott insulator wherein electron-electron correlations and dimerization of V atoms both contribute to the opening of an insulating gap. Optical/thermal/gate-voltage excitation of carriers to the threshold limit to induce the transition to the metallic phase without a crystallographic phase transition (CPT) is seen on Pico-second time scale consistent with the Mott-Hubbard picture [1-3]. On the contrary, infrared spectroscopic studies on VO_2 thin films as well as nano-wires show the clustering of metallic as well as

insulating phase just prior to the MIT [4,5]. In the VO_2(M/R) system the coexistence of the metallic and insulating phases exerts in-plane strain on each other due to their lattice mismatch further adding to the dynamics of the phase transition. Therefore, it will be fair to say that the current understanding of the role of the CPT on the MIT is not unanimous.

Here, we show that a composite film of tetragonal VO_2(A) and monoclinic VO_2(B) phases also exhibits an MIT similar to the one in VO_2(M) to VO_2(R) transition. Extensive TEM and temperature-dependent XRD studies reveal that the film is made of columns of VO_2(A) and VO_2(B) phases and very little M phase. Most importantly, there is no CPT observed in the temperature-dependent x-ray diffraction data across the MIT. The VO_2(A) phase is insulating while the VO_2(B) phase shows a broad MIT at 150 K [6]. However, in the composite, possibly the A phase is under compressive stress while the B phase is under tensile stress and we believe this leads to the dimer induced MIT in this composite VO_2 system. Our findings suggest that a CPT is not necessary for the MIT in VO_2 composite system which we believe will motivate further studies on VO_2 addressing the fundamental question- CPT vs MIT: who leads the game?

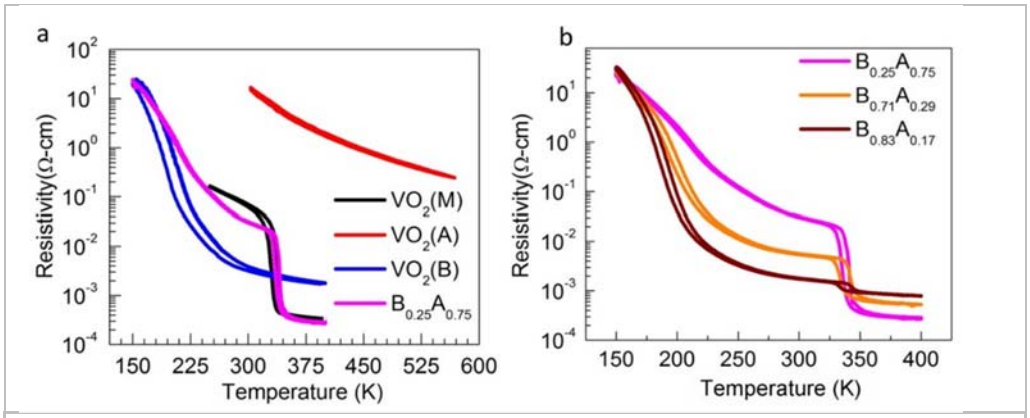

Figure 1: Electrical Transport measurement. (a) Comparison of temperature-dependent resistivity of single phase VO_2(A), VO_2(B), VO_2(M) and BA composite. (b) Temperature-dependent resistivity of different compositions of BA composites in the temperature range of 400 - 150 K.

References

1. J. Jeong *et al.*, *Science* **339**, 1402 (2013);
2. A. Pashkin *et al.*, *Phys. Rev. B* **83**, 195120 (2011);
3. J. Nag *et al.*, *J. Appl. Phys.* **112,** 103532 (2012).
4. M.M. Qazilbash *et al.*, *Science* **318**, 1750 (2007);
5. J. Cao *et al.*, *Nat. Nano* **4**, 732 (2009).
6. A. Srivastava et al. *APL Mat.* **3**, 026101 (2015).

Magnetism and related properties at nm length-scales

D.D. Sarma
Solid State and Structural Chemistry Unit, Indian Institute of Science, Bengaluru 560012

Email: *sarma@sscu.iisc.ernet.in and sarma.dd@gmail.com*
Keywords: magnetic properties, magnetotransport, complex nanomaterials, core-shell structures, heterostructures

There are many manifestations of magnetic interactions within objects and features that are typically in the nm length-scale, leading to a range of interesting and often unexpected properties. Broadly speaking, there are three distinct classes of nano-objects that we have investigated so far, namely (1) nonmagnetic semiconductor nanoparticle hosts doped with magnetic impurities; (2) nanoparticles of bulk magnetic materials; and (3) bulk magnetic materials whose properties are greatly influenced by features that are of nanometric dimensions.

In category 1, the primary motivation comes from the much celebrated class of bulk materials, namely dilute magnetic semiconductors (DMS), with the added incentive arising from the possibility of band-gap tuning with the size of the sample due to the quantum confinement effect. In this context, we critically evaluate whether magnetism of DMS can be sustained independent of the band gap tuning in such NC systems from a theoretical standpoint. [1] At an experimental level, we find these doped semiconductor NCs almost always exhibiting paramagnetic behavior, [2] except for one case where magnetic ordering could be achieved via co-doping of more than one magnetic ions in to the system. [3]

In category 2, we probe magnetic properties, with an emphasis on magnetotransport, of magnetic nanoparticles with complex structures, including core-shell structures and planar heterostructures, to illustrate phenomena [4-8] that challenge well-established concepts of tunnelling magnetoresistance (TMR).

While there are plenty of examples where a bulk antiferromagnet is driven to the ferromagnetic state on doping, there is hardly any reverse example of a ferro or a ferrimagnet driven to an antiferromagnetic state on doping. It turns out that $La_{2-x}Sr_xCuRuO_6$ is one such rare anomaly where the end-member La_2CuRuO_6 is a ferrimagnet, but the hole-doped compositions are antiferromagnetic for all levels of doping. [9] This unusual behavior can be understood in terms of certain nanometric features within the bulk sample that alters the magnetic interactions in a subtle way to bring about this phenomenon. Similarly, anomalous magnetotransport of Sr_2FeMoO_6 can only be understood in terms of

presence of nanometric features within the bulk system that affect its properties drastically. [10]
Depending on the available time, I shall discuss a selection of these results relating to the underlying theme of magnetism and magnetotransport in such complex nanoscopic systems.

*Also at Department of Physics and Astronomy, Uppsala University, Sweden and Council for Scientific and Industrial Research - Network of Institute for Solar Energy (CSIR-NISE), New Delhi, India.

References

1. S. Sapra, D.D. Sarma, S. Sanvito and N.A. Hill, Nano, Lett. **2**, 605 (2002).
2. S. Sapra, J. Nanda, A. Anand, S. V. Bhat and D.D. Sarma, J. Nanosci. Nanotechnol. **3**, 392 (2003); D. D. Sarma, Ranjani Viswanatha, Sameer Sapra, Ankita Prakash and M. Garcia-Hernandez, J. Nanosci. Nanotech. **5**, 1503 (2005).
3. Ranjani Viswanatha, Doron Naveh, James R. Chelikowsky, Leeor Kronik, and D. D. Sarma, J. Phys. Chem. Lett. **3**, 2009 (2012).
4. P. Anil Kumar and D. D. Sarma, Appl. Phys. Lett. **100**, 262407 (2012).
5. V. Thakare, G. Xing, H. Peng, A. Rana, O. Game, P. Anil Kumar, A. Banpurkar, Y. Kolekar, K. Ghosh, T. Wu, D.D. Sarma, and S.B. Ogale, Appl. Phys. Lett. **100**, 172412 (2012).
6. P. Anil Kumar, Sugata Ray, S. Chakraverty, and D.D. Sarma, Appl. Phys. Lett. **103**, 102406 (2013).
7. D.D. Sarma, Sugata Ray, K. Tanaka, M. Kobayashi, A. Fujimori, P. Sanyal, H.R. Kr- ishnamurthy and C. Dasgupta, Phys. Rev. Lett. **98**, 157205 (2007); S. Ray, S. Middey, S. Jana, A. Banerjee, P. Sanyal, R. Rawat, L. Gregoratti and D.D. Sarma, Euro Phys. Lett. **94**, 47007 (2011).
8. Sumanta Mukherjee, Ronny Knut, S. M. Mohseni, T.N. Anh Nguyen, S. Chung, Q. Tuan Le, Johan Åkerman, Johan Persson, Anindita Sahoo, Abhijit Hazarika, Banabir Pal, Sebastian Thiess, Mihaela Gorgoi, P. S. Anil Kumar, Wolfgang Drube, Olof Karis, and D.D. Sarma, Phys. Rev. B 91, 085311 (2015).
9. P. Anil Kumar, R. Mathieu, R. Vijayaraghavan, S. Majumdar, O. Karis, P. Nordblad, B. Sanyal, O. Eriksson, and D.D. Sarma, Phys. Rev. B **86**, 094421 (2012).
10. C. Meneghini, S. Ray, F. Liscio, F. Bardelli, S. Mobilio and D.D. Sarma, Phys. Rev. Lett. **103**, 046403 (2009).

Electromagnetic and electromechanical applications of graphene-based materials

M.S. Sarto*, G. De Bellis, A. Tamburrano, A.G. D'Aloia, F. Marra, A. Rinaldi, L. Paliotta, A. Acquarelli, A. Proietti, A. Bregnocchi
Sapienza University of Rome, Research Center for Nanotechnology applied to Eng. (CNIS),
Sapienza Nanotechnology and Nanoscience Lab. (SNN-Lab)
Dept. Astronautics, Electrical, Energetic Engineering (DIAEE)

Email: *mariasabrina.sarto@uniroma1.it*
Keywords: graphene-based materials, electromagnetic properties, electromechanical properties

The pervasive diffusion of wireless consumer electronics has increased the attention on the risks of electromagnetic interference (EMI), and has pushed towards the development of innovative and cost-effective electromagnetic (EM) shielding solutions. Moreover, EM shielding of radio frequency (RF) radiation in the frequency range up to a few tens of gigahertz is becoming more and more challenging due to the increasing demand for electronic devices integrating smartness and multifunctionality, with lightness, small size, ergonomics, fashion trends.

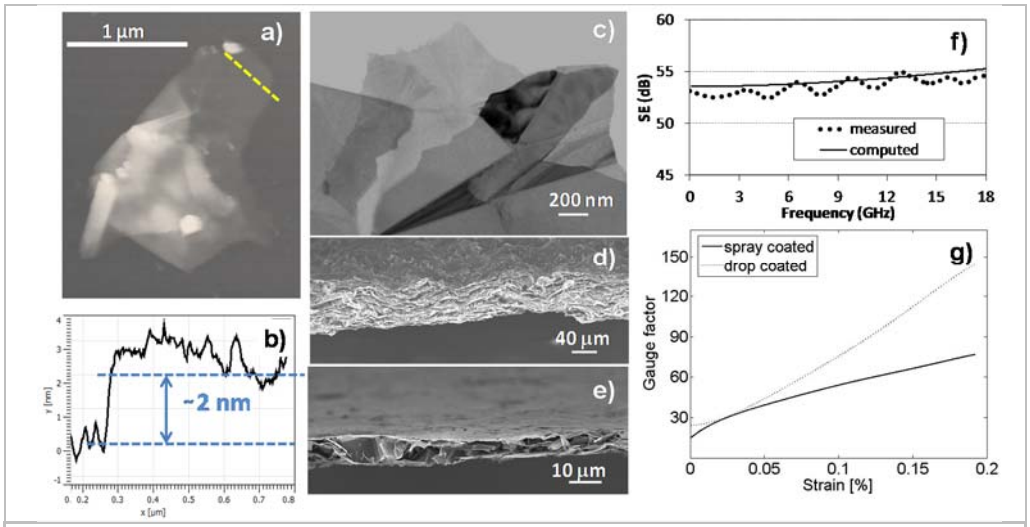

Figure 1: AFM (a,b) and STEM characterization of GNP flakes (b). SEM of the cross section of GNP papers before and after thermal annealing and mechanical compression (d,e). Shielding effectiveness of a GNP paper (f) and gauge factor of GNP-based sensor (g).

Due to their high electrical conductivity, metals are by far the most commonly used materials for EM shielding at RF. However, the use of metals in advanced multifunctional shielding solutions has some limitations, typically related to their high-density that prevents lightweight solutions. Moreover, metals are subjected to corrosion in harsh environment, and most of them are classified as "critical raw materials" by European Commission. In addition, the widespread use of plastics in consumer electronics packaging and the increasing interest in flexible electronics are pushing towards the development of new shielding metal-free solutions. Within this context, recently carbon-based materials have gained popularity thanks to their light weight, resistance to corrosion, electrical and thermal conductivity, multifunctionality [1,2,3]. In particular, carbon nanotube (CNT) and graphene nanomaterials, such as graphene oxide (GO) and multilayer graphene (MLG) micro- and nanosheets, also known as graphene nanoplatelets (GNPs), have been widely investigated in the last decade.
A promising class of graphene-based materials for large-scale exploitation in engineering, and in particular for electromagnetic shielding [4] and strain sensing [5] applications, are GNPs produced by thermochemical exfoliation of intercalated graphite compounds and their derivatives, like GNP-polymer composites [4-6], GNP-papers [7] or GNP-flexible shielding foils.
The presentation will provide an overview of the recent results and application of GNP-based materials for radar-absorbing screen, highly electromagnetic shielding foils, high-sensitivity strain sensors for structural health monitoring applications. An insight on the correlation between production process, structural and morphological characteristics and multifunctional properties of the new materials will be provided.

References

1. Chung DDL. Carbon 39(2), 279–85 (2001).
2. Chung DDL. Carbon 50(9), 3342-53 (2012).
3. Prasek J, Drbohlavova J, Chomoucka J, Hubalek J, Jasek O, Adamc V *et al.* J Mater Chem 21, 15872–84 (2011).
4. G. De Bellis, A.Tamburrano, A.Dinescu, M.L.Santarelli, M.S. Sarto, Carbon 49, 4291-4300 (2011)
5. A. Tamburrano, F. Sarasini, G. De Bellis, A. D'Aloia, M.S. Sarto, Nanotechnology 24(46), 465702 (2013).
6. A.G. D'Aloia, F. Marra, A. Tamburrano, G. De Bellis, M.S. Sarto, Carbon 73, 175–184 (2014).
7. L. Paliotta, G. De Bellis, A. Tamburrano, F. Marra, A. Rinaldi, S.K. Balijepalli, S. Kaciulis, M.S. Sarto, Carbon 89, 260-271 (2015).
8. E. Zanni, G. De Bellis, M. Bracciale, A. Broggi, M.L. Santarelli, M.S. Sarto, C. Palleschi, D. Uccelletti, Nano Lett. 12 (6), 2740–2744 (2012).

Trend to nano-SQUIDs: from magnetic microscopy to the investigation of magnetic nanoparticles and the detection of single electron spin flips

M. Schmelz*[1], V. Zakosarenko[2], T. Schönau[1], S. Anders[1], S. Linzen[1], R. Stolz[1] and H.-G. Meyer[1]
[1]*Leibniz Institute of Photonic Technology, Albert-Einstein-Straße 9, D-07745 Jena, Germany*
[2]*Supracon AG, An der Lehmgrube 11, D-07751 Jena, Germany*

Email: *matthias.schmelz@ipht-jena.de*

Keywords: nanoSQUIDs, cross-type Josephson junction, small spin systems

Superconducting quantum interference devices (SQUIDs) are today's most sensitive sensors for the detection of magnetic flux. They are very versatile and can be used to measure any physical quantity that can be transformed into magnetic flux. In the past, they have successfully been used e.g. in geophysics and biomagnetism. Here, the figure of merit is usually the magnetic field noise $S_B^{1/2}$.

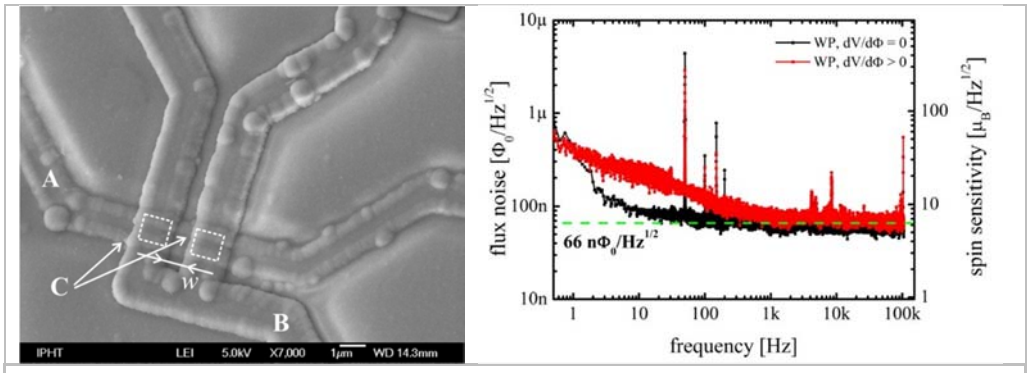

Figure 1: (left) Scanning electron microscope images (SEM) of a SQUID with $(0.8 \times 0.8)\ \mu m^2$ sized Josephson junctions and an inner loop dimension w of 1.5 µm. Areas *C* denote the Josephson junctions formed by the overlap of trilayer (*A*) and wiring layer (*B*). (right) Equivalent flux noise spectrum for SQUID with 0.5 µm loop diameter. The red and black curves correspond to working points (WP) on the slope of the flux-voltage characteristics with $\partial V/\partial \Phi > 0$ and $\partial V/\partial \Phi = 0$, respectively, where the SQUID is insensitive to magnetic flux noise. The equivalent white flux noise corresponds to 66 $n\Phi_0/Hz^{1/2}$.

During the last years there has been growing interest in the investigation of small spin systems and in SQUID microscopy. Here, the coupling of the signal to the SQUID becomes crucial and typically used SQUID sensors are not well

adapted to this task. It has been shown that downsizing the SQUID dimensions may improve the coupling. Whereas SQUIDs typically have dimensions ranging from several 100 µm to mm, nowadays miniature SQUIDs feature loop sizes of about 10 µm and below.

In this talk we will present results on the development of miniature or even nanometer sized SQUIDs with loop dimensions ranging from 10 µm down to 500 nm. They are fabricated in our cross-type Josephson junction technology [1].

The small total capacitance of these submicron junctions leads to the superior noise performance of the devices. Figure 1 (left) shows a scanning electron microscope image of such a device with $(0.8 \times 0.8)\ \mu m^2$ Josephson junctions and an inner loop diameter of $w = 1.5$ µm.

With a loop size of about 500 nm they exhibit an energy resolution of 3.4 h at an operating temperature of 4.2 K, corresponding to an estimated spin sensitivity of better than $7\ \mu_B/Hz^{1/2}$ in the white noise region, as could be seen in Figure 1 (right) [2].

We will show results on the electrical characterization of devices with various pickup loops and discuss options for further improvements, which may push the sensitivity of such devices towards single spin resolution.

These SQUIDs moreover, offer a continuous operation over a broad temperature range down to mK, essential for the investigation of magnetization dynamics. Finally, our approach offers the possibility of the reliable fabrication of homogenous sensor arrays, which may be of particular importance in SQUID microscopy.

References

1. S. Anders, M. Schmelz, L. Fritzsch, R. Stolz, V. Zakosarenko, T. Schönau and H.-G. Meyer, Sub-micrometer-sized, cross-type Nb–AlO_x–Nb tunnel junctions with low parasitic capacitance, Superconductor Science and Technology 22, 064012 (2009).
2. M. Schmelz, Y. Matsui, R. Stolz, V. Zakosarenko, T. Schönau, S. Anders, S. Linzen, H. Itozaki, H.-G. Meyer, Investigation of all niobium nano-SQUIDs based on sub-micrometer cross-type Josephson junctions, Superconductor Science and Technology 28, 015004 (2015).

Nanostructure-Based Fluorescent Biosensors

Kotla Shivaram[*1], R. Gunnella[1], A.M. Giuliodori[2], R. Spurio[2], A. Fabbretti[2], F. Perrozzi[3] and L. Ottaviano[3]
[1]*Physics Division, School of Science and Technology, University of Camerino Via Madonna delle Carceri 9 62032 Camerino (MC)-Italy.*
[2]*School of Biosciences and Veterinary Medicine, University of Camerino Via Gentile III da Varano 62032 Camerino (MC)-Italy.*
[3]*Dipartimento di Scienze Fisiche e Chimiche, Universita' dell'Aquila, Via Vetoio, 67100 L'Aquila, Italy.*

Email: *shiva97895@gmail.com
Keywords: ssDNA: single stranded Deoxyribonucleic acid, oligonucleotide: short fragments of nucleic acids with defined sequence, fluorophore FAM: 6-carboxyfluorescein is a single isomer derivative of fluorescein.

We have studied and investigated the development of a fluorescent biosensor based on graphene oxide (GO) for the analysis of interaction between a fluorophore FAM (Carboxyfluorescein)-labeled single-stranded DNA with its complementary single-stranded DNA oligonucleotide (target). The graphene oxide adsorbs the FAM-labeled single stranded DNA (probe) and quenches its fluorescence. Upon addition of the complementary single stranded DNA oligonucleotide, the probe hybridizes to its target [1] thus producing a double-stranded DNA, which detaches from the GO. The release of the double helix leads to the recovery of dye fluorescence that can be monitored by fluorimetric techniques.

Introduction

Graphene oxide (GO) is a single-atom-thick and two-dimensional carbon material. It is the oxidized form of graphene, with "O" functional groups attached to the sp^2 C basal plane and edges [2]. GO has tremendous attractive and great remarkable electronic, mechanical, and thermal properties [3]. When compared with other nanomaterials GO has some superior properties, high quenching efficiency, good water dispersibility (hydrophilic) due to the presence of the "O" functional groups. These properties make GO a promising nanomaterial for biological applications, including biosensors.
In this study we examined the GO by using Atomic Force Microscopy (AFM) to characterize the GO interaction with ssDNA.

Materials and methods

Pristine GO flakes were prepared using a modified Hummers method and dispersed in water with a concentration of 0.5 mg/mL. Then we tested the GO with buffered solution containing 20mM Tris-HCl pH 7.5, 100mM NH_4Cl, 5 mM KCl, 10mM $Mg(CH_3COO)_2$. The samples were prepared by drop casting, the GO and DNA with buffered solution [1] on 300 nm SiO_2/Si(100) at room temperature. The biomolecules were allowed to adhere to the SiO_2 surface for 5-10 minutes. AFM was performed in air in tapping mode using a Veeco Digital D5000 system.

Samples characterization by AFM

We used atomic force microscopy (AFM) to characterize the GO- DNA complex. Figure 1 (left) shows the AFM image of the GO flakes, whose thickness (about 1.2 nm) is reported in the histogram analysis. Figure 1 (right) shows the typical AFM image of the DNA-GO complex, where the bright areas on the GO surface might be due to the adsorption of DNA. In this complex the thickness is about 3 nm.

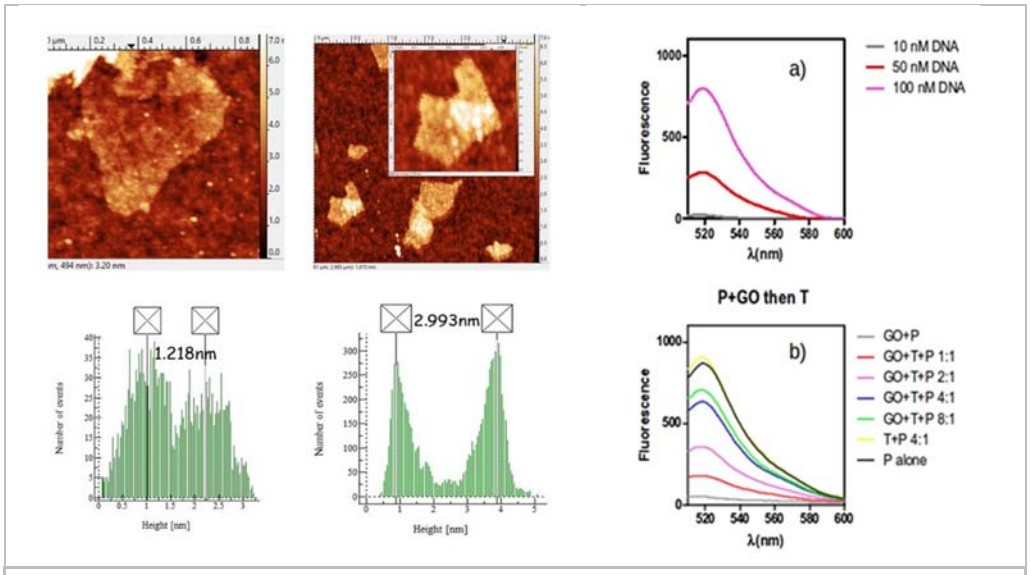

Figure 1 (Left panels) AFM height image of GO sheets deposited on SiO2 substrates (left); AFM height image of DNA-GO complex (right) by histogram analysis; (Right panels) Fluorescence emission spectra (excitation at 495 nm) of ssDNA at different conditions: a) Increasing amounts of fluorescently labeled ssDNA in Tris-HCl buffer with different concentrations; b) Fluorescently labeled ssDNA(100nM) in Tris-HCl buffer + GO in the presence of increasing amounts of target DNA (T).

Spectrofluorimetric analyses of DNA-GO complexes

The fluorescence spectra of ssDNA (5'-FAM-cttgtggaagatgggcaagaagactggagg-3') and ssDNA-GO were measured to monitor the adsorption of ssDNA on GO. As can be seen from Figure 1(a), in the absence of GO the fluorescently labeled ssDNA shows strong fluorescence emission. Furthermore, this emission is proportional to the concentration of ssDNA in solution. However, in the presence of GO, up to ~97% quenching of the fluorescence emission was observed (Figure 1a). This observation indicates that GO can strongly adsorb ssDNA and can efficiently quench its fluorescence. The fluorescently labeled ssDNA-GO complex displayed significant fluorescence enhancement upon addition of complementary target DNA oligonucleotide (Figure 1b). This recovery of fluorescence increases with increasing concentration of the target DNA added to the mixture.

Conclusions

GO can be used as a platform for fast, sensitive, and selective detection of biomolecules. The low cost and large production scale of GO make it a promising material for devising biosensors compared to other nanomaterials.

References

1. Lu, C.-H., Yang, H.-H., Zhu, C.-L., Chen, X. and Chen, G.-N., A Graphene Platform for Sensing Biomolecules. Angew. Chem. Int. Ed. 48: 4785–4787 (2009). doi: 10.1002/anie.200901479.
2. Nan-Fu Chiu, Teng-Yi Huang and Hsin-Chih Lai, Graphene Oxide Based Surface Plasmon Resonance Biosensors, Advances in Graphene Science, M. Aliofkhazraei (Ed.), ISBN: 978-953-51-1182-5, InTech (2013). DOI: 10.5772/56221.
3. F. Perrozzi et al., J. Phys.: Condens. Matter 27, 013002 (2015) doi:10.1088/0953-8984/27/1/013002 Graphene oxide: from fundamentals to applications.

Improved Conversion Efficiency of Dye Sensitized Solar Cell Using Eu doped TiO_2-ZrO_2 Nanocomposite

Laxmi J. Tomar*, Piyush J. Bhatt, Rahul K. Desai, Bishwajit S. Chakrabarty
Applied Physics Department, Faculty of Technology and Engineering, The M. S. University of Baroda, Vadodara, Gujarat, India.

Email: **laxmi_tomar86@yahoo.com*
Keywords: dye sensitized solar cell, nanocomposite, hydrothermal method, optical properties.

Dye Sensitized solar cell have attracted attention in recent years because of their low production cost and ease of fabrication. Michael Gratzel created a low cost Dye Sensitized Solar Cell (DSSC) with TiO_2 and obtained a solar cell efficiency of 10.4% in 1991 [1]. TiO_2 is the most widely used semiconducting material for photo anode. Generally TiO_2 exist in three different phase Anatase, Rutile and Brookite [2]. Among these three phases Anatase is the preferred phase for solar cell application [3]. In the present work we have tried to modify structural and optical properties of TiO_2 by mixing it with ZrO_2 and by doping Eu metal.

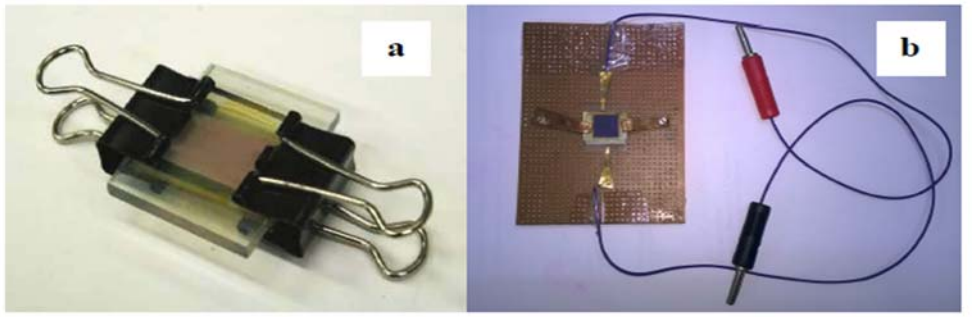

Figure 1: (a) Prepared dye sensitized solar cell, (b) contact arrangements for Dye sensitized solar cell.

TiO_2-ZrO_2 and Eu doped TiO_2-ZrO_2 nanocomposites have been synthesized by hydrothermal method for solar cell application. The structural properties and composition of prepared materials were analyzed by X-ray diffraction spectroscopy and FTIR spectroscopy respectively. The XRD results revealed that prepared samples consist of Anatase and Rutile phases of TiO_2 where as monoclinic and Tetragonal phases of ZrO_2. The average crystallite size of TiO_2-

ZrO_2 and Eu doped TiO_2-ZrO_2 nanocomposites is 17.41 nm and 6.47 nm respectively. The FTIR analysis confirmed the presence of Ti-O-Ti bond. The absorption bands of any impurities have not been observed which shows formation of material in pure form. A red shift of absorption edge has been observed for the prepared samples. The optical bandgap was determined from Tauc´s plot and was found to be 2.15 eV and 2.03 eV for TiO_2-ZrO_2 and Eu doped TiO_2-ZrO_2 nanocomposites respectively. The optical bandgap has been decreased compared to pure TiO_2. The refractive index has been calculated from UV- Visible absorption spectra and it has been increased compare to bulk TiO_2 refractive index.

The high refractive index of the material can trap the photons in the material for longer time, which will be used to generate more electrons in solar cell. Inexpensive and basic dye sensitized solar cells using prepared samples were fabricated. TiO_2-ZrO_2 and Eu doped TiO_2-ZrO_2 nanocomposites were used as photo electrode material. The pomegranate juice was used as a dye and carbon coating through pencil is used as counter electrode. The performance of prepared solar cells was measured by taking I-V characteristics under the illumination. Photovoltaic parameter like open circuit voltage, power conversion efficiency, and fill factor were evaluated for fabricated solar cell. The efficiency has been improved for prepared samples compared to pure TiO_2. The power conversion efficiency of DSSC fabricated with TiO_2, TiO_2-ZrO_2 nanocomposite and Eu doped TiO_2-ZrO_2 nanocomposite was found 0.71%, 1.97% and 6.25% respectively.

References

1. B. O'Regan, M. Grätzel, A low-cost, high-efficiency solar cell based on dye sensitized colloidal TiO_2 films Title, Nature 353, 737 (1991).
2. D. Reyes Coronado, G. Rodriguez Gattorno, M.E. Espinosa Pesqueira, C. Cab, R. de Coss and G. Oskam, Phase-pure TiO2 nanoparticles: anatase, brookite and rutile, Nanotechnology 19, 145605 (2008).
3. S.D. Burnside, V. Shklover, C. Barbe, P. Comte, F. Arendse, K. Brooks, M. Grätzel, Self-organization of TiO_2 nanoparticles in thin films, Chem. Mater. 10, 2419 (1998).

CVD-diamond high-temperature cells for solar concentrating systems

D.M. Trucchi*, M. Girolami, P. Calvani, A. Bellucci
Institute of Structure of Matter, Via Salaria km 29.300 – Monterotondo Scalo (RM) – 00015 Italy

Email: *daniele.trucchi@ism.cnr.it*
Keywords: CVD Diamond; solar concentration; energy conversion; thermionic emission; photoemission

High-temperature solar cells are possible with Photon-enhanced Thermionic Emission (PETE) devices, which represent a novel and very attractive concept for the exploitation of concentrated solar radiation characterized by promising high conversion efficiency. PETE converters rely on the concept that engineered semiconductor structures can provide a thermionic emission, sustained by the high temperatures induced by thermalization of low-energy photons, that is significantly boosted by hot electrons generated by photons with sufficient energy to produce charge couples.

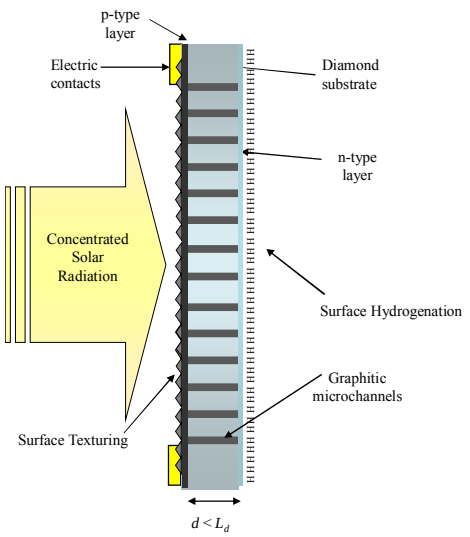

Figure 1: Sketch of the diamond photo-thermionic cathode for high temperature solar cells

Surface nanotexturing combined to surface-hydrogenation, aimed at achieving negative electron affinity conditions and a work function as low as 1.7 eV with nitrogen-doping, are here proposed as a radically new and potentially efficient PETE cathode completely based on chemical-vapor-deposited (CVD) diamond, able to ensure an efficient thermionic emission at temperatures up to 780 °C.

CVD diamond is transparent to solar radiation due to its wide bandgap, consequently advanced and novel techniques are needed for processing diamond to become an efficient sunlight absorbing material (i.e. black diamond). Surface texturing by fs-laser, boron-implantation, buried and distributed graphitic structures and other technological steps allow for the fabrication of an innovative defect engineered diamond cathode to be efficiently exploited for the conversion of concentrated solar radiation.

Diamond Photo-Thermionic Cathode

The cathode structure is sketched in Fig. 1. The active thermionic materials are within a vacuum enclosure, that allows for the electrons transport between the electrodes and for the minimization of thermal losses. A free-standing diamond film (thickness ranging from some to hundreds of micrometers) acts as a photocathode, being directly illuminated by the concentrated sunlight. On its illuminated surface, periodic textured structures with periodicity of hundreds of nanometers, comparable to the solar radiation wavelengths, are developed. It was demonstrated that 1D textures drastically increase the diamond solar absorbance to values > 90 % [1].

Figure 2: Comparison between a transparent and a “textured-black” diamond plate.

Black diamond is the result of this technological process. The cathode is sized in order that absorbed radiation heats the photocathode at a temperature not exceeding 800 °C to avoid hydrogen desorption from the emitting surface. The high diamond thermal conductivity ensures a negligible temperature gradient between the emitting surface and the illuminated one. The surface texturing is also electronically active: since periodic structures are equivalent to periodic defect states in an ideal crystal, they can add additional energy levels within the diamond bandgap. A significant photoelectric enhancement connected to a responsivity increase of two orders of magnitude was measured in surface-textured samples compared to the pristine ones. The control on the surface periodic structure is a key design parameter in diamond-based PETE cathodes, since the additional energy levels depend on the structure morphology, both in terms of density and energy position within the bandgap. Ideally, such defects

should be a large band mimicking the trend of the solar spectrum. A black diamond sample is shown in Figure 2, compared to an untreated one.
The diamond cathode has a front surface p-type doped layer 1) to act as a low resistance ohmic contact; 2) to minimize electron-hole recombination by the formation of a proper band-bending able to locally separate the charge carrier types; 3) to increase the photoelectric boost by introducing in the diamond bandgap additional useful energy states. Boron implantation can be used for the fabrication of the p-type layer. The cathode acts as a defect-engineered semiconductor, where hot electrons, once photogenerated, can travel in the diamond conduction band with a high diffusion length of (175 ± 25) μm [2]. It means that, if the cathode thickness is made shorter than the corresponding electron diffusion length, all the hot electrons will reach the emitting surface even without an accelerating electric field, thus producing an additional contribution of electrons ready for the emission. This is another important design parameter: thicker is the cathode and more is the optical absorption, but less could be the electric boost caused by photoelectrons. On the emitting surface, a thin n-type diamond layer is developed (nitrogen doped to obtain a Fermi level at 1.7 eV from the conduction band minimum) and the surface is hydrogen-terminated to induce NEA conditions. This induces a vacuum level position below the conduction band minimum of about 0.5 eV, guaranteeing virtually no barrier for the electron emission and consequently a very high escape probability. The work function value of 1.7 eV refers to room-temperature conditions, whereas semiconductors bandgap is a decreasing function of temperature. It means that temperature reduces the work function values and, in case of nitrogen-doped diamond at 750 °C, 1.4 eV is reported in literature [3]. Hot electrons induce a decrease of cathode electric conductivity, but the cathode emits also thermal electrons, that have to be refilled from the bulk to the emitting surface. Graphitic conductive micro-channels [4], developed within the diamond bulk and connecting the two cathode surfaces, are able to reduce the cathode series resistance. Graphitic micro-channels were fabricated embedded in the diamond lattice by using ultrashort laser pulses, which are able to transform sharply diamond into graphite with a high spatial resolution (about 1 μm). The presently obtained series resistance is in the range of few hundred of Ohms.

References

1. P. Calvani, A. Bellucci, M. Girolami, S. Orlando, V. Valentini, A. Lettino, D.M. Trucchi, Appl. Phys. A-Mater 117, 25 (2014).
2. J. Ristein, W. Stein, and L. Ley, Phys. Rev. Lett. 78, 1803 (1997).
3. T. Y. Sun, F. A. M. Koeck, and R. J. Nemanich, Advances in Science and Technology 95, 1-10 (2014).
4. M. Girolami, A. Bellucci, P. Calvani, S. Orlando, V. Valentini, and D. M. Trucchi, Appl. Phys. A-Mater 117, 143 (2014).

Gate–Source distance scaling effects in H-terminated diamond MESFETs: optimization of layout and output current density

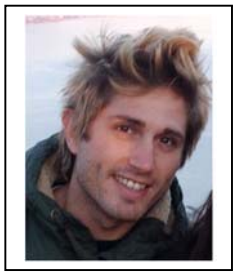

C. Verona[1*], W. Ciccognani[2], S. Colangeli[2], F. Di Pietrantonio[3], E. Giovine[4], E. Limiti[2], M. Marinelli[1] and G. Verona-Rinati[1].

[1]*Dipartimento di Ingegneria Industriale, Università di Roma "Tor Vergata", Via del Politecnico 1, I-00133 Roma, Italy*

[2]*Dipartimento di Ingegneria Elettronica, Università di Roma "Tor Vergata", Via del Politecnico 1, I-00133 Roma, Italy*

[3]*CNR – Istituto di Acustica e Sensoristica "O.M. Corbino" (IDASC), Via del Fosso del Cavaliere, 100 I-00133 Roma, Italy*

[4]*CNR–Istituto di Fotonica e Nanotecnologie, Via Cineto Romano 42, 00156 Rome, Italy*

Email: **claudio.verona@uniroma2.it*

Keywords: CVD diamond, MESFETs, semiconductor device manufacture, output current.

In this work, we report an analysis of gate-source and gate-drain distances on the MESFETs fabricated on H-terminated high-quality single crystal diamond films. The experimental results show that the scaling of the source-gate distance (L_{GS}) is a key factor for enhancing device performance, with positive consequences both on the output current density and device transconductance. On the contrary, the gate-drain distance (L_{GD}) produces less pronounced effects on device performance.

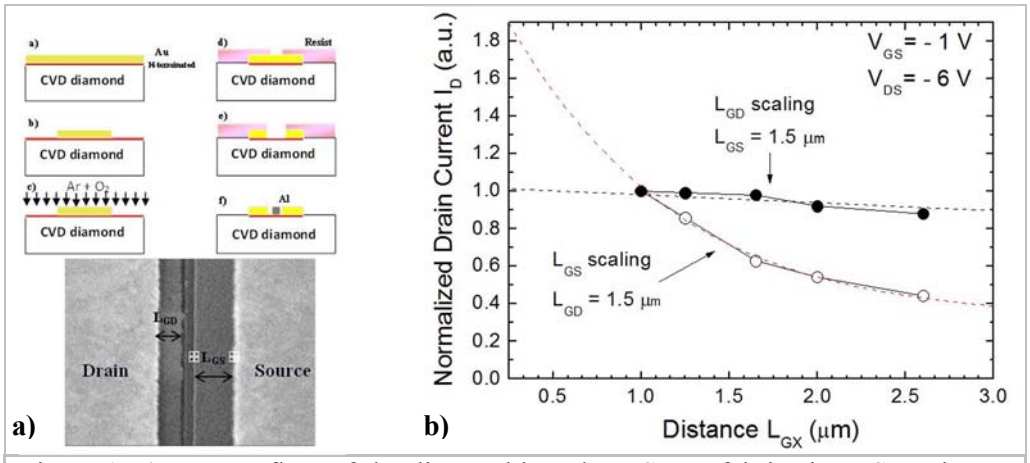

Figure 1: a) Process flow of the diamond based MESFET fabrication. SEM image of a channel geometry; b) normalized drain current density as a function of L_{GS} and L_{GD} distance.

A high-quality intrinsic single crystal diamond film with a thickness of 2 μm was grown by Microwave Plasma Enhanced Chemical Vapor Deposition on commercial low-cost polished synthetic HPHT diamond substrates. H-surface termination was achieved by exposing in-situ the diamond surface to H plasma in the same microwave CVD reactor at the end of the growth.
The diamond MESFET fabrication process, illustrated in Fig.1, consists of the following steps. Gold was thermally evaporated directly onto the H-terminated diamond surface (Fig.1 a). The Au mask, patterned by electron beam lithography (EBL) techniques, was used as electrode for the ohmic contacts of source and drain (Fig.1 b). In order to electrically insulate the devices on the same diamond substrate, the diamond surface was oxidized by using the Reactive Ion Etching (RIE) (Fig.1 c). A second EBL step was performed to realize the drain-source channel. The separation distance between the source and drain contacts was defined by KI/I_2 chemical etching for Au (Fig.1 d-e).
Finally, a single finger gate was patterned by standard lift-off lithographic technique and Aluminum was used to form Schottky contacts (Fig.1 f). In the realized devices, the gate-source (or gate-drain) distances were varied in the range 1.0 ÷ 2.6 μm, while keeping a fixed gate-drain (or gate-source) distance of about 1.5 μm (therefore changing also the total drain-source length). In this way, the devices can be easily tested by choosing which ohmic contact is necessary to be used as the source or drain contact during the tests.
The normalized drain current density as a function of L_{GS} and L_{GD} is shown in Fig.1 b). The normalization was performed with respect to the current measured at L_{GX} of 1 μm. Scaling L_{GD} (full circles) has nearly no effect on the current density, in contrast with the L_{GS} scaling (open circles) which has a noticeable impact on the drain output current density.
This behavior has already been theoretically predicted in other wide band-gap semiconductor technologies, such as GaN-HEMT [1] and 4H-SiC MESFETs [2]. In these references, the authors show that the increase of the current in the active channel associated to a reduction of the gate-source distance is due to the peculiar velocity-field characteristic of GaN 4and H-SiC material, for which the ohmic/linear regime extends up to fields in the order of 100 kV/cm [3]. Such physical property can be transposed to diamond devices, characterized by saturation electric fields [4] very close to the values reported for GaN and SiC. The experimental data, obtained varying the L_{GS}, can be fitted with an exponential function in order to extend the results to a shorter gate-source distance. The drain current is expected to be increased by a factor of about 2 when the L_{GS} distance is shortened from 1 μm down to 0.25 μm.
Breakdown voltage, knee voltage, threshold voltage variations due to changes in gate-source and drain-source distances have been investigated as well.
The obtained results, together with other well established FET design rules, have been used as guidelines for the layout optimization of H-terminated diamond-based MESFETs for RF operation. The optimized device geometry

has a coplanar layout with two gate fingers. The active devices have been characterized in terms of static I-V characteristics, maximum transconductance, maximum output power and small signal S-parameters, for the evaluation of the maximum cutoff frequency f_T and maximum oscillation frequency f_{max}. The normalized DC drain-source characteristics for various gate voltages are reported in Fig. 2.

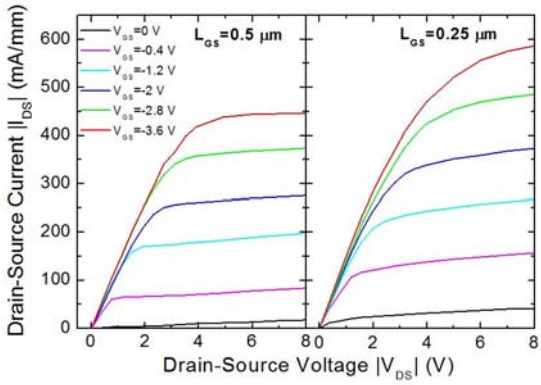

Figure 2: DC drain-source characteristics for various gate biases for devices with 0.5 µm and 0.25 µm gate source distance.

The curves, obtained on a 2x50 µm device, are related to the two different gate source distances i.e. 0.5 µm and 0.25 µm. As expected from the data reported in Fig.1, an increase in the maximum drain current is achieved for the sample realize with L_{GS}= 0.25 µm. Saturated drain current densities as high as 600 mA/mm has been measured.

References

1. S. Russo and A. Di Carlo, IEEE Transactions on Electron Devices 54, 1071 (2007).
2. D. Xiaochuan, Z. Bo and L. Zhaoji, Semic. Sci. Tech. 24, 015011 (2009).
3. J. Khurgin, Y. J. Ding and D. Jena, Appl. Phys. Lett. 91, 252104 (2007).
4. X. Zhou, F. Williams and S. Albin, MRS Online Proceedings Library 1551, 123 (2013).

Author Index